Université Paris Cité

Laboratoire MAP5

Mémoire d'Habilitation à Diriger des Recherches

Spécialité : Mathématiques

Contributions to the modelling of multispecies or multiphasic fluid flows in asymptotic regimes: analysis and simulation

---

Présenté et soutenu publiquement par

Bérénice Grec

le 18 juin 2025

Devant le jury composé de

Marianne Bessemoulin-Chatard	Directrice de recherche, CNRS	Rapportrice
Laurent Chupin	Professeur, Université Clermont Auvergne	Examinateur
Anne-Laure Dalibard	Professeure, Sorbonne Université	Examinatrice
Laurent Desvillettes	Professeur, Université Paris Cité	Examinateur
Maria Groppi	Professor, Università di Parma	Rapportrice
Pauline Lafitte	Professeure, Centrale Supélec	Examinatrice
Frédéric Lagoutière	Professeur, Université de Lyon	Rapporteur
Bertrand Maury	Professeur, Ecole Normale Supérieure	Examinateur

Remerciements

Les travaux présentés dans ce document ont été réalisés depuis mon recrutement au MAP5 et sont le fruit de diverses collaborations, pour lesquelles je suis extrêmement reconnaissante. Je le savais déjà, mais j'ai pu mesurer en ce début d'année 2025 la chance que j'avais d'être aussi bien entourée professionnellement et personnellement, merci ! Je dispose de cet espace pour coucher par écrit plus en détail ma gratitude pour mon environnement de travail si bienveillant et stimulant, ainsi que pour mes amis et ma famille qui rendent ma vie personnelle douce et joyeuse. C'est donc avec plaisir que je m'en empare. Voici donc des remerciements classés à peu près thématiquement, mais aussi de manière un peu aléatoire, ne m'en veuillez pas !

First, I would like to thank most sincerely Marianne Bessemoulin-Chatard, Maria Groppi and Frédéric Lagoutière, who accepted to read carefully this manuscript, write a report and come to my defense. Your kind words on my work really mean a lot to me! Merci également à Laurent Chupin, Anne-Laure Dalibard, Laurent Desvillettes, Pauline Lafitte et Bertrand Maury d'avoir accepté de faire partie de mon jury, c'est un grand honneur pour moi.

Je l'ai mentionné en introduction, je souhaiterais exprimer toute ma reconnaissance à mes co-auteurs, avec lesquels c'est un tel plaisir de travailler.

Laurent, Sébastien, Céline, vous m'avez accompagnée depuis le début de ma carrière, j'ai tant de raisons de vous remercier : depuis la proposition de post-doc et les délégations dans l'équipe REO, jusqu'à nos travaux en commun récents sur la respiration, en passant par toutes nos discussions et repas animés ! Merci également Laurent et Sébastien pour votre relecture attentive de ce manuscrit. Un énorme merci encore à Laurent pour la découverte des équations cinétiques et des modèles de mélanges, pour tes conseils toujours avisés, ainsi que pour les projets et demandes de financement que nous avons faits ensemble, par exemple en collaboration avec la Serbie à l'Université de Novi Sad. À ce sujet, un grand merci à Milana, c'était un bonheur de commencer à travailler avec toi pendant ta thèse, et je suis bien heureuse que nous continuions encore aujourd'hui. Also a huge thanks to Srboljub, it really is a pleasure to work with you, and I am eager to our next collaboration. Also a big thank you to both of you for your nice welcome in Novi Sad, it is truly wonderful to come each time! J'ai eu la joie de travailler avec Andrea dans le cadre de sa thèse, et je suis toujours ravie de nos discussions scientifiques, j'espère que nous reprendrons un travail commun dans le futur.

En 2011, j'ai eu l'opportunité de découvrir le monde des modèles à bas nombre de Mach, et de commencer une collaboration avec Stéphane, Gloria et Yohan. Cela a été un grand plaisir de travailler avec vous toutes ces années. Merci à Yohan pour les séances de travail motivantes, et en particulier lors des stages de Tanja, Davor et Gabrijela et de la thèse de Davor. Ma plus grande gratitude à Gloria, avec qui je continue encore de travailler sur ces sujets, et dont l'amitié, l'enthousiasme et la rigueur scientifique n'ont pas d'égal. Nous avons porté ensemble plusieurs projets Needs, et malgré toute la lourdeur administrative, le partage avec toi rendait la gestion tellement plus facile ! Je ne peux pas non plus passer sous silence ta dextérité hors du commun en LaTeX, la propreté de ce manuscrit te doit tout, et ton efficacité à appréhender de nouveaux outils, par exemple pédagogiques, ton exemple m'a souvent inspirée. Je suis également ravie d'avoir commencé à travailler avec Cédric plus récemment, nos discussions et séances de travail à distance tous les trois fonctionnent admirablement bien, merci.

Un grand merci aussi à Marc, Vincent, Francesco, Laurent, Christèle, Bertrand, Olivier, Nicolas, pour nos travaux communs, j'ai beaucoup apprécié nos travaux communs. In the same way, a big thank you in english to Niclas and Davor, I also really enjoyed our works together. Le CEMRACS a été l'occasion, certaines années, de travailler avec de jeunes collègues. Cette expérience est toujours un plaisir, merci à Amina, Frédérique, Anne, Driss, Dario, Manuel, Ethem, Tan-Trung.

Ma recherche n'est pas figée à la fin de l'écriture de ce manuscrit, un grand merci donc à Frédéric, Hélène, Virginie, Annamaria, Etienne, que je n'ai pas encore cités, pour nos stimulantes discussions en cours, j'espère que nous publierons bientôt ensemble de jolis résultats.

C'est un vrai bonheur de travailler au MAP5, ce laboratoire à taille humaine fait de collègues formidables. Mes premiers remerciements vont à mes co-bureaux de toujours, Flora et Mohamed, je ne monte pas les sept étages à pied que pour la vue, mais plus encore pour votre compagnie, calme et pleine de gentillesse. Flora et Julie, vous êtes devenues des amies précieuses, merci ! Flora, c'est vraiment un grand plaisir de pouvoir partager notre quotidien et nos doutes, nos discussions et tes conseils attentifs et bienveillants sont irremplaçables. J'aime le fait que nous avancions ensemble et partagions les différents aspects du métier et de la carrière d'enseignante chercheuse. Merci aussi pour le partage de la cellule Formation du FEM en 2017 et 2018, et merci à Laurent de nous avoir embarquées en binôme dans ce travail. Merci Julie pour tes passages dans notre bureau, quelle joie de partager thé, chocolats, anecdotes, soucis et conseils avec toi. Sébastien et Anne, vous êtes des phares pour moi, toujours là pour me guider si je cherche mon chemin professionnel, je vous en suis vraiment très reconnaissante.

Je tiens à remercier les directrices successives du laboratoire, pour leur gentillesse et leur dévouement, vous avez toujours aplani toutes les difficultés pour nous : merci Annie, Fabienne et Anne. Merci également à Antoine qui a repris le flambeau avec le même état d'esprit. Pendant le mandat que j'ai fait au CNU, j'ai eu la chance de travailler avec Fabienne, merci également. Bien sûr, le laboratoire ne serait rien sans son secrétariat. Tous mes remerciements à Marie-Hélène pour son grand dévouement et son efficacité hors norme pendant toutes ces années, et à Gladys et Martine qui ont repris cette lourde tâche avec le sourire. Un merci aussi à Camille, qui m'a accompagnée dans les méandres de l'administration jusqu'à la soutenance !

Avant mon arrivée, notre petite équipe, qui n'était pas encore baptisée "MAS" (Modélisation, Analyse & Simulations), ne comptait que deux personnes. J'ai beaucoup apprécié la voir grandir, et je suis très reconnaissante à tous les collègues de l'équipe pour notre fonctionnement égalitaire et apaisé, et bien sûr nos discussions scientifiques, ainsi qu'aux doctorantes et doctorants successifs pour leur présence stimulante et leur joie de vivre. Un grand merci actuellement à Annie, Sébastien, Fabien, Angèle, Camille, Marcela, Clémence, Lucie, Ivan, Mélain.

Sans lister toutes et tous les collègues du laboratoire, j'envoie un grand merci collectif, en particulier pour la sympathique compagnie lors des repas dans la cuisine ou sur la terrasse, ou encore lors du café ou des journées du labo, avec une petite mention spéciale à Julie, Manon, Céline, Marie, Anne, Fabienne, Fabien, Amandine, qui ont toujours un sourire et un petit mot à partager quand elles[1] passent devant notre bureau. Merci également à Rémy, qui combine une gentillesse incroyable avec la possibilité de résoudre tout un tas de problèmes pratiques.

Encore un autre merci pour Gloria et Julie, avec qui j'ai partagé avec bonheur des logements (et de nombreuses tasses de thé) lors de congrès, ainsi qu'à Milana, dont la complicité en conférences à l'étranger m'est également précieuse.

J'ai le plaisir d'enseigner dans une équipe formidable, merci les matheuses et matheux du département Informatique de l'IUT ! Merci à Anne et Sébastien, encore, ainsi qu'à Nathalie

---

[1] féminin neutre ou accord de proximité ?

et Guillaume, actuellement, et Michel, Mélanie, Dominique, Evelyne pendant mes premières années. Le fonctionnement incroyablement bienveillant, motivant et solidaire de cette équipe est tout à fait enthousiasmant, je mesure ma chance de pouvoir concevoir et enseigner nos différents cours en collaboration avec vous. Un merci également à Philippe et à tous nos vacataires, sans qui l'équipe serait bien peu de choses face aux heures à assurer... Un grand merci aux chef·fe·s de département, Daniel, Anne, Hélène, Hassine, Jérôme, qui ont guidé le département à travers les différentes réformes et ont surmonté les diverses complications sans en faire peser le poids sur l'équipe enseignante. Et bien sûr, le département ne tournerait pas sans son secrétariat passé et actuel, un immense merci en particulier en ce moment à Véronique et Hassiba, qui sont d'une efficacité redoutable.

Il est temps de passer aux amis non-mathématiciens, qui équilibrent mes soirées, mes week-ends et mes vacances. Impossible de ne pas commencer par Ini et Tom, votre amitié est tellement présente et importante dans notre vie à tous les trois que je ne sais par où commencer une énumération qui n'en finirait pas. Also vielleicht einfach nur danke, für alles! Nos petits et grands moments ensemble, vos petits et grands cadeaux, vos petites et grandes attentions, vos petits et grands mots gentils, tout est toujours bien, vous êtes incroyables. Merci à Emilie, Pierre-Yves, Charlotte, Sébastien, Véro, Jérémie, Agnès et Jürgen (qui, certes, ne rentrent pas dans la catégorie des non-mathématiciens), c'est toujours un chouette moment avec vous. Juan, Magda, Sébastien, Olga, Martin, Monika, Marc, Nathalie, on ne se voit pas très souvent, mais quelle joie de se retrouver, et d'observer la complicité revenir si facilement, je vous en suis très reconnaissante. Julie[2] et Béa, la magie de nos vacances communes opère à chaque fois, j'ai déjà hâte pour notre prochain voyage. Un grand merci à Angélique pour ton rire communicatif, et à Stéphanie pour nos discussions sur la plage. Merci également à Anna et Christian, pour votre hospitalité hors du commun, on revient toujours sur un petit nuage ! Хотелось бы продолжать по-русски: Сева, Настя, Серёга, Наташа, Вова, Наташа, с вами всегда весело провести время, надеюсь на скорую встречу! А ещё огромное спасибо Мишиной семье, Нина Всеволодовна, Александр Михайлович, Серёга, Аня, за вашу поддержку. Nous avons eu la chance de rencontrer récemment Yves et Florence, c'est toujours très sympa de vous voir, quel que soit le format, merci. Plus récemment encore, nous profitons de la joie de partager de bons moments avec Eda et Burak, notre connivence me fait vraiment chaud au cœur. C'est également à vous que je dois mon pot de soutenance, teşekkürler! Je n'ai pas cité les enfants, mais c'est un bonheur de vous voir grandir, et devenir la nouvelle génération, merci à Sara, Lorenzo, Mathilde, Paul, Louise, Clément, Anaïs, Thomas, Maya, Catherine, Antoine, Victor, Jakob, Sarah, Hannah, Raphaël, Simon, Camille, Lucie, Clara, Sasha, Никита, Дима, Игорь, Наташа, София, Алиса, Женя, Nisan !

Je profite encore de ces lignes pour remercier sincèrement toute ma famille, qui m'entoure avec tant de bienveillance. Une mention spéciale pour mes parents, Joëlle et Christian, dont le soutien est sans faille et la gentillesse inépuisable. Pour finir, je remercie infiniment Миша et Lara, pour tout le bonheur avec vous ! Миша, c'est doux de grandir (ou vieillir ?) avec toi. Mes problèmes scientifiques ont tendance à disparaître si je t'en parle, merci pour cela aussi ! Lara, tu nous éblouis depuis 2013, si le monde de demain est à ton image, ce sera merveilleux. Vos sourires et vos rires à tous les deux, votre amour et vos encouragements me sont tellement précieux, merci pour tout.

---

[2] matheuse aussi, c'est vrai...

Table of contents

CHAPTER 1

Introduction

Avertissement. *Ce document décrit les recherches que j'ai menées après ma thèse, depuis mon arrivée en poste au MAP5 à l'Université Paris Descartes (actuellement Paris Cité). Pour des raisons de cohérence, je ne mentionne pas dans ce manuscrit :*

- ▹ *les travaux liés à mon stage de master [G-33, G-32] et à ma thèse de doctorat [G-31, G-29, G-26, G-17] sur les écoulements complexes en films minces, ainsi qu'un travail sur un modèle de lubrification bi-fluide [G-25] avec mon co-directeur de thèse Laurent Chupin ;*
- ▹ *deux contributions sur la migration cellulaire et l'adhésion des leucocytes [G-19, G-15].*

Les références [G - $\star$] *renvoient à mes travaux avec co-auteurs, listés en page 82, et les références* [$\star$] *à la bibliographie globale (*cf. *p. 92).*

Au cours de mes recherches, je me suis intéressée à différents aspects de la modélisation et de l'analyse mathématique des écoulements de fluides, en particulier des mélanges gazeux ou des fluides diphasiques, dans des régimes d'écoulements spécifiques (limite hydrodynamique d'équations cinétiques ou équations fluides en régime à bas nombre de Mach). J'ai également travaillé sur des applications en sciences du vivant autour de la description de la respiration, ainsi que la prise en compte d'aérosols dans les voies aériennes. En effet, certains modèles mathématiques étudiés dans mes travaux sont particulièrement adaptés à la description de l'aspect multi-espèces de l'air, ou de particules d'aérosols, dans le système respiratoire.

Modèles cinétiques et fluides pour les mélanges gazeux

J'ai, d'une part, étudié des modèles mésoscopiques (cinétiques) pour décrire les gaz multi-espèces, *via* les équations de Boltzmann pour les mélanges, et d'autre part, j'ai analysé des modèles macroscopiques de diffusion pour les mélanges gazeux, en particulier les équations de Maxwell-Stefan et de Fick. Ces deux types de modèles sont liés par une limite hydrodynamique en régime diffusif, qui permet de passer des équations cinétiques aux équations macroscopiques. Ces travaux sont décrits dans le Chapitre 2.

Plus précisément, en théorie cinétique des gaz, on décrit un fluide, ou plus généralement un système constitué d'un grand nombre de particules, par une fonction de distribution f définie sur l'espace des phases, contenant les variables macroscopiques classiques telles que le temps $t \in \mathbb{R}^+$ et l'espace $x \in \mathbb{R}^d$, $d \geq 1$, ainsi que des variables microscopiques supplémentaires, décrivant l'état des particules, typiquement la vitesse $v \in \mathbb{R}^d$. Dans le cas d'un mélange à N espèces, la fonction de distribution est un vecteur de toutes les fonctions de distribution de chaque composant $\boldsymbol{f} = (f_1, \cdots, f_N)^\mathsf{T}$, et son évolution peut être décrite par les équations de Boltzmann pour les mélanges, pour tout $1 \leq i \leq N$

$$\partial_t \boldsymbol{f} + v \cdot \nabla \boldsymbol{f} = \boldsymbol{Q}(\boldsymbol{f}, \boldsymbol{f}). \tag{1.1}$$

Le terme quadratique de collision $\boldsymbol{Q}(\boldsymbol{f}, \boldsymbol{f})$, dont la composante $i \in \{1, \dots, N\}$ est donnée par $\sum_{j=1}^N Q_{ij}(f_i, f_j)$, décrit les interactions intra- et inter-espèces entre les particules par des collisions binaires, et agit uniquement en vitesse de manière non locale.

On peut également adopter un deuxième point de vue en considérant des équations fluides macroscopiques, en définissant les quantités macroscopiques observables de chaque espèce i du mélange, telles que sa densité numérique n_i, sa vitesse macroscopique u_i, et éventuellement sa température T_i, définies par les moments en vitesse de la fonction de distribution f_i contre 1, v et $|v|^2$.

En multipliant (1.1) par la masse molaire m_i de l'espèce i (resp. $m_i v$ et $m_i|v|^2$), et en intégrant en vitesse, on obtient l'équation de conservation de la masse pour l'espèce i (resp. les équations de conservation de la quantité de mouvement et de l'énergie). Ces équations fluides ne sont en général pas fermées, car les flux macroscopiques et les termes intégraux de collision ne peuvent en général pas s'exprimer en fonction de ces moments. Nous renvoyons aux ouvrages de référence sur ces questions, par exemple [101, 54, 52, 51, 200].

Une première approche pour fermer le système consiste à considérer une forme particulière pour la fonction de distribution, typiquement un ansatz maxwellien. Une autre possibilité est de considérer une limite hydrodynamique, où l'on suppose que les collisions sont très fréquentes. Dans mes travaux, on considère également que les effets de diffusion sont prépondérants, et l'on s'intéresse donc à la limite diffusive des équations de Boltzmann multi-espèces. Dans ce cas, on introduit le paramètre $\varepsilon \ll 1$, lié aux nombres de Knudsen et de Mach, et on s'intéresse à la limite $\varepsilon \to 0$. En appliquant une méthode de moments avec un ansatz maxwellien dont les vitesses macroscopiques u_i sont de l'ordre de ε, nous avons obtenu formellement les équations de Maxwell-Stefan sur les quantités macroscopiques [G-18, G-16]. Ces équations appartiennent à la famille des modèles de diffusion croisée. L'équation de conservation de la quantité de mouvement donne en effet une relation entre les flux et les gradients de densité de la forme

$$\nabla n_i = \sum_{j=1}^{N} \frac{n_i n_j \left(u_j - u_i\right)}{D_{ij}}, \qquad 1 \leq i \leq N,$$

où les D_{ij} sont des coefficients de diffusion binaire entre les espèces. Nous avons également considéré plus de moments de la fonction de distribution, ce qui fait intervenir le tenseur de pression, et nous a permis d'obtenir un modèle de Maxwell-Stefan d'ordre supérieur [G-8, G-3].

Par ailleurs, en utilisant un développement de Hilbert ou de Chapman-Enskog, et en considérant l'ordre principal dans les équations de Boltzmann multi-espèces, nous avons obtenu formellement le modèle de Fick [G-6], qui est lui aussi un modèle de diffusion croisée, de la forme

$$u_i = \sum_{j=1}^{N} \varphi_{ij}(n_1, \cdots n_N) \nabla n_j, \qquad 1 \leq i \leq N,$$

où les φ_{ij} dépendent des densités de toutes les espèces et sont liés aux coefficients de diffusion du modèle de Fick.

Limite hydrodynamique des équations de Boltzmann multi-espèces

Pour l'étude de la limite hydrodynamique rigoureuse des équations de Boltzmann pour les mélanges gazeux, on est amené à considérer un développement de la fonction de distribution, soit autour d'une maxwellienne locale, soit autour d'une maxwellienne globale. Dans les deux cas, cela permet de définir un opérateur de Boltzmann linéarisé, qui diffère selon la maxwellienne considérée. Une première étape a été de comprendre les propriétés mathématiques de tels opérateurs linéarisés (caractère auto-adjoint, compacité, trou spectral) [G-22, G-10]. En comparaison avec les travaux antérieurs sur les limites hydrodynamiques de l'équation de

Boltzmann mono-espèce, des difficultés supplémentaires apparaissent en raison de la présence de plusieurs espèces. En particulier, le couplage des espèces nécessite une autre représentation géométrique des collisions binaires, ce qui revient à obtenir une autre représentation de Carleman de l'opérateur de collision de Boltzmann. Dans le cas de la limite vers les équations de Fick, nous avons également été amenés à étudier les propriétés de l'inverse de l'opérateur linéarisé, qui sont liées à celle de l'opérateur direct [G-6].

Après avoir montré une théorie de Cauchy pour les équations de diffusion croisée de la forme Maxwell-Stefan ou Fick dans un cadre perturbatif, on peut ensuite conclure sur la convergence en régime perturbatif des équations de Boltzmann multi-espèces vers le modèle de diffusion croisée correspondant, dépendant du développement asymptotique choisi.

Du point de vue numérique, nous avons reproduit l'approche par moments pour construire un schéma numérique dont le comportement préserve l'asymptotique [G-12], c'est-à-dire que le schéma capture, pour les mêmes paramètres de discrétisation, à la fois des solutions de l'équation cinétique (sous ansatz maxwellien) et des solutions de l'équation de diffusion croisée.

Pour étudier plus en détail le comportement de $\boldsymbol{f}$ autour d'une maxwellienne globale, nous avons également étudié une décomposition micro-macro de la perturbation de la fonction de distribution [G-5]. Nous avons en particulier pu obtenir des estimations d'énergie, qui permettent par exemple de montrer la stabilité de la maxwellienne en temps long.

Par ailleurs, nous nous sommes également intéressés à l'étude d'un modèle fluide avec un terme de relaxation raide de type Maxwell-Stefan [G-13]. Nous montrons qu'à la limite, on obtient un système limite dont le terme correctif de diffusion est de type Fick, pour lequel les vitesses de chaque espèce sont alignées sur une vitesse commune.

Modèles diphasiques à bas nombre de Mach

Dans le cadre d'une collaboration impliquant le CEA, j'ai commencé à travailler sur des modèles thermohydrauliques, décrivant en particulier l'écoulement du liquide de refroidissement dans le circuit primaire des réacteurs nucléaires. On s'intéresse plus spécifiquement aux réacteurs à eau pressurisée, pour lesquels plusieurs éléments sont à prendre en compte : la forte pressurisation du circuit, permettant à l'eau d'être liquide malgré les hautes températures, le fort apport de chaleur par la réaction nucléaire dans le coeur du réacteur, la possibilité d'apparition de petites bulles de vapeur dans le liquide selon les conditions thermodynamiques, et la nécessité de refroidir le circuit via un débit imposé par des pompes pour éviter une surchauffe du cœur. Un élément crucial est qu'en régime nominal ou incidentel, le nombre de Mach associé à l'écoulement du fluide est petit. Dans ce régime, on peut donc filtrer les effets acoustiques, et obtenir un modèle simplifié par rapport aux équations de Navier-Stokes compressibles, mais qui prenne en compte la forte compressibilité due à l'apport de chaleur et la thermodynamique du fluide [155, 77, 78, 62]. Dans ce type de modèles, on a en particulier un découplage entre deux pressions : la pression thermodynamique p_*, qui est constante et intervient dans l'équation d'état, et la pression dynamique $\bar{p}$ dans l'équation sur la quantité de mouvement. Sous forme non conservative, le modèle peut s'écrire sur la vitesse $\boldsymbol{u}$ de l'écoulement, son enthalpie h et $\bar{p}$ de la manière suivante

$$\begin{cases} \operatorname{div} \boldsymbol{u} = \Phi \dfrac{\partial \tau}{\partial h}(h, p_*), \\ \partial_t \boldsymbol{u} + (\boldsymbol{u} \cdot \nabla)\boldsymbol{u} + \tau(h, p_*)\nabla \bar{p} = \tau(h, p_*) \operatorname{div} \sigma(\boldsymbol{u}) + \boldsymbol{g}, \\ \partial_t h + \boldsymbol{u} \cdot \nabla h = \tau(h, p_*)\Phi, \end{cases} \tag{1.2}$$

où Φ décrit la densité de puissance transmise par la réaction nucléaire, $\boldsymbol{g}$ désigne la gravité, et $\sigma(\boldsymbol{u})$ est le tenseur des contraintes visqueuses. L'équation d'état permettant de fermer le système consiste à se donner le volume spécifique $\tau(h, p_*)$ en fonction de l'enthalpie (puisque la pression thermodynamique p_* est constante).

Pour ce modèle, j'ai abordé différents aspects, décrits dans le Chapitre 3. D'une part, nous avons étudié différentes lois d'état, à la fois analytiques (très simples, comme la loi des gaz raidis (*stiffened gas*), ou plus complexes, comme les lois cubiques [G-7]) et tabulées à partir de données expérimentales [G-14]. Dans tous les cas, nous nous sommes attachés à décrire avec précision le changement de phase liquide-vapeur par le biais de l'introduction d'une zone de mélange à saturation. Cette précision est cruciale pour prédire correctement l'évolution de la température dans le fluide, afin de garantir le refroidissement du réacteur. D'autre part, pour ce modèle en régime à bas nombre de Mach, nous pouvons obtenir des solutions asymptotiques, et même des solutions exactes (avec changement de phase) en 1D [G-20]. En introduisant des schémas numériques adaptés, nous présentons des résultats numériques pour des cas tests en 1D et 2D, qui montrent en particulier l'importance de la précision de la loi d'état pour la prédiction de l'apparition de vapeur.

Enfin, nous nous sommes intéressés à un modèle plus complexe autorisant un transfert de masse non instantané entre les phases (déséquilibre du potentiel de Gibbs des deux phases) [G-9], ce qui rajoute au modèle (1.2) une équation de transport sur la fraction massique de vapeur, munie d'un terme source de relaxation vers la valeur à saturation. Dans ce cas, nous avons pu en particulier étudier la relaxation de ce modèle vers le modèle précédent, à la fois formellement et numériquement *via* un schéma préservant l'asymptotique.

Applications à la description du système respiratoire

Je me suis également intéressée à la description de la respiration, pour laquelle différents aspects doivent être pris en compte :

- ▷ d'une part, la géométrie des voies aériennes est un élément crucial, et nécessite la description de l'écoulement de l'air à des échelles très différentes [160] ;
- ▷ d'autre part, les phénomènes à décrire diffèrent le long de la géométrie de l'arbre bronchique (effets convectifs dans les voies respiratoires supérieures, effets diffusifs dans les voies respiratoires inférieures, échanges gazeux dans les alvéoles pulmonaires) [8, 162];
- ▷ enfin, il est intéressant de s'interroger sur les possibles effets de couplage dus à la présence dans l'air de plusieurs gaz, en confrontant les modèles de diffusion croisée mentionnés dans le Chapitre 2.

Mes travaux sur ce sujet sont décrits dans le Chapitre 4. Nous avons en particulier travaillé sur un modèle 0D décrivant les échanges gazeux entre l'air et le sang au niveau des alvéoles pulmonaires, prenant en compte les effets non linéaires dus à la présence conjointe de l'oxygène et du dioxyde de carbone [G-4]. Nous cherchons actuellement à intégrer ce modèle 0D à un modèle 1D du système respiratoire complet considérant les différentes espèces de l'air ou du gaz inhalé, pour lequel nous pourrons discuter la pertinence du modèle de diffusion choisi (en particulier la nécessité, pour certains gaz, de prendre en compte un modèle de diffusion croisée), ainsi que reproduire différents comportements correspondant à des cas pathologiques.

Par ailleurs, les modèles d'écoulement de l'air, qu'ils soient 1D, 2D ou 3D, peuvent être couplés à une équation décrivant la propagation d'aérosols (particules en suspension dans l'air ou aérosols médicamenteux). En considérant que les particules sont une phase dispersée dans l'air, on considère en général qu'elles peuvent être décrites par une fonction de distribution f, dépendant non seulement des variables (t, x, v), mais également possiblement d'autres variables, comme le rayon r ou la température T des particules. Dans tous les cas, f est solution d'une équation de type Vlasov [198, 10]

$$\partial_t f + \nabla_x \cdot (vf) + \nabla_v \cdot (a_v f) + \partial_r (a_r f) + \partial_T (a_T f) = 0,$$

où les termes a_v (resp. a_r et a_T) décrivent l'accélération des particules (resp. leur croissance en taille ou température). Dans ce cas, on peut étudier l'influence des particules sur l'écoulement de l'air, ainsi que les effets hygroscopiques qui induisent des variations de taille et de température des particules. Il est particulièrement intéressant d'analyser comment ces effets influent sur la quantité de dépôt des aérosols, ainsi que sur la localisation de ces dépôts. Dans le cadre d'un projet CEMRACS [G-11], nous avons développé un modèle adapté et obtenu de premières simulations numériques en 2D.

CHAPTER 2

Mesoscopic and macroscopic description of gaseous mixtures

Content of this chapter

This chapter is based on the works [G-24, G-22, G-18, G-16, G-12, G-13, G-10, G-5, G-6, G-8, G-1, G-3], in collaboration with N. Bernhoff, A. Bondesan, L. Boudin, M. Briant, M. (Pavić-)Čolić, V. Pavan, F. Salvarani and S. Simić.

This chapter is dedicated to the study of kinetic and macroscopic models for gaseous mixtures. We first present the Boltzmann equation for mixtures, and macroscopic cross-diffusion models for multi-species flows (Maxwell-Stefan and Fick equations). These two levels of description are linked by the hydrodynamic limit of the kinetic model in the diffusive regime. Formal computations show that both diffusion models can be obtained, either by a moment method or by a perturbative one.

To study the convergence of the solutions of the kinetic model towards the solutions of the macroscopic models, we consider a Hilbert expansion of the distribution function around a local or a global Maxwellian, and we are led to study both corresponding linearized Boltzmann operators for mixtures. In particular, we can prove that these operators are compact, and although they do not provide a negative control on the full distribution function, they possess a spectral gap, which is a crucial property for the analysis, but cannot be proved straightforwardly by extending the mono-species case. In the case of the Fick equations, a Cauchy theory is established, and the convergence in a perturbative setting is proved.

From a numerical point of view, we construct a numerical scheme based on the moment method describing the solutions of both the kinetic (under a Maxwellian ansatz) and the macroscopic Maxwell-Stefan models, which exhibits an asymptotic-preserving behavior.

We also use in the multi-species case a micro-macro decomposition of the perturbation of the distribution function to further study the behavior of the solution around its equilibrium, and we investigate the link between the two macroscopic diffusion models by considering a fluid model with a stiff relaxation term of Maxwell-Stefan type, whose limit system has a Fick-type diffusion correction term.

2.1 Introduction and description of the models

In this chapter, we focus on the kinetic and macroscopic theory of gases, for a mixture of N monatomic species. Such systems of particles can be modelled in several ways, depending on the chosen scale of observation.

2.1.1 Mesoscopic description of mixtures

At the mesoscopic scale, kinetic theory describes a large number of molecules through a distribution function f defined on the phase space, containing the usual macroscopic variables such as time $t \in \mathbb{R}^+$ and space $x \in \mathbb{R}^d$, $d \geq 1$, as well as additional microscopic variables, describing the state of the molecules, typically the velocity $v \in \mathbb{R}^d$. The quantity $f(t,x,v)\,\mathrm{d}x\,\mathrm{d}v$ represents the particle density at time t in an elementary volume centered at (x,v). In the following, for the sake of simplicity, we will write everything down with $d = 3$, except when we restrict ourselves to $d = 1$ (Sections 2.5.2 and 2.6).

In the case of a mixture, the distribution function is a vector of all distribution functions of each components $\boldsymbol{f} = (f_1, \cdots, f_N)^\mathsf{T}$, and its behavior can be described by the following Boltzmann equations for mixtures [64], for any $1 \leq i \leq N$,

$$\partial_t f_i(t,x,v) + v \cdot \nabla f_i(t,x,v) = \sum_{j=1}^{N} Q_{ij}(f_i, f_j). \tag{2.1}$$

In this equation, the interaction between the species is governed by the collision operator Q_{ij}, which is local in time and space but nonlinear and nonlocal in velocity. To describe the microscopic interaction, we only consider binary collisions between a molecule of species i, of molar mass m_i and velocity v', and a molecule of species j, of molar mass m_j and velocity v'_*. The collisions are supposed to be elastic, which means that momentum and energy are conserved during the collision process, and the post-collisional velocities v and v_* of the two particles satisfy

$$m_i v + m_j v_* = m_i v' + m_j v'_*, \tag{2.2a}$$

$$\frac{1}{2} m_i |v|^2 + \frac{1}{2} m_j |v_*|^2 = \frac{1}{2} m_i |v'|^2 + \frac{1}{2} m_j |v'_*|^2. \tag{2.2b}$$

These relations allow to relate the pre- and post-collisional velocities, introducing some parametrization. One possibility is the σ-notation, where the relative velocity $v' - v'_*$ is written as $v' - v'_* = |v - v_*|\sigma$, for $\sigma \in \mathbb{S}^2$, leading to

$$v' = \frac{1}{m_i + m_j} \left(m_i v + m_j v_* + m_j |v - v_*|\sigma \right), \tag{2.3a}$$

$$v'_* = \frac{1}{m_i + m_j} \left(m_i v + m_j v_* - m_i |v - v_*|\sigma \right). \tag{2.3b}$$

This allows to describe the collision operator

$$Q_{ij}(f,g)(v) = \int_{\mathbb{R}^3 \times \mathbb{S}^2} \mathcal{B}_{ij}(v, v_*, \sigma) \left(f' g'_* - f g_* \right) \mathrm{d}\sigma \, \mathrm{d}v_*,$$

with the usual shortcuts $f_* = f(v_*)$, $f' = f(v')$, $f'_* = f(v'_*)$. The cross sections $\mathcal{B}_{ij}$ encode the nature of the microscopic interactions between the species i and j. Due to Galilean invariance, the $\mathcal{B}_{ij}$ are functions of the relative velocity $|v - v_*|$ and a deviation angle only, and are written as follows

$$\mathcal{B}_{ij}(v, v_*, \sigma) = B_{ij}(|v - v_*|, \cos\theta),$$

where the deviation angle $\theta \in [0, \pi]$ is defined by $\cos\theta = (v - v_*) \cdot \sigma / |v - v_*|$. The cross sections are assumed to satisfy, for any $1 \le i, j \le N$, the following properties:

- ▷ a microreversibility property

  $$B_{ij}(|v - v_*|, \cos\theta) = B_{ji}(|v_* - v|, \cos\theta);$$

- ▷ a decomposition into the product of a kinetic part Φ_{ij} and an angular part b_{ij}

  $$B_{ij}(|v - v_*|, \cos\theta) = \Phi_{ij}(|v - v_*|)\, b_{ij}(\cos\theta);$$

- ▷ the kinetic part corresponds to hard-sphere potentials or Maxwell molecules ($\gamma_{ij} = 0$)

  $$\Phi_{ij}(|v - v_*|) = C^{\Phi}_{ij} |v - v_*|^{\gamma_{ij}}, \qquad \text{with } \gamma_{ij} \in [0, 1];$$

- ▷ the angular part is an even function $b_{ij} \in L^1(-1, 1)$ and satisfies a strong form of Grad's cut-off assumption [101], *i.e.* there exist $C_{b1}, C_{b2} > 0$ such that

  $$0 < b_{ij}(\cos\theta) \le C_{b1} |\sin\theta| |\cos\theta| \quad \text{and} \quad b'_{ij}(\cos\theta) \le C_{b2}.$$

  Moreover, we assume that

  $$\min_i \inf_{\sigma_1, \sigma_2} \int \min\left\{ b_{ii}(\sigma_1 \cdot \sigma_3), b_{ii}(\sigma_2 \cdot \sigma_3) \right\} \mathrm{d}\sigma_3 > 0.$$

Remark 2.1. *With these assumptions on the cross sections, it is possible to prove the different results we will mention in the following. Note that more general cross sections can be considered for the Boltzmann equation (see* e.g. *[200]), but we did not tackle the issue of extending our results with fewer assumptions on B_{ij}. Grad's cutoff assumption is interesting mathematically as a first step towards more singular kernels, allowing in particular to decompose the collision operator into a negative part and a positive regularizing one [145, 205, 36, 171].*

Let us state two possible weak forms of this collision operator. For any test function ψ so that the following integrals are well defined, we have

$$\int_{\mathbb{R}^3} Q_{ij}(f,g)(v)\psi(v)\,\mathrm{d}v = \int_{\mathbb{R}^6\times\mathbb{S}^2} B_{ij}(|v-v_*|,\cos\theta) f(v) g(v_*)\left(\psi(v)-\psi(v')\right)\mathrm{d}\sigma\,\mathrm{d}v_*\,\mathrm{d}v, \tag{2.4}$$

and

$$\int_{\mathbb{R}^3} Q_{ij}(f,g)\psi\,\mathrm{d}v = -\frac{1}{2}\int_{\mathbb{R}^6\times\mathbb{S}^2} B_{ij}\left(f'g'_* - fg_*\right)\left(\psi'+\psi'_*-\psi-\psi_*\right)\mathrm{d}\sigma\,\mathrm{d}v_*\,\mathrm{d}v.$$

From the weak form, one can in particular obtain the following well-known conservation properties [192, 167, 64]

$$\int_{\mathbb{R}^3} Q_{ij}(f,g)(v)\,\mathrm{d}v = 0,$$
$$m_i\int_{\mathbb{R}^3} v\,Q_{ij}(f,g)(v)\,\mathrm{d}v + m_j\int_{\mathbb{R}^3} v\,Q_{ji}(g,f)(v)\,\mathrm{d}v = 0,$$
$$\frac{1}{2}m_i\int_{\mathbb{R}^3} |v|^2 Q_{ij}(f,g)(v)\,\mathrm{d}v + \frac{1}{2}m_j\int_{\mathbb{R}^3} |v|^2 Q_{ji}(g,f)(v)\,\mathrm{d}v = 0.$$

It is sometimes convenient to handle the Boltzmann equation (2.1) under the following vectorial form

$$\partial_t \boldsymbol{f} + v\cdot\nabla\boldsymbol{f} = \boldsymbol{Q}(\boldsymbol{f},\boldsymbol{f}), \tag{2.5}$$

where the i-th component of $\boldsymbol{Q}(\boldsymbol{f},\boldsymbol{f})$ is given by $\sum_{j=1}^N Q_{ij}(f_i,f_j)$.

Let us now describe the collision invariants. The relation

$$\sum_{i,j=1}^N \int_{\mathbb{R}^3} Q_{ij}(f,g)(v)\psi_i(v)\,\mathrm{d}v = 0$$

holds if and only if $\boldsymbol{\psi} = (\psi_1,\cdots,\psi_N)^\mathsf{T} \in \mathbb{E}$, with

$$\mathbb{E} = \mathrm{Span}\{\boldsymbol{e}_1,\cdots,\boldsymbol{e}_N, v_1\boldsymbol{m}, v_2\boldsymbol{m}, v_3\boldsymbol{m}, |v|^2\boldsymbol{m}\}, \tag{2.6}$$

where $\boldsymbol{e}_i$ is the i-th vector of the canonical basis of $\mathbb{R}^N$ and $\boldsymbol{m} = (m_1,\cdots,m_N)^\mathsf{T}$.

The H-theorem for the mixture Boltzmann operator [64] states that the distributions $\boldsymbol{f}$ satisfying, for all $1\le i,j\le N$,

$$Q_{ij}(f_i,f_j)(v) = 0, \qquad \forall v\in\mathbb{R}^3, \tag{2.7}$$

are the local Maxwellian distributions with the same bulk velocity and temperature, *i.e.* of the form

$$f_i(t,x,v) = n_i(t,x)\left(\frac{m_i}{2\pi k_B T(t,x)}\right)^{3/2}\exp\left(-\frac{m_i|v-u(t,x)|^2}{2k_B T(t,x)}\right), \qquad 1\le i\le N.$$

The quantities $(n_i)_{1\leq i\leq N}$, u and T are the macroscopic quantities of the mixture, and k_B is the Boltzmann constant. We can also derive the global equilibrium states, *i.e.* cancelling the collision and transport operators, which are the global Maxwellian distributions $\boldsymbol{\mu} = (\mu_1, \cdots, \mu_N)^\mathsf{T}$, with

$$\mu_i(v) = \bar{n}_i \left(\frac{m_i}{2\pi k_B \bar{T}}\right)^{3/2} \exp\left(-\frac{m_i|v-\bar{u}|^2}{2k_B\bar{T}}\right), \qquad 1 \leq i \leq N,$$

with constant physical observables $(\bar{n}_i)_{1\leq i\leq N}$, $\bar{u}$ and $\bar{T}$. In particular, local Maxwellians (*i.e.* with any macroscopic states n_i, u_i and T_i) are not in general equilibrium states of the mixture Boltzmann operator, nor solutions of (2.7), in contrary to the mono-species case.

Finally, let us relate the macroscopic quantities for species i (number density n_i, macroscopic velocity u_i and energy) with the moments of the distribution function f_i as follows

$$n_i = \int_{\mathbb{R}^3} f_i \,\mathrm{d}v, \tag{2.8a}$$

$$n_i u_i = \int_{\mathbb{R}^3} v f_i \,\mathrm{d}v, \tag{2.8b}$$

$$n_i|u_i|^2 + n_i e_i = \int_{\mathbb{R}^3} |v|^2 f_i \,\mathrm{d}v, \tag{2.8c}$$

where e_i is the partial internal energy. In the special case of a (monatomic) ideal gas, it is related to the temperature T_i of the species by $e_i = \frac{3}{2}\frac{k_B T_i}{m_i}$. Macroscopic equations are written on these quantities.

Remark 2.2. *We do not discuss in this manuscrit other collision operators, in particular the well-known family of BGK and ES-BGK models, which have the same properties of conservation of moments and dissipation of entropy as the Boltzmann operator [25, 4]. The main idea consists in replacing the bilinear collision operator* $\boldsymbol{Q}$ *by a relaxation operator towards a local Maxwellian equilibrium. Extensions of the BGK model were introduced to capture correctly the hydrodynamic limit in particular in the case of mixtures [109, 44, 28, 33]. A large computational advantage of these models is that the operators are very easy to compute numerically, compared to the full Boltzmann operator.*

2.1.2 Macroscopic diffusion models for mixtures

As we mentioned, at the macroscopic scale, a mixture of fluid is described by macroscopic quantities, typically the number density n_i of species i, its macroscopic velocity u_i, and possibly its temperature T_i. We only focus in this section on the macroscopic description of mass transport by diffusion in gaseous mixtures (meaning that convection is neglected). Many diffusion models have been proposed and discussed in the literature since the 19th century [104, 85, 163, 194], and we are interested in two of them, the Maxwell-Stefan and the Fick models. It is confortable to formulate diffusion in terms of fluxes, defined for species i as $J_i = n_i u_i$ (diffusion flux per unit mass). We can also define global quantities for the mixture: we will denote by $n_{\text{tot}} = \sum_i n_i$ the total number density and by $J_{\text{tot}} = \sum_i J_i$ the total flux.

Moreover, because the diffusion models we will consider lie in the class of cross-diffusion models, involving interactions between all species, it will be convenient to write the models vectorially, in order to handle all species simultaneously. We will denote $\boldsymbol{n} = (n_1, \cdots, n_N)^\mathsf{T}$, $\boldsymbol{u} = (u_1, \cdots, u_N)^\mathsf{T}$, $\boldsymbol{J} = (J_1, \cdots, J_N)^\mathsf{T}$.

As we shall see, both the Maxwell-Stefan and the Fick models are based upon the mass conservation of species, but differ in the way diffusion mechanism is described, and the way the system is closed. Let us describe briefly these two models.

Maxwell-Stefan equations

The Maxwell-Stefan model gives relations between the fluxes and the number densities, steming from momentum equations and considerations on forces [208, 173, 135, 34]. They are written under the following form, for any $1 \leq i \leq N$,

$$\partial_t n_i + \nabla \cdot J_i = 0, \tag{2.9a}$$

$$\nabla n_i = \sum_{j=1}^{N} \frac{1}{D_{ij}} \left(n_i J_j - n_j J_i \right), \tag{2.9b}$$

where $D_{ij} > 0$ is the binary diffusion coefficient between species i and j, for $i \neq j$. The Maxwell-Stefan relations (2.9b) can be rewritten under a matrix form in the following way

$$\nabla \boldsymbol{n} = \boldsymbol{A}(\boldsymbol{n}) \boldsymbol{J},$$

where the coefficients $\alpha_{ij}(\boldsymbol{n})$ of the matrix $\boldsymbol{A}(\boldsymbol{n})$ are defined by $\alpha_{ij}(\boldsymbol{n}) = \frac{n_i}{D_{ij}}$, if $i \neq j$ and $\alpha_{ii}(\boldsymbol{n}) = -\sum_{j \neq i} \frac{n_j}{D_{ij}}$.

One of the main issue of these equations is the need of a closure condition, since the Maxwell-Stefan relations are not linearly independent; indeed, $\boldsymbol{A}(\boldsymbol{n})$ is not invertible, since $\sum_j \alpha_{ij}(\boldsymbol{n}) = 0$. First, observe that the total number of molecules n_{tot} is homogeneous in space $\nabla n_{\text{tot}} = 0$. A standard assumption, used in particular to provide a good mathematical framework for the analysis of the equations, is the so-called equimolar diffusion assumption [135], stating that the total flux is zero

$$J_{\text{tot}} = \sum_{i=1}^{N} J_i = 0. \tag{2.10}$$

This assumption obviously implies from the mass conservation equation that the total number of molecules n_{tot} is constant.

However, it has been proved in [31] that, at least in a perturbative setting, is it enough to close the Maxwell-Stefan system with the assumption of a constant total number density n_{tot} and a divergence-free total flux $\nabla \cdot J_{\text{tot}} = 0$. We note that in dimensions higher than one, this relation is not enough to reconstruct the whole vector J_{tot}. This assumption is thus less restrictive than the equimolar diffusion one.

The mathematical analysis of the Maxwell-Stefan model has gained interest in the last fifteen years, and is mentioned in Section 2.2.

Fick equations

The Fick equations, on the other hand, link the fluxes to the gradients of the number densities, and are based on constitutive relations [108, 97]. They are written under the following form

$$\partial_t n_i + \nabla \cdot J_i = 0,$$

$$J_i = \sum_{j=1}^{N} \varphi_{ij}(\boldsymbol{n}) \nabla n_j.$$

The associated vectorial form of the Fick equations is

$$\boldsymbol{J} = \boldsymbol{F}(\boldsymbol{n}) \nabla \boldsymbol{n}, \tag{2.11}$$

where $\boldsymbol{F}(\boldsymbol{n}) = (\varphi_{ij}(\boldsymbol{n}))_{1\leq i,j\leq N}$ is the Fick diffusion matrix. These equations can be rewritten on the number densities only as

$$\partial_t \boldsymbol{n} + \nabla \cdot (\boldsymbol{F}(\boldsymbol{n})\nabla \boldsymbol{n}) = 0, \tag{2.12}$$

where we recognize a parabolic setting if $\boldsymbol{F}(\boldsymbol{n})$ is positive semi-definite. As the Maxwell-Stefan one, the matrix $\boldsymbol{F}$ is not invertible, and a closure condition is needed. For the form (2.12) of the equations, it is written on the total number density n_{tot}, which is supposed to be constant in time and space as for the Maxwell-Stefan model.

Discussion on both models

Of course, there is a structural analogy between these two systems, and some authors proposed numerical methods to link the physical coefficients in both formulations [96, 97, 34]. The physical derivation of both models is nevertheless different: in the Fick model, the diffusion fluxes are determined by constitutive relations of phenomenological nature. More precisely, in the thermodynamics of irreversible processes viewpoint, close to equilibrium, linear considerations are invoked to model the fluxes as linear combinations of the gradients of potentials, related to the gradients of the species densities. In the Maxwell-Stefan model, diffusion is regarded as a source of momentum exchange between the species, which is balanced by the gradients of partial pressures, and the main assumption is the fact that the different species have different macroscopic velocities on macroscopic time scales [172, 115].

As we shall see in the following, the obtention of these two models from the Boltzmann equation is also different, and is the topic of Sections 2.3 and 2.5.

2.1.3 Hydrodynamic limit

A natural question is then to obtain these diffusion equations from the kinetic description in the hydrodynamic limit in a diffusive scaling. To this end, the Boltzmann equation is written under a non-dimensional form, which enlightens two non-dimensional numbers, the Knudsen (Kn) and the Mach (Ma) numbers. The Knudsen number, related to the collision frequency, is defined as the ratio of the mean free path to the characteristic length of the system, and thus describes if the gas is rarefied or not. Its inverse appears in front of the collision term in (2.1). The Mach number on the other hand is the ratio of the characteristic velocity to the speed of sound, and appears in front of the time derivative in (2.1). The diffusive scaling consists in focusing on the fluid regime, meaning that collisions are very frequent (*i.e.* Kn is small), and on diffusion effects, meaning that convection ones are neglected (Ma is therefore also small). Choosing both numbers of order $\varepsilon \ll 1$, *i.e.* $\mathrm{Kn} = \mathrm{Ma} = \varepsilon$, we obtain the diffusive scaling of the Boltzmann equations for mixtures, for any $1 \leq i \leq N$

$$\varepsilon \partial_t f_i + v \cdot \nabla f_i = \frac{1}{\varepsilon} \sum_{j=1}^{N} Q_{ij}(f_i, f_j). \tag{2.13}$$

We then focus on the limit $\varepsilon \to 0$ of this equation. In the case of the monospecies Boltzmann equation, this procedure has been widely studied in the literature [76, 48, 6, 47, 59, 13, 14, 12, 81] by means of two different methods.

- ▷ The perturbative method is based on Hilbert or Chapman-Enskog expansions [117, 79, 54], meaning that the distribution function is written as a series of the Knudsen number ε, whose terms are determined from solving the equations obtained by identifying the powers of ε.

- ▹ The moment method consists in determining a hierarchy of equations satisfied by the moments of the distribution function [102, 101, 143], and closing this hierarchy by a relation obtained from minimizing an entropy functional. This method aims at capturing in a satisfactory way the dynamics of a flow which could be not very close to the local equilibrium.

In the current chapter, we are mainly interested in extending such results to the hydrodynamic limit in the case of mixtures, in the diffusive scaling.

2.2 Analysis of the cross-diffusion models for mixtures

Before diving into the hydrodynamic limits, let us describe some properties of the cross-diffusion models we introduced, namely the Maxwell-Stefan and the Fick ones.

2.2.1 Analysis of the Maxwell-Stefan equations

The interest in the mathematical analysis of the Maxwell-Stefan equations is fairly recent [97, 34]. In [G-24], we proved a preliminary result on the existence of a solution to the Maxwell-Stefan equations with the equimolar diffusion closure condition (2.10), in the special case of three-species diffusion with $D_{12} = D_{13}$. This very special case allows to rewrite the equations in order to have a simple uncoupled heat equation on species 1, leading to handle the coupling only in the equation for species 2 (species 3 being determined by the closure condition).

In further works, existence results have been obtained with the equimolar diffusion closure condition, mainly by passing to entropic variables [131, 58]. Moreover, let us mention the work [31], in which the closure condition is not equimolar diffusion, but only an incompressible setting. More precisely, inspired by micro-macro decomposition techniques, the velocities are split into a kernel part belonging to Ker $\boldsymbol{A}$ and an orthogonal part. As opposed to the entropy method, a hypocoercive strategy exploits the properties of $\boldsymbol{A}$ without the need of computing its explicit structure. Moreover, instead of eliminating one last species, a symmetric role is given to all the species variables.

As far as the numerical analysis of these equations is concerned, we proposed in [G-24], again with the equimolar diffusion assumption, a simple one-dimensional numerical scheme. The mass conservation equation is discretized in a very standard way on a staggered grid, and the Maxwell-Stefan equations are solved by expressing the quantities for one species (for example n_N and J_N) in terms of quantities for all other species due to the closure condition. This allows to write a modified matrix of size $N-1$, which is invertible, and the system can thus be solved by a standard Gauss elimination method. In the case of three species, we obtain a 2×2 system, which is solved explicitly. In the special case when $D_{12} = D_{13}$, the L^∞-stability of the scheme is proved under a CFL condition depending on the diffusion coefficients.

Numerical simulations allow in particular to reproduce the well-known Duncan and Toor experiment [74]. In this experiment, a ternary mixture is put in an isolated device. Two of the three gases (H_2 and CO_2) are separated by a membrane, whereas the number density of the third one (N_2) is constant in the whole device. When the membrane is removed, nitrogen and carbon dioxide start diffusing. Due to a larger friction coefficient, carbon dioxide drags nitrogen, even though its number density gradient is zero. This effect is called the uphill diffusion. This disequilibrium eventually reaches a point where the density gradient for nitrogen has a stronger effect than the friction forces, and the standard diffusion then takes over until reaching the global equilibrium.

Further works have proposed numerical schemes for the Maxwell-Stefan equations with various numerical methods (for example with finite differences [119], finite elements [164] or finite volumes [49], splitting methods [94]).

2.2.2 Analysis of the Fick equations

A perturbative Cauchy theory for the Fick equations (2.12) can be obtained in the torus $\mathbb{T}^3$ from the properties of the matrix $\boldsymbol{F}(\boldsymbol{n})$, stated in the following proposition.

Proposition 2.3 ([G-6])**.** *Assume that* $\boldsymbol{n}(0,x)$ *is bounded from below by a positive constant and that the initial perturbation* $\tilde{\boldsymbol{n}}(0,x)$ *is small enough in* H^2*. Under suitable assumptions on the matrix* $\boldsymbol{F}(\boldsymbol{n})$*, a perturbative solution* $\boldsymbol{n}(t,x) = \bar{\boldsymbol{n}} + \tilde{\boldsymbol{n}}(t,x)$ *of the Fick equation* (2.12) *with the closure condition of constant* $n_{\text{tot}} = \sum_i \bar{n}_i$*, satisfies the following properties*

- *the number density* $\boldsymbol{n}$ *remains positive bounded from below by a positive constant;*
- *the* H^2_x*-norm of the perturbation* $\tilde{\boldsymbol{n}}$ *decays exponentially in time, with an explicit decay rate.*

Remark 2.4. *Actually, this result also holds in* H^s *for any* $s > 3/2$*, for which the injection* $H^s \hookrightarrow L^\infty$ *holds.*

Let us describe why the Fick model does not completely fall into the standard parabolic structure, and the main ideas of the proof of this proposition. This will also allow to discuss the properties needed for the matrix $\boldsymbol{F}(\boldsymbol{n})$ (we shall see in Section 2.5.1 that these assumptions correspond to the form of the coefficients obtained from the hydrodynamic limit).

- The coefficients $\varphi_{ij}(\boldsymbol{n})$ of the matrix $\boldsymbol{F}(\boldsymbol{n})$ are supposed to have the following form: $\varphi_{ij}(\boldsymbol{n}) = n_i \breve{\varphi}_{ij}(\boldsymbol{n})$, corresponding to the following decomposition of the matrix $\boldsymbol{F}(\boldsymbol{n}) = \boldsymbol{D}(\boldsymbol{n})\breve{\boldsymbol{F}}(\boldsymbol{n})$, where $\boldsymbol{D}(\boldsymbol{n}) = \mathrm{Diag}(\boldsymbol{n})$.

- The kernel of $\breve{\boldsymbol{F}}$ is spanned by the vector $\boldsymbol{nm} = (n_1 m_1, \cdots, n_N m_N)^\top$, with the convenient abuse of notation that $(\boldsymbol{fg})_i := f_i g_i$, for any $1 \le i \le N$. Outside its kernel, the matrix $\breve{\boldsymbol{F}}$ is strictly negative as long as $\boldsymbol{n} > 0$, thus endowing the system with a standard degenerate nonlinear parabolic structure, if it was not for the dilatation by $\boldsymbol{n}$. The issue to obtain a complete Cauchy theory reduces to preventing the appearance of a singularity.

- Thus, a perturbative setting around a global equilibrium $\bar{\boldsymbol{n}} > 0$ allows to avoid such a singularity, as long as the perturbation is small enough. The perturbed equation takes the form
$$\partial_t \tilde{\boldsymbol{n}} + \nabla \cdot (\boldsymbol{D}(\bar{\boldsymbol{n}})\breve{\boldsymbol{F}}(\boldsymbol{n})\nabla\tilde{\boldsymbol{n}}) = -\nabla \cdot (\boldsymbol{D}(\tilde{\boldsymbol{n}})\breve{\boldsymbol{F}}(\boldsymbol{n})\nabla\tilde{\boldsymbol{n}}), \tag{2.14}$$
with a homogeneous closure condition $\sum_i \tilde{n}_i = 0$. Due to the presence of $\boldsymbol{D}(\bar{\boldsymbol{n}})$, we could think of working in the weighted $L^2_x(\bar{\boldsymbol{n}}^{-1/2})$-norm. However, even dropping the nonlinear term, a direct estimate would yield a negative feedback on the orthogonal of the kernel of $\breve{\boldsymbol{F}}$, and the kernel quantity (spanned by $\boldsymbol{nm}$) cannot be easily controlled, even at the main order.

- We thus introduce a rescaling in time and space in order to transform (2.14) into a degenerate parabolic equation for which the projection on the kernel remains constant in time at the main order. This is done by defining $\mathfrak{n} = (\mathfrak{n}_i)_{1\le i\le N}$, with $\mathfrak{n}_i = \tilde{n}_i(t/m_i\bar{n}_i^2, \sqrt{m_i\bar{n}_i}x)$. In this way, when applying the spectral gap of $\breve{\boldsymbol{F}}$, it is applied to $\mathfrak{n}/\bar{\boldsymbol{n}}\boldsymbol{m}$, and it remains to control the kernel part. When evaluating the scalar product with $\bar{\boldsymbol{n}}\boldsymbol{m}$ at the main order, we have exactly $(\frac{\mathfrak{n}}{\bar{\boldsymbol{n}}\boldsymbol{m}}, \bar{\boldsymbol{n}}\boldsymbol{m}) = (\mathfrak{n}, \mathbf{1})$ (where $\mathbf{1} := (1, \cdots, 1)^{\mathsf{T}}$), which is zero thanks to the closure condition.

- The nonlinear terms are at higher order, and Sobolev controls on $\check{\boldsymbol{F}}$ ensure that they remain small for small initial data. Grönwall's lemma then allows to end the proof.

Remark 2.5. *The analysis presented here can be extended to the case of a non-zero convective velocity, meaning that* $\boldsymbol{J} = \boldsymbol{F}(\boldsymbol{n})\nabla\boldsymbol{n} + \boldsymbol{X}(\boldsymbol{n})$*, for some vector field* $\boldsymbol{X}$*. The main issue is then to control the convective term, which is ensured under a continuity assumption of* $\boldsymbol{X}(\boldsymbol{n})$ *with respect to* $\boldsymbol{n}$*, allowing to treat this term as the nonlinear ones.*

Let us now tackle the hydrodynamic limit of the Boltzmann equation for mixtures in the diffusive scaling.

2.3 Moment method: the Maxwell-Stefan limit

We first start by applying the moment method, which leads to the Maxwell-Stefan diffusion model.

2.3.1 Formal derivation of the model and diffusion coefficients

The method relies on writing f_i as a local Maxwellian in the velocity variable, *i.e.* the following ansatz

$$f_i(t,x,v) = n_i(t,x)\left(\frac{m_i}{2\pi k_B T(t,x)}\right)^{3/2} \exp\left(-\frac{m_i|v-u_i(t,x)|^2}{2k_B T(t,x)}\right), \tag{2.15}$$

which becomes after scaling

$$f_i^\varepsilon(t,x,v) = n_i^\varepsilon(t,x)\left(\frac{m_i}{2\pi k_B T(t,x)}\right)^{3/2} \exp\left(-\frac{m_i|v-\varepsilon u_i^\varepsilon(t,x)|^2}{2k_B T(t,x)}\right), \tag{2.16}$$

where we assumed that all species have the same macroscopic temperature $T(t,x)$.

Remark 2.6. *It has been proved in [123] that, in the diffusive scaling, even if the species temperatures are different, they satisfy* $T_i(t,x) = T(t,x) + \mathcal{O}(\varepsilon^2)$*, which justifies that we choose a unique temperature for all species.*

In the following, we also work in an isothermal setting, meaning that the temperature is assumed to be uniform and constant $T(t,x) = T$.

When computing the first two moments in velocity of the scaled Boltzmann equation (2.13), and using the ansatz (2.16), we obtain

$$\varepsilon\partial_t n_i^\varepsilon + \varepsilon\nabla\cdot(n_i^\varepsilon u_i^\varepsilon) = 0, \tag{2.17a}$$

$$\varepsilon^2\partial_t(n_i^\varepsilon u_i^\varepsilon) + \varepsilon^2\nabla\cdot(n_i^\varepsilon u_i^\varepsilon \otimes u_i^\varepsilon) + \frac{k_B T}{m_i}\nabla n_i^\varepsilon = \frac{1}{\varepsilon}\sum_{j=1}^N \int_{\mathbb{R}^3} v\, Q_{ij}(f_i^\varepsilon, f_j^\varepsilon)\,\mathrm{d}v. \tag{2.17b}$$

From (2.17a), we obviously obtain at the limit the mass conservation equation

$$\partial_t n_i + \nabla\cdot J_i = 0,$$

where $n_i = \lim_{\varepsilon\to 0} n_i^\varepsilon$ and $J_i = \lim_{\varepsilon\to 0} n_i^\varepsilon u_i^\varepsilon$. The limit when ε tends to zero of the left hand side of (2.17b) leads to the term $k_B T \nabla n_i/m_i$, which corresponds to the left hand side of (2.9b) multiplied by $k_B T/m_i$. The computation of the right hand side of (2.17b) can be done very easily using the ansatz in the special case of Maxwell molecules, which means that the angular part Φ_{ij} is constant ($\gamma_{ij} = 0$), and the cross sections thus only depend on the deviation angle θ. In this case, the computations are done completely explicitly in polar coordinates, by using the weak form of the Boltzmann operator (2.4) with $\psi(v) = v$ and with the expression of $v' - v$ given by the collision rule (2.3a). We obtain

$$\frac{1}{\varepsilon}\sum_{j=1}^{N}\int_{\mathbb{R}^3} v\, Q_{ij}(f_i^\varepsilon, f_j^\varepsilon)\,\mathrm{d}v = \sum_{j=1}^{N} \frac{2\pi m_j \|b_{ij}\|_{L^1}}{m_i + m_j} n_i^\varepsilon n_j^\varepsilon (u_j^\varepsilon - u_i^\varepsilon). \tag{2.18}$$

In [G-18], the limit when $\varepsilon \to 0$ of this term gives the right-hand side of the Maxwell-Stefan equations (2.9b), with the diffusion coefficients

$$D_{ij} = \frac{(m_i + m_j) k_B T}{2\pi m_i m_j \|b_{ij}\|_{L^1}}. \tag{2.19}$$

These computations have been extended to the case of analytic factorized cross sections [124], with Grad's angular cutoff assumption, *i.e.* for Φ_{ij} having the form of a specific power series.

For general cross sections, explicit computations cannot be done anymore. However, it is of interest to check if in this case, the asymptotic limit still has the form of the Maxwell-Stefan diffusion model, and to investigate how the coefficients D_{ij} are related to the microscopic quantities, *i.e.* an extension of (2.19). In [G-16], we tackle this problem for a very general class of cross sections, only assumed to satisfy Grad's angular cutoff assumption and standard Galilean properties for any $(v, v_*, \sigma) \in \mathbb{R}^6 \times \mathbb{S}^2$, which are

$$\mathcal{B}_{ij}(v + w, v_* + w, \sigma) = \mathcal{B}_{ij}(v, v_*, \sigma), \qquad \mathcal{B}_{ij}(\Theta v, \Theta v_*, \Theta\sigma) = \mathcal{B}_{ij}(v, v_*, \sigma),$$

for any $w \in \mathbb{R}^3$ and any rotation $\Theta \in O^+(\mathbb{R}^3)$. In this case, we proved the following proposition.

Proposition 2.7 ([G-16])**.** *We have that, for any $1 \le i \le N$,*

$$\lim_{\varepsilon\to 0}\frac{1}{\varepsilon}\sum_{j=1}^{N}\int_{\mathbb{R}^d} v\, Q_{ij}(f_i^\varepsilon, f_j^\varepsilon)\,\mathrm{d}v = \sum_{j=1}^{N}\frac{1}{D_{ij}} n_i n_j (u_j - u_i), \tag{2.20}$$

where the coefficients D_{ij} have the following expression

$$\frac{1}{D_{ij}} = \frac{1}{6 k_B T}\left(\frac{m_i}{2\pi k_B T}\right)^{3/2}\left(\frac{m_j}{2\pi k_B T}\right)^{3/2}\mathcal{I},$$

only depending on the masses $(m_i)_i$, the temperature T and an integral of the form

$$\mathcal{I} = \frac{m_j}{(m_i + m_j)}\int_{\mathbb{R}^6\times\mathbb{S}^2}\mathcal{B}_{ij}(v, v_*, \sigma) e^{-\frac{m_i}{2k_B T}v^2 - \frac{m_j}{2k_B T}v_*^2}(v_* - v + |v - v_*|\sigma)\cdot(v - v_*)\,\mathrm{d}\sigma\,\mathrm{d}v_*\,\mathrm{d}v.$$

This means that at the limit $\varepsilon \to 0$, the scaled Boltzmann equations (2.13) formally converge to the Maxwell-Stefan equations, with the diffusion coefficients given by the expression above.

Another expression, allowing to deduce directly the positivity of the associated diffusion coefficients, is

$$\mathcal{I} = m_i \int_{\mathbb{R}^6 \times \mathbb{S}^2} \mathcal{B}_{ij}(v, v_*, \sigma) e^{-\frac{m_i}{2k_BT}v^2 - \frac{m_j}{2k_BT}v_*^2} (v' - v)^2 \, \mathrm{d}\sigma \, \mathrm{d}v_* \, \mathrm{d}v. \tag{2.21}$$

The proof of this result results from the algebraic structure of the terms involved. Indeed, when computing the moment of order 1 of Q_{ij} over ε using the ansatz (2.16), we have the following observations:

- using the weak form (2.4) with $\psi(v) = v$, a change of variable in v and v_* as $v + \varepsilon u_i$ and $v_* + \varepsilon u_j$ leads to the quantity $u_i - u_j$ in the terms in v;

- an expansion with respect to ε of the exponential terms (coming from the ansatz on f_i), together with parity arguments, imply that at the main order, it remains terms of order ε, thus cancelling the division by ε, and that the integrand is proportional to

  $$[(u_i - u_j) \cdot (v' - v)] \, (v' - v);$$

- this term can be seen as a matrix operator acting on $u_i - u_j$, which commutes with the rotations of $O^+(\mathbb{R}^3)$, and is thus a scalar times the identity matrix (this comes from a standard linear algebra result, also a corollary of Schur's lemma). The scalar value is then any component of $v' - v$ squared, or their mean value $\frac{1}{3}|v' - v|^2$.

The other expression of $\mathcal{I}$ comes from the same scheme of proof with the use of another weak form of the Boltzmann operator.

Remark 2.8. *It can be proved that the Maxwell-Stefan diffusion coefficients given by* (2.21) *can actually also be written in terms of the linearized Boltzmann operator* $\mathcal{L}$ (2.33) *defined in Section 2.4.1. On the other hand, we shall see that Fick diffusion coefficients involve the inverse of this operator.*

Remark 2.9. *Observe that, at the asymptotic limit, the Maxwell-Stefan diffusion model is not closed. A natural question is to wonder whether the closure condition can also be retrieved (at least formally) from the kinetic level. First, summing the mass conservation equations for each species* (2.17a) *implies that*

$$\partial_t n_{\mathrm{tot}} + \nabla \cdot J_{\mathrm{tot}} = 0,$$

and the momentum conservation equations for each species (2.17b) *with masses that* $\nabla n^{\varepsilon}_{\mathrm{tot}} = \mathcal{O}(\varepsilon^2)$*, thus* $\nabla n_{\mathrm{tot}} = 0$*. Further, the moment of order 2 of the Boltzmann equations* (2.13) *summed over i combined with the ansatz* (2.16) *gives*

$$(3\partial_t n_{\mathrm{tot}} + 5\nabla \cdot J_{\mathrm{tot}}) k_B T = 0,$$

which in turns implies that the total number of molecules n_{tot} *is uniform and constant, and that the total flux* J_{tot} *is divergence free. We point out that the classical equimolar diffusion assumption* $J_{\mathrm{tot}} = 0$ *has not been obtained in this derivation, but a weaker condition on its divergence, which was discussed in Section 2.1.2.*

2.3.2 Justification of the Maxwellian ansatz

The key ingredient of the previous approach is the ansatz that the distribution function has the form of a local Maxwellian. Let us briefly explain why this ansatz is relevant, even if not in a fully rarefied regime.

Indeed, when prescribing the values of the moments of the distribution function (2.8), the local Maxwellian (2.15) is obtained by applying the Maximum Entropy Principle (MEP) in [5]. This principle is a constrained variational formulation, which determines the approximate velocity distribution [73, 173, 134]. The functional to be maximized is the kinetic entropy, defined as

$$\mathcal{H}(t,x) = -\sum_{i=1}^{N} \int_{\mathbb{R}^3} f_i \log(f_i)\, \mathrm{d}v. \tag{2.22}$$

The constraints are taken to be the moments, *i.e.* the macroscopic variables which determine the state space. Physically, the maximization of the entropy is the search for the most probable distribution function. Since the only information we have about the system is its macroscopic state, we look for a distribution function compatible with these macroscopic variables maximizing the entropy.

To derive the Maxwell-Stefan model, it is enough to choose the number density, the momentum and the energy as constraints. The proof relies on defining the Lagrangian

$$\int_{\mathbb{R}^3} \sum_{i=1}^{N} \left(f_i \log(f_i) + \lambda_{n_i} f_i + \sum_{k=1}^{3} \lambda_{u_i}^{(k)} v^{(k)} f_i + \lambda_{e_i} |v|^2 f_i \right) \mathrm{d}v,$$

where $v^{(k)}$ is the k-th component of v, and λ_{n_i}, $\lambda_{u_i}^{(k)}$ and λ_{e_i} are the Lagrange multipliers associated to the constraints. The extremum of the functional is obtained by computing the variations of the Lagrangian with respect to f_i, which gives the Maxwellian form of the distribution function. The computation of the moments combined with the constraints then gives the values of the multipliers.

Remark 2.10. *In Section 2.3.3, we derive formally from the kinetic level a higher order Maxwell-Stefan model, taking into account viscous dissipation. This also relies on a Maxwellian ansatz, which can be derived in the same way, with the constraints* (2.8a)–(2.8b) *and the full pressure tensor*

$$n_i u_i^{(k)} u_i^{(\ell)} + p_i^{(k\ell)} = \int_{\mathbb{R}^3} v^{(k)} v^{(\ell)} f_i \,\mathrm{d}v. \tag{2.23}$$

We proved in [G-8] that the Maxwellian

$$f_i(t,x,v) = n_i(t,x) \left(\frac{n_i(t,x)}{2\pi} \right)^{3/2} (\det P_i(t,x))^{-1/2} \times \exp\left(-\frac{n_i(t,x)}{2} (v - u_i(t,x))^{\mathsf{T}} P_i^{-1}(t,x)(v - u_i(t,x)) \right) \tag{2.24}$$

is the unique solution of the Maximum Entropy Principle under these constraints. In this expression, $P_i = (p_i^{(k\ell)})_{1\le k,\ell\le 3}$ *is the full (diagonal) pressure tensor.*

Actually, the core ideas of the closure by the MEP can be reinterpreted using Levermore's formalism [143]. As we discussed in [G-16], this approach can be seen a Galerkin method for solving the Boltzmann equation. Let us describe in a few words how it is stated for mixtures with Levermore's notations.

Introducing the entropy function $\eta(\boldsymbol{f}) = -\sum_i f_i \log(f_i) + f_i$ (which is consistent with the entropy (2.22)), its associated conjugate convex function is the exponential function $\eta^*(\boldsymbol{f}) = \sum_i \exp(f_i)$. The space $\mathbb{E}$ defined in (2.6) is the equilibrium subspace. Introducing the tensors $\mathsf{C}_1, \cdots, \mathsf{C}_N$ defined by

$$\mathsf{C}_1 = \begin{bmatrix} m_1 v \\ 0 \\ \vdots \\ 0 \end{bmatrix}, \qquad \cdots \qquad , \mathsf{C}_N = \begin{bmatrix} 0 \\ \vdots \\ 0 \\ m_N v \end{bmatrix},$$

we define $\mathbb{M} = \operatorname{Span}\{\boldsymbol{e}_1, \cdots, \boldsymbol{e}_N, \mathsf{C}_1, \cdots, \mathsf{C}_N, |v|^2 \boldsymbol{m}\} \supset \mathbb{E}$, and $(\mathsf{M}_k(v))_{1 \le k \le 2N+1}$ the tensorially formulated basis of $\mathbb{M}$. Observe that the subspace $\mathbb{M}$ produces the macroscopic moments (number density, momentum and energy). Indeed, we define a realizable moment R, for which there exists $\boldsymbol{f}$ such that $\mathsf{R}_k = \sum_i \int_{\mathbb{R}^3} [\mathsf{M}_k(v)]_i f_i \,\mathrm{d}v$, for $\mathsf{M}_k \in \mathbb{M}$. In our procedure, from the definition of the prescribed macroscopic quantities (2.8), we have

$$\mathsf{R} = (n_1, \cdots, n_N, m_1 n_1 u_1, \cdots, m_N n_N u_N, \mathcal{E}),$$

where $\mathcal{E} = \sum_i m_i n_i |u_i|^2/2 + m_i n_i e_i/2$ is the total energy. We look for $\boldsymbol{f}$ under the form $\boldsymbol{f} = \nabla \eta^*(\mathsf{a} \cdot \mathsf{M}(v)) = \exp(\mathsf{a} \cdot \mathsf{M}(v))$, where $\mathsf{a} \in \mathbb{M}$ and

$$[\mathsf{a} \cdot \mathsf{M}(v)]_i = \sum_{k=1}^{2N+1} \mathsf{a}_k \cdot [\mathsf{M}_k(v)]_i, \qquad 1 \le i \le N.$$

We have a correspondance between a and R *via* the Euler condition

$$\mathsf{R} = \nabla_{\mathsf{a}} \left(\int_{\mathbb{R}^3} \eta^*(\mathsf{a} \cdot \mathsf{M}(v)) \,\mathrm{d}v \right) = \nabla_{\mathsf{a}} \left(\sum_i \int_{\mathbb{R}^3} \exp([\mathsf{a} \cdot \mathsf{M}(v)]_i) \,\mathrm{d}v \right). \tag{2.25}$$

Computing the right-hand side of (2.25) can be done explicitly, and leads to a system of equations for a depending on R. This system is solved by the exact same computations as the ones on the Lagrange multipliers in the MEP. Finally, inserting the expression of a in the relation for $\boldsymbol{f}$ leads to the Maxwellian form of the distribution function.

2.3.3 Higher-order Maxwell-Stefan model

In the Maxwell-Stefan model, viscous dissipation is not included. To take into account this effect, we can extend the model with the momentum flux balance laws.

As we have seen before, the first two moments in velocity of the scaled Boltzmann equation coupled with the ansatz (2.16) give mass and momentum balance laws for each species, see (2.17a)–(2.17b) with (2.18). As for the third moment, we consider in [G-8] the whole pressure tensor, and not only its trace part as in (2.8c). The partial pressure tensor $p_i^{(k\ell)}$ for species i is defined by

$$p_i^{(k\ell)} = \int_{\mathbb{R}^3} c_i^{(k)} c_i^{(\ell)} f_i \,\mathrm{d}v,$$

where $c_i = v - \varepsilon u_i$. Equivalently, we have that

$$\varepsilon^2 n_i u_i^{(k)} u_i^{(\ell)} + p_i^{(k\ell)} = \int_{\mathbb{R}^3} v^{(k)} v^{(\ell)} f_i \,\mathrm{d}v. \tag{2.26}$$

As discussed in Section 2.3.2, using a Maxwellian ansatz can be justified by the Maximum Entropy Principle, under the constraints of the prescribed moments. Here, we take into account higher-order approximations by extending the state space and using the constraint (2.26) instead of (2.8c) (*cf.* Remark 2.10). This leads us to use a scaled version of the Maxwellian (2.24), where each u_i is replaced by εu_i.

In the case of Maxwell molecules, using these constraints, we can compute the moment equations extending (2.17) as follows

$$\varepsilon\left(\partial_t n_i + \nabla\cdot(n_i u_i)\right) = 0,$$
$$\varepsilon^2\left(\partial_t(n_i u_i) + \nabla\cdot(n_i u_i\otimes u_i)\right) + \nabla\cdot P_i = \sum_{j=1}^N \frac{k_B T}{D_{ij}} n_i n_j (u_j - u_i),$$

where D_{ij} is defined in (2.19) and $P_i = (p_i^{(k\ell)})_{1\le k,\ell\le 3}$. These moment equations are also completed by a momentum flux balance law, which we do not write here for the sake of concision. The computations are very similar to the standard Maxwell-Stefan model, using the weak form (2.4) and the moments of the distribution function. The collision terms on the right hand side are computed explicitly in the case of Maxwell molecules in polar coordinates. We can however state the energy balance law, obtained by summing component-wise the momentum flux balance laws

$$\begin{aligned}\varepsilon^3\Big(\partial_t(n_i|u_i|^2) + \nabla\cdot(n_i|u_i|^2 u_i)\Big) + \varepsilon\Big(3\partial_t p_i + 2\nabla\cdot(u_i\cdot P_i) + 3\nabla\cdot(p_i u_i)\Big)\\ = \sum_{j=1}^N \frac{k_B T}{(m_i+m_j)D_{ij}}\left\{\frac{6}{\varepsilon}\Big(n_i p_j - n_j p_i\Big) + 2\varepsilon n_i n_j\Big(m_j|u_j|^2 + (m_i - m_j)u_i\cdot u_j - m_i|u_i|^2\Big)\right\},\end{aligned} \tag{2.27}$$

where $p_i = \sum_{k=1}^3 p_i^{(kk)}$.

Proposition 2.11 ([G-8]). *Formally, taking the limit when ε tends to zero leads to the following set of equations, which generalizes the Maxwell-Stefan model to the case of higher-order moments, for $1\le i\le N$*

$$\partial_t n_i + \nabla\cdot J_i = 0, \tag{2.28a}$$
$$\nabla\cdot P_i = \sum_{j=1}^N \frac{k_B T}{D_{ij}}\left(n_i J_j - n_j J_i\right), \tag{2.28b}$$

where the partial pressure tensor is diagonal and decomposed as $P_i^{(k\ell)} = \left(p_i + \mathscr{P}_i^{(k\ell)}\right)\delta_{k\ell}$, $1\le k,\ell\le 3$, and the traceless part $\mathscr{P}_i^{(\ell\ell)}$ is given by an explicit local relation, depending on the masses, the microscopic cross sections via *the diffusion coefficients D_{ij} and other moments of the angular function b_{ij}, the number densities, as well as the partial pressures.*

The main observation leading to this limit system is that at the main order (ε^{-1}), the momentum flux balance laws are pointwise relations forming a linear system for the unknowns $\mathscr{P}_i^{(k\ell)}$. The matrix of this system can be proved to be invertible since it is diagonally dominant, and the partial pressure tensor to be diagonal. Further, the properties of the system on $\mathscr{P}_i^{(k\ell)}$ lead to the following compatibility condition on the equation of state

$$p_i = \theta(t,x)n_i,$$

where the function θ does not depend on species i, and is related to the (common) temperature in the ideal gas law.

Let us comment on the structure of the obtained higher-order model (2.28). The main difference with the usual Maxwell-Stefan model (2.9) is that the momentum exchange between the species is not balanced solely by the gradients of partial pressures. One must take into account the diagonal terms of the traceless part of the pressure tensor, determined by a set of algebraic relations. In the isothermal case (when θ is a known constant), the system is closed. In the non-isothermal case, the system is not closed, and one must add an equation to close the system, which is the energy conservation for the mixture, obtained from (2.27) by summing over all species i. In this equation, the term at order ε^1 disappears when summing (actually the whole right-hand side disappears), and the main order term is the one of order ε, which leads to

$$3\partial_t\left(\sum_{i=1}^{N} p_i\right) + 2\nabla\cdot\left(\sum_{i=1}^{N} u_i\cdot P_i\right) + 3\nabla\cdot\left(\sum_{i=1}^{N} p_i u_i\right) = 0.$$

Numerical scheme Since the structure (in terms of partial differential equations) of this higher-order Maxwell-Stefan model is very similar to the classical Maxwell-Stefan one, we extended naturally in [G-3] the simple 1D scheme mentioned in Section 2.2.1, which handles the model with the equimolar diffusion closure assumption. In order to determine the partial pressures p_i, we choose the ideal gas law $p_i = k_B T n_i$ (isothermal). The only extension consists in solving the linear system on $\mathscr{P}_i^{(11)}$ (in 1D) at each iteration in order to update the values of the traceless parts of the pressure tensor. We show on Figure 2.1 the evolution at different times of the number densities for the Duncan and Toor experiment. We observe the uphill diffusion phenomenon on species N_2, and diffusion towards the global equilibrium. We also observe that the diffusion process is faster for species H_2 and CO_2 than for N_2, which is standard with a Maxwell-Stefan model.

In order to quantify the influence of taking into account the complete pressure tensor, we compare the number densities and pressures at a given time obtained with the higher-order model with the ones obtained with the classical Maxwell-Stefan model on Figure 2.2, for nitrogen, which is the species with the unusual diffusion process. We observe that the higher-order model has a slower evolution than the classical one, both on the number density and the total pressure, thus showing that the viscous effects have an influence on the diffusion rate. Note that the asymptotic values of the pressure are not the same between the two models, since the asymptotic value of the traceless part of the pressure tensor is not zero in the higher-order model.

Contrary to the classical Maxwell-Stefan model, which only involves the binary diffusion coefficients D_{ij}, for $i \neq j$, the higher-order model involves the self-diffusivities D_{ii} as well as the second moment of the angular part of the cross sections b_{ij}, which are not given in the literature and have to be computed. For these quantities, we imposed the restrictive condition that $\int_{-1}^{1} \eta^2 b_{ij}(\eta)\,\mathrm{d}\eta = \gamma \|b_{ij}\|_{L^1}$, and we studied the influence of this parameter γ. Figure 2.3 compares the number densities and the pressure for hydrogen at a given time for different values of γ, and shows that the difference in the dynamics between the two models is influenced by this parameter.

Prospect

> It would be of interest to study the two cross-diffusion Maxwell-Stefan systems (lower and higher-order) in order to compare the different diffusion time scales, and in particular to see

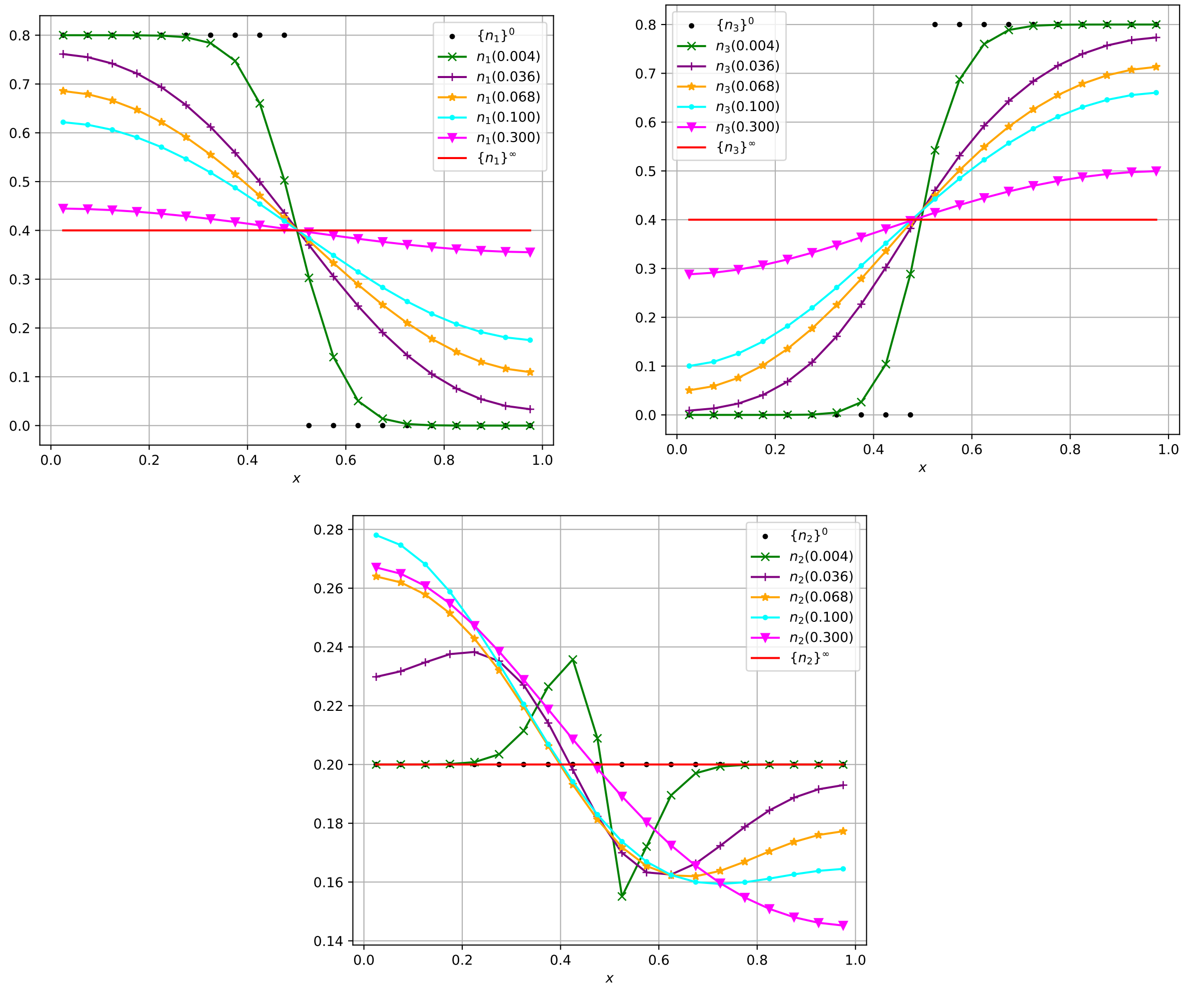

Figure 2.1: Evolution of the number densities for H_2 and CO_2 (first line) and N_2 along time

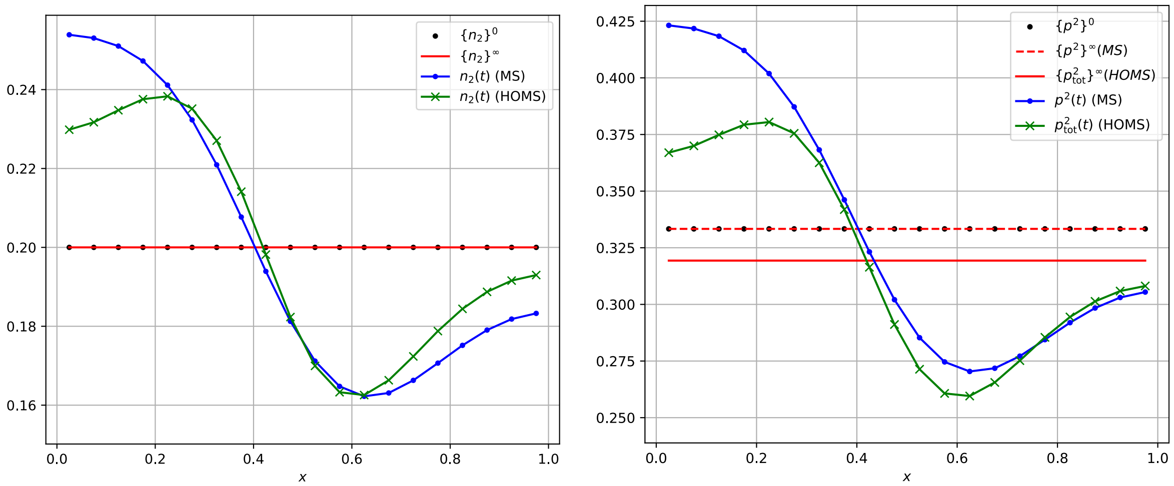

Figure 2.2: Comparison of the number densities (left) and pressure (right) for H_2 at a given time between the Maxwell-Stefan (MS) model and the higher-order (HOMS) model

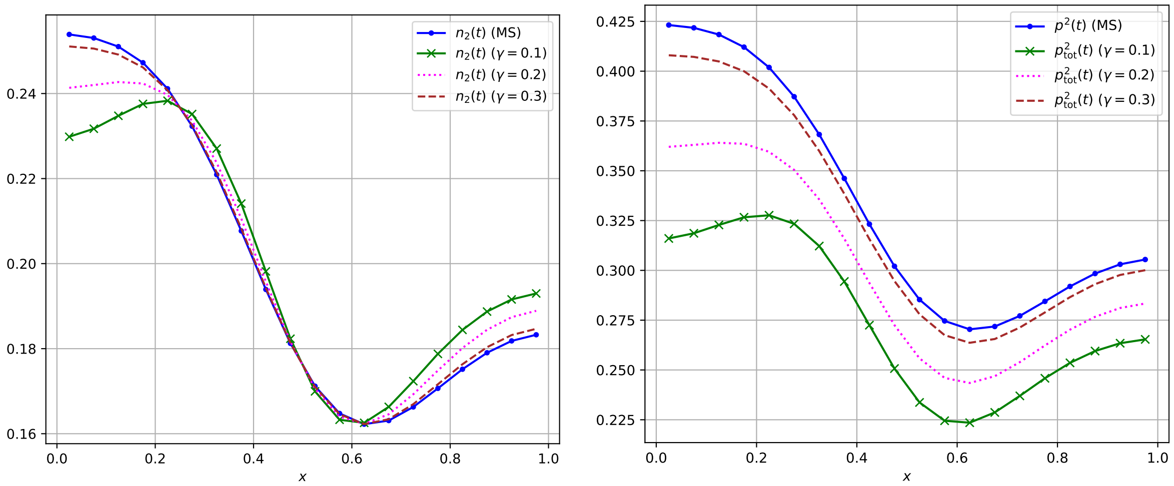

Figure 2.3: Influence of the parameter γ on the number densities (left) and pressure (right) for H_2 at a given time

if we can obtain explicit rates of convergence, explaining the discrepancy when taking into account the full pressure tensor. This could give some information about the regime in which the classical Maxwell-Stefan model is relevant, and when the higher-order model is necessary.

2.4 Perturbative method around a local Maxwellian

2.4.1 Introduction

After the formal derivation of the Maxwell-Stefan equations from the Boltzmann equations for mixtures, the next step is to prove the rigorous convergence of the kinetic model towards the macroscopic one.

Let us briefly recall previous approaches on the rigorous convergence in the mono-species case, in a perturbative setting around a local (for compressible limits) or global (for incompressible limits) equilibrium. In [59], inspired from Caflisch's works [48] in a compressible case, the authors prove the convergence of the distribution function to a Maxwellian equilibrium, whose macroscopic quantities satisfy the macroscopic fluid equations. These methods lead to solutions local in time, since they depend on the regularity of the solutions of the limit system. Further, the pioneering works of Bardos, Golse and Levermore [13, 12] lead the path to global existence results, from techniques coming from proving a decay to equilibrium.

- ▷ The entropy method is adapted to the perturbative case by Golse and Saint Raymond [99, 100] to prove the rigorous convergence of weak solutions (à la DiPerna and Lions) of the Boltzmann equation towards the weak solutions (à la Leray) of the Navier-Stokes equations.
- ▷ Other works are based on a micro-macro decomposition and the nonlinear energy method [111, 113].
- ▷ The hypocoercive formalism and explicit spectral gap estimates can also used to prove the convergence towards a Maxwellian whose macroscopic quantities satisfy the Navier-Stokes equations [169, 170, 43].

The extension of these results in the mixture case is not straightforward.

I will now describe the context in which my contributions can be set. As we mentioned previously, two different approaches can be used for obtaining (formally) the hydrodynamic limit of a kinetic model: the moment method and the perturbative method. For the latter, in the mathematical analysis of the scaled Boltzmann equation for mixtures, two choices can be made for the expansion of the distribution function.

- We can consider an expansion around a global Maxwellian

  $$\boldsymbol{f} = \boldsymbol{n\mu} + \varepsilon \boldsymbol{g}. \tag{2.29}$$

  In this case the macroscopic quantities are contained (at least partially) in the perturbation $\boldsymbol{g}$, and we are led to study this perturbation. It is thus natural to define the (vectorial) weighted space $L^2((\boldsymbol{n\mu})^{-1/2})$ by its scalar product

  $$\langle \boldsymbol{f}, \boldsymbol{g}\rangle_{\boldsymbol{n\mu}} := \langle \boldsymbol{f}, \boldsymbol{g}\rangle_{L^2((\boldsymbol{n\mu})^{-1/2})} = \sum_{i=1}^{N} \int_{\mathbb{R}^3} f_i g_i (n_i \mu_i)^{-1}\, \mathrm{d}v, \tag{2.30}$$

  in which most of the analysis will be done in the following. When $\boldsymbol{n} = \boldsymbol{1}$, it becomes the weighted space $L^2(\boldsymbol{\mu}^{-1/2})$, with the scalar product $\langle \cdot, \cdot \rangle_{\boldsymbol{\mu}}$.

  Observe that another possible choice would be to choose the perturbation of the form $\varepsilon(\boldsymbol{n\mu})^{1/2}\boldsymbol{g}$, which would allow to work in a non weighted L^2-space. This is actually the case in several contributions [G-22, G-5], but for the sake of consistency, we shall discuss in this manuscript all results in the weighted space.

- We can also consider an expansion around a local Maxwellian, involving the macroscopic quantities

  $$\boldsymbol{f} = \boldsymbol{n}\boldsymbol{M}^{\varepsilon} + \varepsilon \boldsymbol{g}, \tag{2.31}$$

  where

  $$M_i^{\varepsilon} = \left(\frac{m_i}{2\pi k_B T(t,x)}\right)^{3/2} \exp\left(-\frac{m_i |v - \varepsilon u_i^{\varepsilon}(t,x)|^2}{2 k_B T(t,x)}\right). \tag{2.32}$$

  Let us mention that since the Maxwellian $\boldsymbol{M}^{\varepsilon}$ contains the macroscopic velocity $\varepsilon \boldsymbol{u}$, which is scaled of order ε, it also depends on ε, and we chose to emphasize this dependence in the notation. The difficulty is then contained in the analysis with this local Maxwellian (which is not an equilibrium).

The two expansions induce two different linearized Boltzmann operators:

- the linearized operator $\boldsymbol{\mathcal{L}} = (\mathcal{L}_i)_i$ around the global Maxwellian, which is defined by

  $$\mathcal{L}_i(\boldsymbol{g}) = \sum_{j=1}^{N} \left(Q_{ij}(n_i\mu_i, g_j) + Q_{ij}(g_i, n_j\mu_j)\right); \tag{2.33}$$

- the linearized operator $\boldsymbol{L}^{\varepsilon} = (L_i^{\varepsilon})_i$ around the local Maxwellian, which is defined by

  $$L_i^{\varepsilon}(\boldsymbol{g}) = \sum_{j=1}^{N} \Big(Q_{ij}(n_i M_i^{\varepsilon}, g_j) + Q_{ij}(g_i, n_j M_j^{\varepsilon})\Big).$$

  Let us note that in this case, we again chose to emphasize the dependence in ε of the linearized operator in the notation.

In a previous work [42], the authors obtained a Cauchy theory and the convergence of the multi-species Boltzmann equation towards equilibrium (relying on the spectral gap for the linearized operator $\boldsymbol{\mathcal{L}}$ around a global Maxwellian, and an adaptation of the method by Guo for the linear perturbed equation). However, this linearization cannot be used for the convergence in the diffusive limit towards the Maxwell-Stefan system. Indeed, for the hydrodynamic limit, the expansion on the distribution function is not around the global Maxwellian, but around a local one, whose macroscopic quantities satisfy (at the limit) the Maxwell-Stefan equations. This local Maxwellian $\boldsymbol{n}\boldsymbol{M}^\varepsilon$ actually corresponds to the ansatz (2.16), and contains the macroscopic quantities involved in the limit diffusion model, in a consistent way with the moment method.

The linearization around a local Maxwellian induces a series of difficulties with respect to the mono-species case. First, symmetry properties of the linearized operator are lost, since the introduction in the Maxwellian of macroscopic velocities εu_i ruins the microscopic conservation of energy (2.2b) when $u_i \neq u_j$, and thus $M_i^{\varepsilon\prime} M_{j*}^{\varepsilon\prime} \neq M_i^\varepsilon M_{j*}^\varepsilon$. This implies that $\boldsymbol{L}^\varepsilon$ is not self-adjoint, which prevents to use classical methods for the analysis of its spectrum.

Further, an important element is the function space in which the spectral gap is proved for $\boldsymbol{L}^\varepsilon$. Indeed, in order to rely on the spectral gap property of $\boldsymbol{\mathcal{L}}$ (see Proposition 2.14), which is naturally set in the weighted $L^2(\boldsymbol{\mu}^{-1/2})$ space, we choose to work in the same space, meaning that the weight is not the local Maxwellian involved in the linearized operator.

The rigorous convergence in a perturbative setting was the main topic of Andrea Bondesan's PhD thesis. With the expansion (2.31), we are led to study the following perturbed Boltzmann equation on $\boldsymbol{g}$

$$\varepsilon\partial_t \boldsymbol{g} + v\cdot\nabla_x \boldsymbol{g} = \frac{1}{\varepsilon}\boldsymbol{L}^\varepsilon(\boldsymbol{g}) + \boldsymbol{Q}(\boldsymbol{g},\boldsymbol{g}) + \boldsymbol{S}^\varepsilon,$$

where the source term contains the following contributions

$$\boldsymbol{S}^\varepsilon = -\partial_t \boldsymbol{M}^\varepsilon - \frac{1}{\varepsilon} v\cdot\nabla_x \boldsymbol{M}^\varepsilon + \frac{1}{\varepsilon^2}\boldsymbol{Q}(\boldsymbol{M}^\varepsilon,\boldsymbol{M}^\varepsilon).$$

We mention here the main steps of the proof, which was developed in the doctoral work of Andrea Bondesan [29], and we will give some details in the following sections.

- First, a Cauchy theory is needed for the Maxwell-Stefan equations in a perturbative setting [31] (see Section 2.2).

- Then, one has to choose a suitable local Maxwellian and its macroscopic quantities. Let us mention that in the hydrodynamic limit, even if the $\frac{1}{\varepsilon}\boldsymbol{L}^\varepsilon$ was controlled with an explicit spectral gap estimate, the source term (involving in particular $\frac{1}{\varepsilon^2}\boldsymbol{Q}(\boldsymbol{M}^\varepsilon,\boldsymbol{M}^\varepsilon)$) is of a higher order of magnitude, and thus a priori not controlled. This is the main reason to tune in a fine way the choice of the local Maxwellian, in particular choosing its macroscopic values $\boldsymbol{n}$ and $\boldsymbol{u}$ to be perturbed solutions of the Maxwell-Stefan equations, in order to have a control of the form $\boldsymbol{M}^\varepsilon - \boldsymbol{\mu} = \mathcal{O}(\varepsilon)$. In concrete terms, these macroscopic quantities are chosen as perturbations of solutions of the Maxwell-Stefan system as follows $\boldsymbol{n} = \bar{\boldsymbol{n}} + \varepsilon\tilde{\boldsymbol{n}}$ (and similarly $\boldsymbol{u} = \bar{\boldsymbol{u}} + \varepsilon\tilde{\boldsymbol{u}}$), where the bar quantities are solutions of the Maxwell-Stefan equations, and the tilde quantities are small perturbations (of order ε). This allows to use the Cauchy theory we mentioned above.

- Further, the stability of the spectral gap is proved (see Section 2.4.3) to control the microscopic terms. Observe that the obtained spectral gap is of the form

$$\langle \boldsymbol{L}^\varepsilon(\boldsymbol{g}),\boldsymbol{g}\rangle_{\boldsymbol{\mu}} \leq -\lambda\|\boldsymbol{g} - \boldsymbol{\pi}_{\boldsymbol{\mathcal{L}}}(\boldsymbol{g})\|_{\boldsymbol{\mu}}^2 + \varepsilon\|\boldsymbol{\pi}_{\boldsymbol{\mathcal{L}}}(\boldsymbol{g})\|_{\boldsymbol{\mu}}^2,$$

which differs from standard spectral gap results. First, the weight of function space in which the spectral gap is proved is not the one associated to the perturbation (local Maxwellian $\boldsymbol{M}^\varepsilon$), but to the global Maxwellian $\boldsymbol{\mu}$. Second, the projection $\boldsymbol{\pi}_{\boldsymbol{\mathcal{L}}}$ is not the projection on $\operatorname{Ker} \boldsymbol{L}^\varepsilon$ but the one on the kernel of the standard linear operator $\boldsymbol{\mathcal{L}}$ arising from the global Maxwellian $\boldsymbol{\mu}$.

- It remains to control the fluid part. This is done by extending hypocoercivity methods to the mixture case [170, 43].

- The stability of this local Maxwellian in the Boltzmann equation is thus proved (*i.e.* $\varepsilon \boldsymbol{g}$ tends to zero), and the convergence towards the Maxwell-Stefan equations in a perturbative setting is obtained.

2.4.2 Properties of the linearized operator around a global Maxwellian

Before diving into the spectral gap property of the linearized operator $\boldsymbol{L}^\varepsilon$, let us first mention preliminary results on $\boldsymbol{\mathcal{L}}$.

The operator $\boldsymbol{\mathcal{L}}$ appears as the sum of a negative multiplicative operator involving the collision frequency $\boldsymbol{\nu} > 0$, and an integral operator $\boldsymbol{\mathcal{K}} = \boldsymbol{\mathcal{K}}_1 + \boldsymbol{\mathcal{K}}_2 + \boldsymbol{\mathcal{K}}_3$, which is expected to satisfy a compactness property. Using the definition of $\boldsymbol{\mathcal{L}}$ and of the collision operator, as well as the conservation of energy (2.2b) in the Maxwellians, we get

$$
\begin{aligned}
[\boldsymbol{\mathcal{K}}_1]_i(\boldsymbol{g}) &= -n_i \sum_{j=1}^N \int_{\mathbb{R}^3\times\mathbb{S}^2} B_{ij}(|v-v_*|,\cos\theta)\mu_i(v) g_j(v_*)\,\mathrm{d}\sigma\,\mathrm{d}v_*,\\
[\boldsymbol{\mathcal{K}}_2]_i(\boldsymbol{g}) &= n_i \sum_{j=1}^N \int_{\mathbb{R}^3\times\mathbb{S}^2} B_{ij}(|v-v_*|,\cos\theta)\mu_i(v') g_j(v'_*)\,\mathrm{d}\sigma\,\mathrm{d}v_*,\\
[\boldsymbol{\mathcal{K}}_3]_i(\boldsymbol{g}) &= n_j \sum_{j=1}^N \int_{\mathbb{R}^3\times\mathbb{S}^2} B_{ij}(|v-v_*|,\cos\theta)\mu_j(v'_*) g_j(v')\,\mathrm{d}\sigma\,\mathrm{d}v_*,\\
\nu_i &= n_j \sum_{j=1}^N \int_{\mathbb{R}^3\times\mathbb{S}^2} B_{ij}(|v-v_*|,\cos\theta)\mu_j(v_*)\,\mathrm{d}\sigma\,\mathrm{d}v_*.
\end{aligned}
$$

Proposition 2.12 ([G-22])**.** *The linearized operator* $\boldsymbol{\mathcal{K}} = \boldsymbol{\mathcal{L}} - \boldsymbol{\nu}\,\mathrm{Id}$ *is compact from* $L^2(\boldsymbol{\mu}^{-1/2})$ *to* $L^2(\boldsymbol{\mu}^{-1/2})$.

The proof follows a standard path for such compactness results.

- The core of the work is to write each operator under a kernel form

  $$\int_{\mathbb{R}^3} k_i(v,w) g(w) \mu(w)^{-1/2}\,\mathrm{d}w.$$

  It is of course obvious for $\boldsymbol{\mathcal{K}}_1$, but needs some work for $\boldsymbol{\mathcal{K}}_2$ and $\boldsymbol{\mathcal{K}}_3$.

- We use the characterization of a compact operator as an operator satisfying a uniform decay at infinity and an equicontinuity property. These two properties follow from bounds on the growth in v of the L^1-norm (in w) of the kernel k_i, as well as $L^2(\mathbb{R}^3 \times \mathbb{R}^3)$-bounds on both variables.

Let us now briefly discuss the obtention of a kernel form. In the case of $\boldsymbol{\mathcal{K}}_3$, as well as in the case of the terms in $\boldsymbol{\mathcal{K}}_2$ for which $m_j = m_i$, the kernel form is obtained following Grad's approach [103], with a succession of suitable changes of variables. The geometrical argument of Grad is based on the ω-parametrization of the collision rules:

$$v' = \frac{m_i v + m_j v_*}{m_i + m_j} + \frac{m_j}{m_i + m_j}\Big[v - v_* - 2\big((v - v_*)\cdot\omega\big)\omega\Big], \tag{2.34a}$$

$$v'_* = \frac{m_i v + m_j v_*}{m_i + m_j} - \frac{m_i}{m_i + m_j}\Big[v - v_* - 2\big((v - v_*)\cdot\omega\big)\omega\Big]. \tag{2.34b}$$

It consists in performing the change of variable $(v_* - v, \omega)$ into the decomposition of $v_* - v$ parallel and orthogonal to ω. However, this approach fails in the case of different masses.

We detail succinctly the case of the terms in $\boldsymbol{\mathcal{K}}_2$ for which $m_j \neq m_i$, which needs a novel approach. We can write

$$[\boldsymbol{\mathcal{K}}_2]_i(\boldsymbol{g}) = n_i \sum_{j=1}^{N} \int_{\mathbb{R}^3} \left(\int_{\mathbb{S}^2} B_{ij}(v, v_*, \sigma) \mu_i(v') \mu_j(v'_*)^{1/2} \, \mathrm{d}\sigma \right) g_j(v'_*) \mu_j(v'_*)^{-1/2} \, \mathrm{d}v_*. \tag{2.35}$$

From the conservation of energy (2.2b), we have

$$\mu_i(v')\mu_j(v'_*)^{1/2} = \mu_i(v)\mu_j(v_*)\mu_j(v'_*)^{-1/2} = \mu_j(v_*)^{1/2}\mu_i(v')^{1/2}. \tag{2.36}$$

The main idea is then to change variables by transforming (v', v_*) into (v, v'_*), which takes into account properly the crossing effect between the species. The obtention of a kernel form thus relies on the following observation: there exists a constant $\mathfrak{C}$ such that for all i, j with $m_i \neq m_j$, we have

$$m_i|v'|^2 + m_j|v_*|^2 \geq \mathfrak{C}\left(m_i|v|^2 + m_j|v'_*|^2 \right). \tag{2.37}$$

Combining (2.36) with (2.37), the terms in the parenthesis in (2.35) lead to the kernel form of $\boldsymbol{\mathcal{K}}_2$. The proof of inequality (2.37) is obtained by using $|v - v_*|\sigma = v - v_* - 2(\omega\cdot(v - v_*))\omega$ in the collision rules (2.34), which allows to rewrite it in the following way

$$(\mathbb{I}_3 - 2\frac{m_i}{m_i + m_j}\omega\omega^\mathsf{T})v_* = v'_* - 2\frac{m_i}{m_i + m_j}\omega\omega^\mathsf{T} v,$$

where $\mathbb{I}_3$ is the identity matrix of $\mathbb{R}^3$. Defining the matrix $X = \mathbb{I}_3 - 2\frac{m_i}{m_i+m_j}\omega\omega^\mathsf{T}$, we have $X v_* = v'_* + (X - \mathbb{I}_3)v$. It is possible to compute $\det X = (m_j - m_i)/(m_i + m_j)$, and thus to invert X in the case of different masses. This allows to write the following relation

$$\begin{pmatrix} \sqrt{m_i}v' \\ \sqrt{m_j}v_* \end{pmatrix} = \mathbb{X} \begin{pmatrix} \sqrt{m_i}v \\ \sqrt{m_j}v'_* \end{pmatrix},$$

where the block matrix $\mathbb{X}$ is defined by blocks involving X and the masses. We can thus estimate its norm, giving the needed lower bound.

Remark 2.13. *Note that another Carleman representation for the multi-species Boltzmann operator has been proved in [42] of the following form*

$$\int_{\mathbb{R}^3\times\mathbb{S}^2} B_{ij}(|v - v_*|, \cos\theta) f_i(v') f_j(v'_*) \, \mathrm{d}\sigma \, \mathrm{d}v_*$$
$$= C_{ij} \int_{\mathbb{R}^3} \frac{1}{|v - v_*|} \int_{H^{ij}_{vv_*}} \frac{B_{ij}(v - V(v_*, u), \frac{u - v_*}{|u - v_*|})}{|u - v_*|} f_i(u) \, \mathrm{d}H(u) \, f_j(v_*) \, \mathrm{d}v_*, \tag{2.38}$$

where $V(u,v_*) = v_* + \frac{m_i}{m_j}(u-v)$, *and* $\mathrm{d}H$ *denotes the Lebesgue measure on the hyperplane* $H^{ij}_{vv_*}$, *which is orthogonal to* $v-v_*$ *and passing through* $\frac{m_i+m_j}{2m_j}v - \frac{m_i-m_j}{2m_j}v_*$. *This also allows to deduce a kernel form of the operator* $\boldsymbol{\mathcal{K}}$.

Further, the kernel of the linearized operator $\boldsymbol{\mathcal{L}}$ is spanned by the functions $\phi^{(r)}$, $1 \le r \le N+4$, defined by

$$\begin{aligned}
\boldsymbol{\phi}^{(i)}(v) &= \frac{1}{\sqrt{\boldsymbol{n}}}\boldsymbol{e}_i\boldsymbol{n}\boldsymbol{\mu}, \qquad 1 \le i \le N,\\
\boldsymbol{\phi}^{(N+k)}(v) &= \frac{v_k}{\sqrt{\sum_j m_j n_j}}\boldsymbol{m}\boldsymbol{n}\boldsymbol{\mu}, \qquad 1 \le k \le 3,\\
\boldsymbol{\phi}^{(N+4)}(v) &= \frac{1}{\sqrt{6\sum_j n_j}}(\boldsymbol{m}|v|^2 - 3)\boldsymbol{n}\boldsymbol{\mu}.
\end{aligned}$$

These functions form an orthonormal basis of $\operatorname{Ker}\boldsymbol{\mathcal{L}}$ in $L^2((\boldsymbol{n}\boldsymbol{\mu})^{-1/2})$. Let us denote by $\boldsymbol{\pi}_{\boldsymbol{\mathcal{L}}}$ the orthogonal projection on $\operatorname{Ker}\boldsymbol{\mathcal{L}}$ in $L^2((\boldsymbol{n}\boldsymbol{\mu})^{-1/2})$. In [42], the following spectral gap property of the linearized operator $\boldsymbol{\mathcal{L}}$ around a global Maxwellian is proved.

Proposition 2.14. *The operator* $\boldsymbol{\mathcal{L}}$ *is a closed self-adjoint operator in* $L^2((\boldsymbol{n}\boldsymbol{\mu})^{-1/2})$. *There exist* $C_{\boldsymbol{\mathcal{L}}}, \lambda_{\boldsymbol{\mathcal{L}}} > 0$ *such that for all* $\boldsymbol{g} \in L^2((\boldsymbol{n}\boldsymbol{\mu})^{-1/2})$, *we have*

$$\langle \boldsymbol{\mathcal{L}}(\boldsymbol{g}), \boldsymbol{g}\rangle_{\boldsymbol{n}\boldsymbol{\mu}} \le -\lambda_{\boldsymbol{\mathcal{L}}}\|\boldsymbol{g} - \boldsymbol{\pi}_{\boldsymbol{\mathcal{L}}}(\boldsymbol{g})\|^2_{L^2(\langle v\rangle^\gamma(\boldsymbol{n}\boldsymbol{\mu})^{-1/2})} \le -\lambda_{\boldsymbol{\mathcal{L}}}\|\boldsymbol{g} - \boldsymbol{\pi}_{\boldsymbol{\mathcal{L}}}(\boldsymbol{g})\|^2_{\boldsymbol{n}\boldsymbol{\mu}} \tag{2.39}$$

and

$$\|\boldsymbol{\mathcal{L}}(\boldsymbol{g})\|_{\boldsymbol{n}\boldsymbol{\mu}} \le C_{\boldsymbol{\mathcal{L}}}\|\boldsymbol{g}\|_{L^2(\langle v\rangle^\gamma(\boldsymbol{n}\boldsymbol{\mu})^{-1/2})},$$

where $\langle v\rangle^\gamma = (1+|v|^2)^{\gamma/2}$.

Remark 2.15. *In [G-6], we tracked the explicit dependence of the constants involved in the control estimates of* $\boldsymbol{\mathcal{L}}$ *with respect to the number densities* $\boldsymbol{n}$. *This allows us to obtain an explicit formula for* $\lambda_{\boldsymbol{\mathcal{L}}}$ *depending on the masses, the cross sections, the collision frequencies and the number densities.*

2.4.3 Stability of the spectral gap

We can now focus on the properties of the linearized operator $\boldsymbol{L}^\varepsilon$ around the local Maxwellian $\boldsymbol{M}^\varepsilon$, which satisfies the following almost spectral gap property. We assume in this section that $\boldsymbol{\mathcal{L}}$ is the linearized operator around $\boldsymbol{\mu}$ (*i.e.* $\boldsymbol{n} = 1$ in the expansion) for simplicity, since the macroscopic number densities are carried by the local Maxwellian (2.32).

Theorem 2.16 ([G-10])**.** *There exists* $\delta > 0$ *such that for any* $\boldsymbol{g} \in L^2(\boldsymbol{\mu}^{-1/2})$, *we have*

$$\langle \boldsymbol{L}^\varepsilon(\boldsymbol{g}), \boldsymbol{g}\rangle_{\boldsymbol{\mu}} \le -\left(\lambda_{\boldsymbol{\mathcal{L}}} - \varepsilon R^\varepsilon(\boldsymbol{u})\right)\|\boldsymbol{g} - \boldsymbol{\pi}_{\boldsymbol{\mathcal{L}}}(\boldsymbol{g})\|^2_{L^2(\langle v\rangle^\gamma\boldsymbol{\mu}^{-1/2})} + \varepsilon R^\varepsilon(\boldsymbol{u})\|\boldsymbol{\pi}_{\boldsymbol{\mathcal{L}}}(\boldsymbol{g})\|^2_{L^2(\langle v\rangle^\gamma\boldsymbol{\mu}^{-1/2})},$$

where

$$R^\varepsilon(\boldsymbol{u}) = C(\delta)\max_{1\le i\le N}\left\{n_i^{1-\delta}|u_i|\left(1 + \varepsilon|u_i|e^{\frac{4m_i}{1-\delta}\varepsilon^2|u_i|^2}\right)\right\}.$$

Let us mention the different steps of the proof, without going into the technical details and the tedious computations.

- The first step is the penalization of the operator $\boldsymbol{L}^{\varepsilon}$ by the operator $\boldsymbol{\mathcal{L}}$, by splitting the Dirichlet form as follows

  $$\langle \boldsymbol{L}^{\varepsilon}(\boldsymbol{g}), \boldsymbol{g} \rangle_{\boldsymbol{\mu}} = \langle \boldsymbol{\mathcal{L}}(\boldsymbol{g}), \boldsymbol{g} \rangle_{\boldsymbol{\mu}} + \langle (\boldsymbol{L}^{\varepsilon} - \boldsymbol{\mathcal{L}})(\boldsymbol{g}), \boldsymbol{g} \rangle_{\boldsymbol{\mu}}.$$

  The first term is obviously handled by the spectral gap property (2.39) of $\boldsymbol{\mathcal{L}}$.

- As for the second part, it can be split into different terms $\mathcal{T}_k$, each containing a factor of the form $\boldsymbol{M}^{\varepsilon} - \boldsymbol{\mu}$ for different velocity variables. We naturally expect the local Maxwellian to remain close to the global one, since the macroscopic quantities of the two Maxwellians are close to each other at order ε. We can estimate the growth of the difference by the growth of the global one $\boldsymbol{\mu}$, in the following way

  $$|\boldsymbol{M}^{\varepsilon}(w) - \boldsymbol{\mu}(w)| \leq \varepsilon R^{\varepsilon}(\boldsymbol{u}) \boldsymbol{\mu}^{\delta}(w),$$

  for $w \in \{v, v_*, v', v'_*\}$ and for any $\delta \in (0,1)$. This term is indeed of order ε, but only displays $\boldsymbol{\mu}^{\delta}$ instead of a full $\boldsymbol{\mu}$ to be dealt with in the weighted space. The terms $\mathcal{T}_k$ involving v and v_* are easy to bound.

- However, it remains to handle the ones involving v' and v'_*. We use the explicit kernel form from the Carleman representation (2.38) (and a corresponding one when switching velocities v' and v'_*). In a similar way as in [42], the kernels are bounded pointwise so as to regain a full Maxwellian decay. This is possible because of a smoothing effect in weights, meaning that the kernel features an exponential decay that can compensate a loss $\boldsymbol{\mu}^{\frac{1-\delta}{2}}$, and thus regain a full Maxwellian decay for a good choice of δ. This smoothing effect is of the form, for some constant $\zeta > 0$,

  $$|k_i| \leq C(|v - v_*|^{\gamma} + |v - v_*|^{\gamma - 2}) e^{-\delta\zeta |v - v_*|^2 - \delta\zeta \frac{\left||v|^2 - |v_*|^2\right|^2}{|v - v_*|^2}} \mu_i(v)^{\delta/2} \mu_{i/j}(v_*)^{-\delta/2},$$

  which has to be bounded with the weights.

  - For the term involving the velocity variable v', the last term is this inequality is $\mu_i(v_*)^{-\delta/2}$, which makes the bound easier to obtain.
  - In the case of the velocity variable v'_*, the last term features $\mu_j(v_*)^{-\delta/2}$, meaning that the Maxwellians each decrease with a different rate (depending on the species' mass m_i and macroscopic velocity u_i). This comes from the fact that the component i of the integral operator also involve components g_j ($j \neq i$) of $\boldsymbol{g}$, and has to be estimated in $L^2(\mu_i^{-1/2})$, even though g_j lives in $L^2(\mu_j^{-1/2})$. This mixing of exponential decays requires to use an appropriate decomposition of the velocities.

2.5 Perturbative method around a global Maxwellian

As we discussed in Section 2.4.1, when performing an expansion with respect to the small parameter ε, one can choose to expand the distribution function around a global Maxwellian, or around a local one. In this section, we shall now investigate the case of an expansion around a global Maxwellian $\boldsymbol{\mu}$ of the form (2.29), meaning that we will be dealing directly with the linearized operator $\boldsymbol{\mathcal{L}}$.

2.5.1 Derivation of the Fick model from the Boltzmann equations

As we discussed in Section 2.1.2, the cross-diffusion Fick model is also used in the literature besides the Maxwell-Stefan model to describe diffusion of mixtures. We described previously the obtention of the Maxwell-Stefan equations as the hydrodynamic limit of the Boltzmann equations, and a natural question is whether the structure of the Fick equations (2.11) can also be retrieved as an hydrodynamic limit of the same Boltzmann equations for mixtures. This is the aim of this section. Let us first describe the formal computations leading to this structure.

As we already stated, we now consider an expansion around a global Maxwellian $\boldsymbol{f} = \boldsymbol{n}\boldsymbol{\mu} + \varepsilon \boldsymbol{g}$. Obviously, the moment of order zero of the scaled Boltzmann equations (2.5) gives, at the main order (ε), the mass conservation equation for each species, involving the first moment of $\boldsymbol{g}$ in the flux $\boldsymbol{J} = \int \boldsymbol{g} v \,\mathrm{d}v$. When injecting the expansion in the Boltzmann equation, the order ε^{-1} is trivial since $\boldsymbol{Q}(\boldsymbol{n}\boldsymbol{\mu}, \boldsymbol{n}\boldsymbol{\mu}) = 0$, and order ε^0 gives, for any $1 \leq i \leq N$

$$[\boldsymbol{\mathcal{L}}\boldsymbol{g}]_i = \mu_i v \cdot \nabla n_i. \tag{2.40}$$

Remark 2.17. *Since we know (*cf. *Section 2.4.2) that the operator* $\boldsymbol{\mathcal{L}}$ *is the sum of a compact and a multiplicative operator, and that its kernel is non trivial, Fredholm's alternative ensures the existence of a solution* $\boldsymbol{g}$ *to this equation provided* $\boldsymbol{\mu} v \cdot \nabla \boldsymbol{n} \in (\operatorname{Ker} \boldsymbol{\mathcal{L}})^{\perp}$ *(using that* $\boldsymbol{\mathcal{L}}$ *is selfadjoint) [G-22]. We computed in [G-6] that this condition corresponds to the fact that the total number density* n_{tot} *is constant in space. This leads the compatibility condition that* n_{tot} *has to be constant for the Fick equations.*

Further, the inversion of $\boldsymbol{\mathcal{L}}$ leads to

$$\boldsymbol{g} = \boldsymbol{\mathcal{L}}^{-1}(\boldsymbol{\mu} v \cdot \nabla \boldsymbol{n}) + \boldsymbol{\chi}, \tag{2.41}$$

with $\boldsymbol{\chi} \in \operatorname{Ker} \boldsymbol{\mathcal{L}}$. This allows to deduce the flux $\boldsymbol{J} = \int \boldsymbol{g} v \,\mathrm{d}v$ with the following arguments.

- We use the selfadjointness of $\boldsymbol{\mathcal{L}}^{-1}$ on its domain $(\operatorname{Ker} \boldsymbol{\mathcal{L}})^{\perp}$ in the weighted $L^2((\boldsymbol{n}\boldsymbol{\mu})^{-1/2})$-space.
- We write the relation between the flux and $\boldsymbol{\mu} v$ in a tensorial way, and algebraic arguments similar to the ones used in Proposition 2.7 allow to recognize a relation of the form $\boldsymbol{J} = \boldsymbol{F}(\boldsymbol{n}) \nabla \boldsymbol{n}$, where the coefficients $\varphi_{ij}(\boldsymbol{n})$ of $\boldsymbol{F}(\boldsymbol{n})$ are given by
$$\varphi_{ij}(\boldsymbol{n}) = n_i \Big\langle \boldsymbol{\mathcal{L}}^{-1}\left(V \boldsymbol{\mu}_i \boldsymbol{e}_i - \boldsymbol{\pi}_{\boldsymbol{\mathcal{L}}}(V \mu_i \boldsymbol{e}_i)\right), V \boldsymbol{\mu}_j \boldsymbol{e}_j - \boldsymbol{\pi}_{\boldsymbol{\mathcal{L}}}(V \mu_j \boldsymbol{e}_j) \Big\rangle_{\boldsymbol{n}\boldsymbol{\mu}}, \tag{2.42}$$
with $V = (v_1 + v_2 + v_3)/3$.
- We use the explicit form of the kernel of $\boldsymbol{\mathcal{L}}$, which is spanned by the functions $\boldsymbol{\phi}^{(r)}$, $1 \leq r \leq N + 4$, to compute the part involving $\boldsymbol{\chi}$. This gives an additional vector field $\boldsymbol{X}(\boldsymbol{n})$, which depends on $\boldsymbol{n}$ since $\operatorname{Ker} \boldsymbol{\mathcal{L}}$ and the scalar product both involve $\boldsymbol{n}$.

We thus obtain formally the following model of Fick type

$$\partial_t \boldsymbol{n} + \nabla \cdot (\boldsymbol{F}(\boldsymbol{n}) \nabla \boldsymbol{n}) + \nabla \cdot \boldsymbol{X}(\boldsymbol{n}) = 0.$$

In order to obtain a Cauchy theory for this model, in a perturbative setting, we can apply the results of Section 2.2.2 (in particular Remark 2.5), provided the matrix $\boldsymbol{F}(\boldsymbol{n})$ satisfies the required properties. The diffusion coefficients of this cross-diffusion model are given by (2.42), and depend on the inverse of the linearized Boltzmann operator $\boldsymbol{\mathcal{L}}^{-1}$. We are thus led to study the properties of this operator, and in particular its spectral gap property, which follows from the properties of the linearized operator $\boldsymbol{\mathcal{L}}$ itself.

Proposition 2.18 ([G-6])**.** *The operator $\boldsymbol{\mathcal{L}}^{-1}$ is a closed self-adjoint operator in $(\operatorname{Ker}\boldsymbol{\mathcal{L}})^{\perp}$, and for all $\boldsymbol{h} \in (\operatorname{Ker}\boldsymbol{\mathcal{L}})^{\perp}$, we have*

$$\langle \boldsymbol{\mathcal{L}}^{-1}(\boldsymbol{h}), \boldsymbol{h}\rangle_{\boldsymbol{n\mu}} \leq -\frac{\lambda_{\boldsymbol{\mathcal{L}}}}{C_{\boldsymbol{\mathcal{L}}}^2}\|\boldsymbol{h}\|_{\boldsymbol{n\mu}}^2$$

and

$$\|\boldsymbol{\mathcal{L}}^{-1}(\boldsymbol{h})\|_{\boldsymbol{n\mu}} \leq \|\boldsymbol{h}\|_{L^2(\langle v\rangle^{\gamma}(\boldsymbol{n\mu})^{-1/2})} \leq \frac{1}{\lambda_{\boldsymbol{\mathcal{L}}}}\|\boldsymbol{h}\|_{\boldsymbol{n\mu}},$$

with constants $\lambda_{\boldsymbol{\mathcal{L}}}$ and $C_{\boldsymbol{\mathcal{L}}}$ whose dependence with respect to the number densities $\boldsymbol{n}$ is known explicitly.

From this, it is possible to ensure the claimed properties of the diffusion coefficients of the Fick model. Indeed, with the decomposition $\boldsymbol{F}(\boldsymbol{n}) = \boldsymbol{D}(\boldsymbol{n})\breve{\boldsymbol{F}}(\boldsymbol{n})$, defined in Section 2.2.2, we can compute explicitly $\operatorname{Ker}\breve{\boldsymbol{F}}(\boldsymbol{n}) = \operatorname{Span}(\boldsymbol{nm})$, as well as a control on the eigenvalues of the matrix $\breve{\boldsymbol{F}}(\boldsymbol{n})$ by using the spectral gap property of $\boldsymbol{\mathcal{L}}^{-1}$, again with respect to $\boldsymbol{n}$. This allows to deduce that $\breve{\boldsymbol{F}}(\boldsymbol{n})$ is coercive outside its kernel (for positive number densities $\boldsymbol{n} > 0$). We also have Sobolev estimates on the full matrix $\boldsymbol{F}(\boldsymbol{n})$ by continuity arguments with respect to $\boldsymbol{n}$. These properties are enough to apply Proposition 2.3 and deduce a Cauchy theory in a perturbative setting.

Remark 2.19 (Rigorous convergence towards the Fick equations)**.** *With an expansion around a local Maxwellian (as for Maxwell-Stefan equations) whose macroscopic quantities are perturbations of the solution of the Fick equations $\boldsymbol{n} = \bar{\boldsymbol{n}} + \varepsilon\tilde{\boldsymbol{n}}$ and $\boldsymbol{u} = \boldsymbol{X}(\bar{\boldsymbol{n}}) + \varepsilon\tilde{\boldsymbol{u}}$, one can prove the stability of the Maxwellian by applying the result of [30], and the convergence of the solution of the Boltzmann equation towards the solution of the Fick equations in a perturbative setting.*

2.5.2 Micro-macro decomposition

In the previous section, we observed that at the limit $\varepsilon \to 0$, the distribution function $\boldsymbol{f}$ tends to a distribution $\boldsymbol{n\mu}$ whose macroscopic quantity $\boldsymbol{n}$ is a perturbative solution of the Fick equations. This suggests to perform a micro-macro decomposition of the distribution function, in order to separate the macroscopic quantities from the microscopic part and the main order part of $\boldsymbol{n}$ from the perturbation. The method consists in considering the equilibrium perturbation as the sum of a macroscopic part and a microscopic one. The macroscopic part lives in a finite-dimensional subspace, and the associated coordinates solve some conservation laws of fluid type, whereas the microscopic part still solves a kinetic equation. Nevertheless, the microscopic part appears in the macroscopic conservation laws, in a intermediated way betwwen fluid and kinetic models. This decomposition plays an important role in the study of both mathematical and numerical properties of the solution of the linearized Boltzmann equation.

In the mono-species case, the micro-macro decomposition method has been introduced in [112, 113, 146, 147], and was used for different purposes (*e.g.* hypocoercivity estimates [72], large-time behavior studies [170], propagation of one-dimensional waves [148]). Furthermore, this method is a major tool in numerical analysis to build asymptotic-preserving schemes, allowing for instance to preserve some physical quantities [92], or some hydrodynamic limit [17], or quantify uncertainty [71]. In the case of mixtures, preliminary works have been done [42], as well as studies for a BGK approximation [130, 128]. In [G-5], we tackled the micro-macro decomposition for mixtures, and the corresponding energy method [147]. We studied the following decomposition

$$\boldsymbol{f} = \bar{\boldsymbol{n}}\boldsymbol{\mu} + \varepsilon(\boldsymbol{g}^0 + \boldsymbol{g}^1),$$

where $\bar{\boldsymbol{n}}$ is constant, and the perturbation $\boldsymbol{g}$ is split into the sum of its macroscopic part $\boldsymbol{g}^0 \in \operatorname{Ker} \boldsymbol{\mathcal{L}}$ and microscopic part $\boldsymbol{g}^1 \in (\operatorname{Ker} \boldsymbol{\mathcal{L}})^\perp = \operatorname{Im} \boldsymbol{\mathcal{L}}$. It satisfies the following equation

$$\partial_t \boldsymbol{g} + v \cdot \nabla \boldsymbol{g} - \boldsymbol{\mathcal{L}}(g) = \boldsymbol{Q}(\boldsymbol{g}, \boldsymbol{g}). \tag{2.43}$$

Let us define the macroscopic quantities associated to the perturbation $\boldsymbol{g}^0$ as follows

$$\begin{aligned} \tilde{n}_i &= \langle \boldsymbol{g}^0, \boldsymbol{\phi}^{(i)} \rangle_{\bar{\boldsymbol{n}}\boldsymbol{\mu}}, \qquad && 1 \le i \le N, && (2.44a) \\ q_k &= \langle \boldsymbol{g}^0, \boldsymbol{\phi}^{(N+k)} \rangle_{\bar{\boldsymbol{n}}\boldsymbol{\mu}}, \qquad && 1 \le k \le 3, && (2.44b) \\ e &= \langle \boldsymbol{g}^0, \boldsymbol{\phi}^{(N+4)} \rangle_{\bar{\boldsymbol{n}}\boldsymbol{\mu}}. && && (2.44c) \end{aligned}$$

The method relies on the orthogonal decomposition of the functional space onto $\operatorname{Ker} \boldsymbol{\mathcal{L}}$ and $(\operatorname{Ker} \boldsymbol{\mathcal{L}})^\perp$, and we define the orthogonal projections $\boldsymbol{P}^0$ and $\boldsymbol{P}^1$ on these subspaces. We then have the following result.

Proposition 2.20 ([G-5])**.** *The fluid quantities of $\boldsymbol{g}^0$ satisfy the following conservation laws*

$$\partial_t \tilde{n}_i + \sqrt{\frac{\bar{n}_i}{\sum_j m_j \bar{n}_j}} \nabla \cdot q + \langle \boldsymbol{P}^0(v \cdot \nabla \boldsymbol{g}^1), \boldsymbol{\phi}^{(i)} \rangle_{\bar{\boldsymbol{n}}\boldsymbol{\mu}} = 0, \qquad 1 \le i \le N, \tag{2.45a}$$

$$\partial_t q_k + \frac{1}{\sqrt{\sum_j m_j \bar{n}_i}} \partial_{x_k} \left(\sum_i \sqrt{\bar{n}_i} \tilde{n}_i + \sqrt{\frac{2}{3} \sum_j \bar{n}_j e} \right) + \langle \boldsymbol{P}^0(v \cdot \nabla \boldsymbol{g}^1), \boldsymbol{\phi}^{(N+k)} \rangle_{\bar{\boldsymbol{n}}\boldsymbol{\mu}} = 0, \qquad 1 \le k \le 3 \tag{2.45b}$$

$$\partial_t e + \sqrt{\frac{2 \sum_j \bar{n}_j}{3 \sum_j m_j \bar{n}_j}} \nabla \cdot q + \langle \boldsymbol{P}^0(v \cdot \nabla \boldsymbol{g}^1), \boldsymbol{\phi}^{(N+4)} \rangle_{\bar{\boldsymbol{n}}\boldsymbol{\mu}} = 0, \tag{2.45c}$$

where $q = (q_1, q_2, q_3)$.

The projection of the Boltzmann equation (2.5) on $\operatorname{Ker} \boldsymbol{\mathcal{L}}$ and $(\operatorname{Ker} \boldsymbol{\mathcal{L}})^\perp$ leads to the following equations

$$\begin{aligned} &\partial_t \boldsymbol{g}^0 + \boldsymbol{P}^0(v \cdot \nabla \boldsymbol{g}^0) + \boldsymbol{P}^0(v \cdot \nabla \boldsymbol{g}^1) = 0, \\ &\partial_t \boldsymbol{g}^1 + \boldsymbol{P}^1(v \cdot \nabla \boldsymbol{g}^0) + \boldsymbol{P}^1(v \cdot \nabla \boldsymbol{g}^1) - \boldsymbol{\mathcal{L}} \boldsymbol{g}^1 = \boldsymbol{Q}(\boldsymbol{g}, \boldsymbol{g}). \end{aligned}$$

By inverting $\boldsymbol{\mathcal{L}}$ on $(\operatorname{Ker} \boldsymbol{\mathcal{L}})^\perp$, we can express $\boldsymbol{g}^1$ from the second equation, and insert it in the first one

$$\partial_t \boldsymbol{g}^0 + \boldsymbol{P}^0(v \cdot \nabla \boldsymbol{g}^0) + \boldsymbol{P}^0 \Big(v \cdot \nabla \boldsymbol{\mathcal{L}}^{-1} \Big(\partial_t \boldsymbol{g}^1 + \boldsymbol{P}^1(v \cdot \nabla \boldsymbol{g}^0) + \boldsymbol{P}^1(v \cdot \nabla \boldsymbol{g}^1) - \boldsymbol{Q}(\boldsymbol{g}, \boldsymbol{g}) \Big) \Big) = 0. \tag{2.46}$$

Let us detail how an energy estimate can be obtained with this decomposition.

- ✍ We can first multiply (2.43) by $\boldsymbol{g}$ and use the spectral gap of $\boldsymbol{\mathcal{L}}$ to control some norm of $\boldsymbol{g}^1$ (related to the $L^2((\boldsymbol{n\mu})^{-1/2})$-norm). In this process, in order to handle the terms coming from the quadratic operator $\boldsymbol{Q}$, we impose a smallness condition on the $L^\infty_{t,x}$-norm of $\boldsymbol{g}$ in the same way as in [147]. We can also obtain the control of norms of the time and space derivatives of $\boldsymbol{g}^1$ in a similar way. However, the control of the macroscopic part $\boldsymbol{g}^0$ is then missing.

- Such a control will be obtained by a lower bound on the term $\|\boldsymbol{P}^1(v \cdot \nabla \boldsymbol{g}^0)\|_{\bar{\boldsymbol{n}}\boldsymbol{\mu}} = \|v \cdot \nabla \boldsymbol{g}^0\|_{\bar{\boldsymbol{n}}\boldsymbol{\mu}} - \|\boldsymbol{P}^0(v \cdot \nabla \boldsymbol{g}^0)\|_{\bar{\boldsymbol{n}}\boldsymbol{\mu}}$. The terms $v \cdot \nabla \boldsymbol{g}^0$ and $\boldsymbol{P}^0(v \cdot \nabla \boldsymbol{g}^0)$ can both be computed explicitly, and involve the macroscopic quantities (2.44). Contrary to the monospecies case, where the density is not controlled, we can obtain a control of the norm of the space derivative of the full macroscopic quantities. The key idea to this novel estimate is to take advantage of the specific structure of the conservation law (2.45b), and handle $\sum_i \sqrt{\bar{n}_i}\nabla\tilde{n}_i + \sqrt{\frac{2}{3}\sum_j \bar{n}_j}\nabla e$ as a whole, instead of only $\nabla\tilde{n}_i$ and ∇e separately. Moreover, Cauchy-Schwarz inequality is only used on a fraction of this macroscopic term, keeping the other part to give further control using the conservation laws. In the end, we control a positive definite quadratic form of $\nabla \boldsymbol{g}^0$, which is equivalent to the $L^2((\bar{\boldsymbol{n}}\boldsymbol{\mu})^{-1/2})$-norm.

- A control of $\boldsymbol{g}^0$ (not only its space derivative), is still missing but needed, since the nonlinear term involves $\boldsymbol{g}$, and not only $\boldsymbol{g}^1$ (since $\boldsymbol{Q}(\boldsymbol{g}^0, \boldsymbol{g}^0) \neq 0$), and derivatives of this quadratic term involve both derivatives of $\boldsymbol{g}$ and $\boldsymbol{g}$ itself. When multiplying (2.46) by $\boldsymbol{g}^0$, we observe that there is no way to exhibit such an estimate. In order to circumvent this problem, we introduce the antiderivative in space of $\boldsymbol{g}^0$, which restricts the analysis to the 1D case. Nevertheless, in this case, we can obtain a roughly similar energy estimate on the space derivative of the antiderivative of $\boldsymbol{g}^0$, giving some control on $\boldsymbol{g}^0$ itself. We then also impose a smallness condition on the $L^\infty_{t,x}$-norm of the antiderivative of $\boldsymbol{g}^0$.

- Combining all these estimates with a suitable choice of constants allows to obtain a lower order estimate, controlling basically the $H^1_{t,x}$-norm of $\boldsymbol{g}$ by its initial value. However, this estimate is not closed, in the sense that the requirement of the smallness assumption concerns $L^\infty_{t,x}$-norms, and $H^1_{t,x}$ does not continuously inject in $L^\infty_{t,x}$. Therefore, we derive a higher-order estimate involving more derivatives with respect to t and x, by derivating the equations as many times as necessary and estimating in the same way as for the lower-order one. We finally obtain the controls of $H^5_{t,x}$-norms of $\boldsymbol{g}^0$ and $\boldsymbol{g}^1$ by their initial values. This time, the estimate is closed, since $H^5_{t,x} \hookrightarrow W^{2,\infty}_{t,x}$, which is the norm involved in the higher-order smallness assumption. Then, as long as the initial data is small enough in $H^5_{t,x}$, the solution remains small in $H^5_{t,x}$, which proves in particular the stability of the global Maxwellian in large time as stated below.

Theorem 2.21 ([G-5])**.** *For any global Maxwellian $\bar{\boldsymbol{n}}\boldsymbol{\mu}$, provided the perturbation $\boldsymbol{g}$ is initially small enough in $H^s_x(L^2((\bar{\boldsymbol{n}}\boldsymbol{\mu})^{-1/2}))$, for $s \geq 5$, there exists a constant C such that*

$$\|\boldsymbol{f}(t,x,v) - \bar{\boldsymbol{n}}\boldsymbol{\mu}\|_{H^s_{t,x}(L^2((\bar{\boldsymbol{n}}\boldsymbol{\mu})^{-1/2}))} \leq C, \qquad \lim_{t\to\infty} \|\boldsymbol{f}(t,x,v) - \bar{\boldsymbol{n}}\boldsymbol{\mu}\|_{H^s_{t,x}(L^2((\bar{\boldsymbol{n}}\boldsymbol{\mu})^{-1/2}))} = 0.$$

2.6 Numerical approach for the hydrodynamic limit

Since the convergence of the Boltzmann equation for mixtures towards the Maxwell-Stefan equations has been proved in the diffusive limit, we are interested in deriving a numerical scheme which could capture the behavior of both the physical solutions to the Boltzmann equations in a rarefied regime and describe the solutions of the Maxwell-Stefan equations in the fluid regime. Because the collision term (and, in a lesser way, the transport term) become stiffer when the parameter ε tends to zero, this requires a careful treatment. For example, for moderately rarefied regimes, the macroscopic description is not precise enough but the kinetic methods for the Boltzmann equation struggle with the stiffness of the collision operator. In this context, the need of a scheme able to describe both regimes, *i.e.* an asymptotic-preserving (AP) scheme, arises. In particular, a satisfactory numerical scheme needs to describe properly the solutions in both regimes while maintaining discretization parameters independent of ε.

Several approaches have been used to develop such AP schemes. Let us mention splitting methods [91, 68], IMEX schemes [69, 70], or the micro-macro decomposition already mentioned in Section 2.5.2 [17, 142, 92]. A further IMEX approach, introduced by [86], is to use a penalization method on the collision term by a suitable linear BGK operator, allowing to handle the nonlinear term explicitly, while the linear BGK operator is treated implicitly. However, in the diffusive scaling, the transport term is also stiff (although less than the collision term), and this stiffness prevents from extending in a straightforward way the techniques mentioned above. In the case of linear collision operators, several authors overcame this difficulty [133, 129, 50]. In [G-12], we propose a numerical approach for the full mixture Boltzmann operator circumventing these difficulties by imposing a Maxwellian ansatz, and using the moment method.

2.6.1 Description of the scheme

Inspired by the theoretical results on the asymptotic limit towards the Maxwell-Stefan equations, we propose a numerical scheme based on the moment method [G-12]. Such a scheme relies on the same ansatz (2.16) that the distribution functions are at local Maxwellian states, and on the computation of their moments.

The numerical scheme is based on the discretization of the two moment equations (2.17a)–(2.17b) with an explicit computation of the collision term as in (2.18) for Maxwell molecules (or possibly (2.20) for general cross sections). We tackle only the case of dimension 1 ($d = 1$) because the extension to higher dimensions of the proofs on the properties of the scheme is not straightforward. The system in 1D is thus

$$
\begin{gathered}
\partial_t n_i + \partial_x J_i = 0, \\
\varepsilon^2 \partial_t J_i + \varepsilon^2 \partial_x (n_i u_i^2) + \frac{k_B T}{m_i} \partial_x n_i = \sum_{j=1}^{N} \frac{1}{D_{ij}} n_i n_j (u_j - u_i).
\end{gathered}
$$

The right-hand side of the momentum equation, involving the interaction between all species, can be written under a matrix form as

$$
\varepsilon^2 \partial_t J_i + \varepsilon^2 \partial_x (n_i u_i^2) + \frac{k_B T}{m_i} \partial_x n_i = [\boldsymbol{A}(\boldsymbol{n}) \boldsymbol{J}]_i,
$$

where $\boldsymbol{n} = (n_i)_i$ and $\boldsymbol{J} = (J_i)_i$ are the vectors of the number densities and the fluxes, and $\boldsymbol{A}(\boldsymbol{n})$ is the Maxwell-Stefan matrix.

Let us define Δx and Δt the discretization parameters in space and time, and denote by $\star_{i,\ell}^n$ an approximate value of $\star_i(n\Delta t, \ell \Delta x)$. We use a staggered dual grid, so that the number densities n_i are evaluated at points $\ell \Delta x$, whereas the fluxes J_i are evaluated at points $(\ell + 1/2)\Delta x$.

Let us describe the main ideas of the scheme.

- ✍ Time discretization: the nonlinear term $\varepsilon^2 \partial_x (n_i u_i^2)$ is treated explicitly, whereas the linear term $\partial_x n_i$ and the Maxwell-Stefan contribution $\sum_j n_i n_j (u_j - u_i)/D_{ij}$ are treated implicitly.
- ✍ Space discretization:
  - ▷ Since the momentum equation is evaluated at points $(\ell + 1/2)\Delta x$, the values of n_i at these points (involved in the Maxwell-Stefan term and in the nonlinear one) have to be interpolated from the staggered grid. We shall see that, in order to ensure nonnegativity of the number densities, an appropriate choice is to impose $n_{i,\ell+1/2} = \min(n_{i,\ell}, n_{i,\ell+1})$.

▷ The nonlinear term is rewritten as $\varepsilon^2\partial_x(n_i u_i^2) = \varepsilon^2\partial_x(J_i^2/n_i)$, when $n_i \neq 0$. In this derivative, the values of the fluxes at the grid points $\ell\Delta x$ are computed as the mean between the values at the staggered points $(\ell+1/2)\Delta x$ and $(\ell-1/2)\Delta x$.

✍ We rely on two rewritings of the scheme. First, the vectorial form, which is given for any n, ℓ, by:

$$\frac{\boldsymbol{n}_\ell^{n+1}-\boldsymbol{n}_\ell^n}{\Delta t}+\frac{\boldsymbol{J}_{\ell+1/2}^{n+1}-\boldsymbol{J}_{\ell-1/2}^{n}}{\Delta x}=0, \tag{2.47a}$$

$$[\boldsymbol{A}(\boldsymbol{n})\boldsymbol{J}]_{\ell+1/2}^{n+1}-\varepsilon^2\frac{\boldsymbol{J}_{\ell+1/2}^{n+1}}{\Delta t}=k_BT\frac{\boldsymbol{n}_{\ell+1}^{n+1}-\boldsymbol{n}_\ell^{n+1}}{\boldsymbol{m}\Delta x}+\varepsilon^2\boldsymbol{S}_{\ell+1/2}^n, \tag{2.47b}$$

where we used the following abuse of notation $\boldsymbol{n}/\boldsymbol{m} = (n_i/m_i)_{1\leq i\leq N}$, and where the explicit source term $\boldsymbol{S}$ is given by

$$\boldsymbol{S}_{\ell+1/2}^n=\frac{(\boldsymbol{J}_{\ell+3/2}^n+\boldsymbol{J}_{\ell+1/2}^n)^2}{4\boldsymbol{n}_{\ell+1}^n\Delta x}-\frac{(\boldsymbol{J}_{\ell+1/2}^n+\boldsymbol{J}_{\ell-1/2}^n)^2}{4\boldsymbol{n}_{\ell}^n\Delta x}-\frac{\boldsymbol{J}_{\ell+1/2}^n}{\Delta t}.$$

✍ Second, the matrix form of the scheme: introducing $\mathbf{n} = ((n_{i,\ell})_\ell)_i$ the vector of all number densities at all grid points, and similarly for the fluxes $\mathbf{J}$, the scheme can be written under the form

$$\begin{aligned}\mathbf{M}_{11}\mathbf{n}+\mathbf{M}_{12}\mathbf{J}&=\mathbf{b}_1,\\ \mathbf{M}_{21}\mathbf{n}+\mathbf{M}_{22}(\mathbf{n})\mathbf{J}&=\mathbf{b}_2,\end{aligned}$$

where $\mathbf{M}_{11}$, $\mathbf{M}_{12}$ and $\mathbf{M}_{21}$ are constant diagonal matrices, and $\mathbf{M}_{22}(\mathbf{n})$ comes from the Maxwell-Stefan term and depends on the number densities. This can be rewritten again as

$$\mathbb{M}(\mathbb{y}_1)\mathbb{y}=\mathbb{b}, \tag{2.48}$$

where $\mathbb{y}_1 = \mathbf{n}$, $\mathbb{y}_2 = \mathbf{J}$, $\mathbb{y} = (\mathbb{y}_1, \mathbb{y}_2)^\mathsf{T}$ and $\mathbb{M}$ (resp. $\mathbb{b}$) is a block matrix (resp. vector). Equation (2.48) can then be solved by a Newton fixed point method.

2.6.2 Existence and positivity of a solution

The different choices described previously, as well as the vectorial and matrix forms of the scheme allow to prove several properties of the scheme, in particular the existence of a solution and the nonnegativity of the number densities.

Proposition 2.22. *There exists a solution* $\mathbb{y} = (\mathbf{n}, \mathbf{J})^\mathsf{T}$ *to the numerical scheme* (2.47). *Moreover, for* ε *small enough, we can prove that a solution* $\mathbb{y} = (\mathbf{n}, \mathbf{J})^\mathsf{T}$ *satisfies that* $\mathbf{n}$ *is nonnegative.*

Let us mention some elements of the proof.

✍ The nonnegativity of the number densities is proved using the parabolic setting of the cross-diffusion equation and following an idea by [3]. It relies on introducing an auxiliary scheme similar to (2.47b) but with a modified Maxwell-Stefan matrix $\hat{\boldsymbol{A}} = \boldsymbol{A}([\boldsymbol{n}]_+)$, where $[\star]_+ = \max(\star, 0)$ denotes the positive part of $\star$. The key point is then to prove some properties on this modified matrix $\hat{\boldsymbol{A}}$, in particular that it is invertible, and properties on the coefficients of its inverse $\hat{\boldsymbol{A}}^{-1}$:

- the diagonal coefficients are nonnegative;
- the extra diagonal coefficients all contain a factor containing a component of $[\boldsymbol{n}]_+$.

Then, expressing $\boldsymbol{J}$ as $\hat{\boldsymbol{A}}^{-1}$ applied to all terms of (2.47b) , and inserting it in the mass conservation equation, we obtain a diffusion equation on the solution $\hat{\boldsymbol{n}}$ of this auxiliary system, and we can derive a priori estimates by multiplying by the negative part $[\hat{\boldsymbol{n}}_\ell^{n+1}]_-$. Now, the extra diagonal terms involving $[\hat{\boldsymbol{n}}_{\ell+1/2}]_+ \times [\hat{\boldsymbol{n}}_\ell]_-$ are zero, because of the definition of $\hat{\boldsymbol{n}}_{\ell+1/2} = \min(\hat{\boldsymbol{n}}_\ell, \hat{\boldsymbol{n}}_{\ell+1})$. As for the diagonal terms, they have a definite sign up to a term of order ε^2, which is controlled for ε small enough, as long as the terms $\varepsilon^2 \boldsymbol{S}^n_{\ell+1/2}$ tend to zero when ε tend to zero. This allows to prove an a priori estimate on $[\hat{\boldsymbol{n}}_\ell^{n+1}]_-$, and in the end that

$$\|[\hat{\boldsymbol{n}}_\ell^{n+1}]_-\|^2 \leq 0.$$

The number densities $\hat{\boldsymbol{\mathsf{n}}}$ are thus nonnegative, and are therefore also solutions of the original system.

✍ The existence is easily proved by considering a similar auxiliary scheme for (2.48), in which $\boldsymbol{\mathsf{n}}$ is replaced by $[\boldsymbol{\mathsf{n}}]_+$ in $\boldsymbol{\mathsf{M}}_{22}(\boldsymbol{\mathsf{n}})$, allowing to define $\hat{\mathbb{M}}$ and $\hat{\mathbb{y}}_1$, $\hat{\mathbb{y}}$. Block computations and the diagonally dominant property lead to the invertibility of the matrix $\hat{\mathbb{M}}$. We apply Schaefer's fixed point theorem to conclude the existence of a solution $\hat{\mathbb{y}}$, which is also a solution to the original system since the number densities have been proved to be nonnegative.

2.6.3 Asymptotic-preserving behavior

Numerical tests were run on the standard Duncan and Toor experiment [74] mentioned before, which involves a three-species mixture in which one species (N_2) is initially at equilibrium (see Section 2.2.1). Whereas the diffusion on the other two species is standard, the density of N_2 presents a uphill diffusion behavior, which is a well-known feature of the Maxwell-Stefan equations, *i.e.* the species is dragged out of equilibrium by the movement of the other species and the friction properties of the species involved in the mixture.

The simulations of the scheme (2.48) are run with a constant diffusion CFL condition of the form $\Delta t \leq C \Delta x^2$, independent of the value of ε. The influence of the regime, *i.e.* the behaviors observed for different values of ε, is showed on Figure 2.4 for the three species at the same time. We observe in particular that for large values of ε, other phenomena than diffusion are involved, whereas the Maxwell-Stefan behavior is well-captured for small values of ε.

The AP-behavior is showed on Figure 2.5, where we observe that the solutions of the scheme (2.48) indeed converge to the solutions of the Maxwell-Stefan equations, approximated by the scheme mentioned in Section 2.2.1.

Prospect

A natural follow-up of this work is to derive a full kinetic AP scheme for the mixture Boltzmann equation in the diffusive scaling, without relying on a Maxwellian ansatz, and restricting ourselves to the macroscopic quantities. This could be done for example either *via* a micro-macro decomposition for mixtures [137], or by extending the projective integration method introduced in [9] to the diffusive asymptotic regime. Another path could be to follow recent results based on preserving hypocoercivity [72] at the discrete level [22, 23].

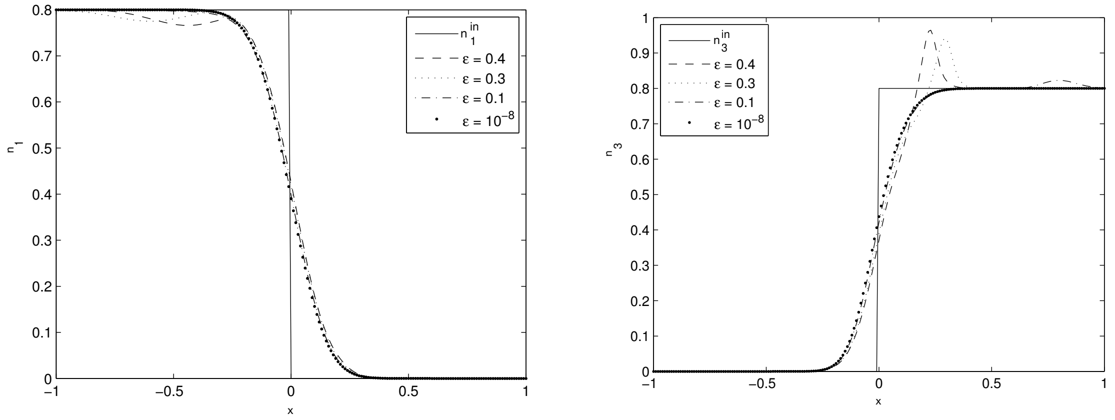

(a) H_2 (b) CO_2

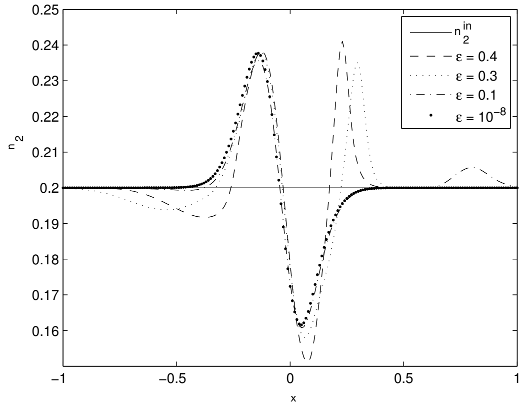

(c) N_2

Figure 2.4: Influence of the rarefaction regime (parameter ε) at time $t = 0.01$

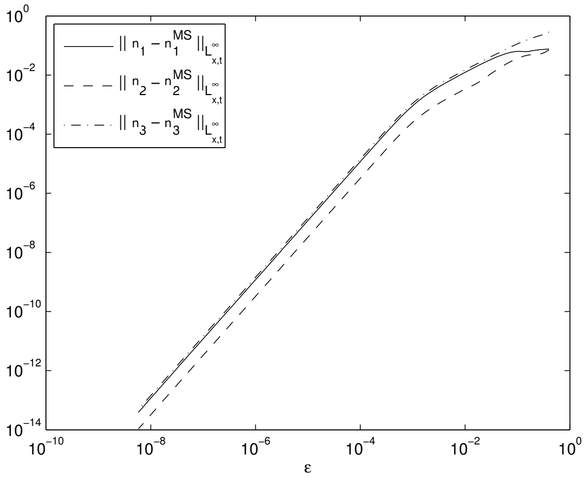

Figure 2.5: Convergence of the solutions of the scheme for the moments of the Boltzmann equation towards the solutions of the Maxwell-Stefan equations

2.7 Stiff dissipative hyperbolic formalism for diffusion models

Additionally to the hydrodynamic limits of the Boltzmann equation for mixtures, leading to the Maxwell-Stefan or the Fick models, we also investigated at the macroscopic level a system of fluid equations for mixtures with a stiff relaxation term of Maxwell-Stefan diffusion type. By applying the formalism of [55], we obtained in [G-13] a limit system of Fick type, where the species velocities tend to align to a bulk velocity when the relaxation parameter remains small. More precisely, let us consider the system on the number densities n_i and velocities u_i of any species i, $1 \leq i \leq N$

$$\partial_t n_i + \nabla \cdot (n_i u_i) = 0, \tag{2.49a}$$

$$\partial_t (n_i u_i) + \nabla \cdot (n_i u_i \otimes u_i) + \nabla P_i(n_i) + \frac{1}{\varepsilon} \sum_{j=1}^{N} a_{ij}(u_j - u_i) = 0, \tag{2.49b}$$

where $a_{ij} = n_i n_j / D_{ij}$, and the partial pressure of species i is given by the ideal gas law $P_i(n_i) = k_B T n_i$. We can prove the following result.

Proposition 2.23 ([G-13])**.** *The system* (2.49) *formally reduces to the following system when ε remains small*

$$\partial_t n_i + \nabla \cdot (n_i u_i) = \varepsilon \nabla \cdot \left(\sum_{j=1}^{N} \ell_{ij} \nabla P_j(n_j) \right), \tag{2.50a}$$

$$\partial_t (\rho_{\text{tot}} u) + \nabla \cdot (\rho_{\text{tot}} u \otimes u) + \nabla P_{\text{tot}} = 0, \tag{2.50b}$$

where we defined $\rho_{\text{tot}} = \sum_i m_i n_i$, $\rho_{\text{tot}} u = \sum_i m_i n_i u_i$ and $P_{\text{tot}} = \sum_i P_i(n_i)$, and the coefficients ℓ_{ij} are linked to the pseudoinverse of the matrix $\mathbb{A} = (a_{ij})_{i,j}$.

We observe on the reduced system that (2.50a) provide the mass conservation for each species, with a diffusive term of Fick type, appearing as a correction of order ε to the main convective flux. Equation (2.50b) is the only one available on the momentum, involving the total momentum of the mixture.

Let us describe how the formalism of Chen, Levermore and Liu [55] can be applied to the system (2.49).

- First, introducing the vector

  $$\mathsf{W} = \left(n_1, \cdots, n_N, n_1 u_1^{\mathsf{T}}, \cdots, n_N u_N^{\mathsf{T}} \right)^{\mathsf{T}},$$

  the system becomes

  $$\partial_t \mathsf{W} + \nabla \cdot \mathsf{F}(\mathsf{W}) + \frac{1}{\varepsilon} \mathsf{R}(\mathsf{W}) = 0, \tag{2.51}$$

  where F is the convective flux and R is the relaxation term of Maxwell-Stefan type.

- The relaxation term is endowed with a matrix $\mathbb{Q}$ such that $\mathbb{Q}\mathsf{R}(\mathsf{W}) = 0$. This yields the $N+1$ conserved quantities

  $$\mathsf{w} = \mathbb{Q}\mathsf{W} = \left(n_1, \cdots, n_N, \sum_{i=1}^{N} n_i u_i^{\mathsf{T}} \right)^{\mathsf{T}}.$$

  In addition, we assume that each such w determines a local equilibrium value $\mathcal{E}(\mathsf{w})$, satisfying $\mathbb{Q}\mathcal{E}(\mathsf{w}) = \mathsf{w}$. Associated with $\mathbb{Q}$ are $N+1$ conservation laws

  $$\partial_t \mathbb{Q}\mathsf{W} + \nabla \cdot (\mathbb{Q}\mathsf{F}(\mathsf{W})) = 0.$$

- If W is of the form $\mathcal{M}(\mathsf{w})$, with $\mathbb{Q}\mathcal{M}(\mathsf{w}) = \mathsf{w}$, then the previous equations relates $\partial_t \mathsf{w}$ to $-\nabla \cdot \mathbb{Q}\mathsf{F}(\mathcal{M}(\mathsf{w}))$. We can then deduce from (2.51) that
$$(\mathbb{I} - D_{\mathsf{w}}\mathcal{M}(\mathsf{w})\mathbb{Q})\nabla \cdot \mathsf{F}(\mathcal{M}(\mathsf{w})) + \frac{1}{\varepsilon}\mathsf{R}(\mathcal{M}(\mathsf{w})) = 0. \tag{2.52}$$
where $\mathbb{I}$ is the identity matrix.

- At the main order, one would only consider the equilibrium, leading to (2.50) with $\varepsilon = 0$. Taking into account the correction, we use the expansion at first order
$$\mathsf{W} = \mathcal{E}(\mathsf{w}) + \varepsilon\mathcal{M}^{(1)}(\mathsf{w})$$
in (2.52), and the order ε^0 leads to an expression of $\mathcal{M}^{(1)}$ provided the pseudoinversion of $D_{\mathsf{W}}\mathsf{R}(\mathcal{E}(\mathsf{w}))$. Last, the system is obtained from the equation on the conserved quantities w using the expansion and the expression of $\mathcal{M}^{(1)}$.

- In our case, it boils down to computing the pseudoinverse, as well as the correction term, whose expression involves $\mathbb{Q}$, $D_{\mathsf{W}}\mathsf{F}(\mathcal{E}(\mathsf{w}))$, $\mathbb{I} - D_{\mathsf{w}}\mathcal{M}(\mathsf{w})\mathbb{Q}$ and $\nabla \cdot \mathsf{F}(\mathcal{E}(\mathsf{w}))$. The pseudoinversion is considered by carefully determining the prescribed range and null space. Since R is linked to the matrix $\mathbb{A}$, whose range and null space are known explicitly, we can link its pseudoinverse to the pseudoinverse of $\mathbb{A}$. Further, block matrix computations lead to the claimed form of the limit system.

- Finally, the formalism of [55] also provides a simple criterion to ensure the local equilibrium hyperbolicity and the first-order correction dissipativity property, namely the existence of a strictly convex entropy. In our case, it is the total energy, which can be computed explicitly as the sum of the kinetic and internal energies
$$\eta = \sum_{i=1}^{N} \left\{ \frac{1}{2} n_i u_i^2 + k_B T n_i \left(\ln\left(\frac{n_i}{n_0}\right) - 1 \right) \right\}. \tag{2.53}$$

Prospect

This work could be extended to the non isothermal case, to see the influence of the temperature on the relaxation approximation. Moreover, it would be interesting to run numerical simulations to recover the behavior we have highlighted in this formalism.

2.8 Further works and prospects

In this section, I mention possible future works and perspectives on kinetic and macroscopic models for complex gases, some of which are already collaborations in progress.

2.8.1 Multiscale description

As we have seen, depending on the rarefaction regime, a kinetic or a fluid description can be used to model the behavior of a gas mixture. The kinetic description allows to capture rarefied regimes, at the cost of a higher complexity (and higher numerical costs), whereas the fluid limit only holds for small Knudsen numbers, but is much simpler to handle. In some applications, the flow can be locally rarefied, but fluid in other parts of the domain. In such a case, it would be of interest to couple spatially the two models.

Together with Etienne Bernard, Laurent Boudin, Virginie Ehrlacher, and Annamaria Massimini during her post-doctoral work, we investigate the spatial coupling of the Boltzmann equation with the Maxwell-Stefan systems. Indeed, in order to model solar cells based on semiconducting thin films, two regimes of description are needed. Let us explain very shortly the working of this device. The photovoltaic phenomena accounting for the efficiency of the whole solar cell occur inside a thin film, which is produced *via* a Physical Vapor Deposition process. More precisely, a substrate wafer is introduced in a hot chamber where different chemical species are injected under a gaseous form, best described by a kinetic model. Molecules deposit on the substrate surface, so that a thin film layer grows. In addition, the different components diffuse inside the bulk of the film, and a macroscopic model is enough in this part. In the end, the efficiency of the solar cell depends on the final chemical composition of the film.

Inspired by the work [136], we want to consider a Chapman-Enskog expansion of the distribution functions to derive criteria to determine the best regime to use in a given subdomain. This defines a hybrid kinetic/fluid model (and solver) with an automatic domain decomposition. Interface conditions would then be dealt with using a micro-macro decomposition of the distribution.

2.8.2 Polyatomic gases

In an effort to enhance the modelling of (mixtures of) gases, it is natural to extend the models to polyatomic gases. Indeed, all the works mentioned here have been conducted for mixtures of monatomic gases, and the extension to polyatomic gases is a challenging issue, since the number of degrees of freedom is larger, and the interactions between the different species are more complex. More precisely, the effect of the internal structure of a polyatomic molecule is reflected on the energy conservation law during a collision. Usually, an additional internal energy variable is introduced, either discrete or continuous [41, 64, 26, 27]. This new internal energy variable implies more difficulties to tackle the analysis of the Boltzmann equations, in particular one first step of the analysis of an hydrodynamic limit, namely the investigation of the properties of the linearized Boltzmann operator, for instance its compactness property (as in Section 2.4.2 for monatomic gases). With Niclas Bernhoff, Laurent Boudin and Milana Čolić, we reviewed in [G-1] the different compactness and Fredholm properties obtained in the literature for single polyatomic gases or for gas mixtures, with various assumptions on kernels and on the description of the microscopic collision process [18, 19, 32, 20, 45]. We showed the analogies and differences between the results and the different strategies of proof presented in the literature.

2.8.3 Dense gases

Together with Laurent Boudin and Srboljub Simić, we started to work on the kinetic description of dense gases. The starting point of our study was to obtain from the kinetic level the macroscopic models of so-called non-simple mixtures [35]. For such mixtures, the momentum balance law for each species contain additional gradient terms to the usual pressure gradient, involving the chemical potential and the enthalpy. This comes from the fact that the specific energy of the mixture depends on the densities of all species not only by summing up the contributions of all species. One possible idea to describe such mixtures at the mesoscopic level would be to take into account long range interactions, which falls in the scope of dense gases [54].

To this end, we intend to investigate the properties of mixtures of gases described by Enskog models, for which the collisions between two molecules are delocalized (in the sense that the two molecules are not exactly at the same point when the collision occurs). This leads to a non-local collision operator, involving some equivalent cross section taking into account the spatial correlations in the gas. The mathematical analysis of this model is a challenging task, since the obtention of an H-theorem is already an issue [189, 53, 15, 185]. In the monospecies case, the asymptotic of a slightly delocalized gas in the fluid regime (meaning that the delocalizing factor is of the same order as the Knudsen number) is tackled by Desvillettes and Perthame in [60, Part 2, Sections 14&15], obtaining a correction of the equation of state at the limit. We aim at extending formally this result to the mixture case, and carry out further studies on the mixture collision operator for dense gases.

2.8.4 Comparison with experimental data

Let us mention that in the previous hydrodynamic limits, from the Boltzmann equations for mixtures to the Maxwell-Stefan or the Fick equations, a special care has been taken to give explicit constants for the convergence rates to equilibrium.

It would be interesting to compare experimentally measured relaxation times with the theoretical convergence rates. Preliminary discussions with members of the IUSTI laboratory (Aix-Marseille Université) had been initiated a few years ago, and I hope that this collaboration will take shape.

Experimental data could also be useful to quantify the regimes in which the higher-order Maxwell-Stefan model is needed instead of the Maxwell-Stefan one, or even models taking into account further phenomena.

CHAPTER 3

Low Mach number models for diphasic flows

Content of this chapter

This chapter is based on the works [G-23, G-20, G-21, G-14, G-9, G-7], in collaboration with S. Dellacherie, G. Faccanoni and Y. Penel, as well as M. Bernard, O. Lafitte, E. Nayir and T. Nguyen during CEMRACS projects.

This chapter focuses on the derivation and analysis of low Mach number thermohydraulic models for diphasic flows, in the context of pressurized water reactors. We derive a model in the low Mach number regime which is less costly than compressible models, but more precise than incompressible models. Due to a decoupling of the pressure between a constant thermodynamic one and a dynamic one, this low Mach number model presents a specific structure closer to incompressible models, but with large compressibility effects due to the heating. We focus on describing accurately the thermodynamic properties of the fluid, both for representing phase change and for the equation of state of a pure phase, which is a key element for applications in order to prevent apparition of vapor in the core of a nuclear reactor.

In particular, we provide analyses with analytical and tabulated equations of state.
For this model, we are able to provide explicit steady-state solutions, and in 1D, even explicit time-dependent solutions. We derive accurate and well-balanced numerical schemes, and provide reference test cases for industrial 3D codes as well as numerical results on academic test cases.

We also consider, in an analogous way to the hierarchy of compressible models with different desequilibria between the phases, the analysis of a low Mach number model with non-instantaneous mass transfer, and its relaxation limit towards the first model, both formally and numerically with an asymptotic-preserving approach.

3.1 Derivation of low Mach number models for diphasic flows

3.1.1 Context of the study

In the context of pressurized water reactors (PWR), we are interested in the modelling, the analysis and the numerical simulation of the flow of the coolant fluid, water. Schematically, the functioning of such a nuclear reactor is plotted on Figure 3.1, and we focus our analysis on the primary circuit, involving the coolant fluid, and more precisely on the core of the reactor.

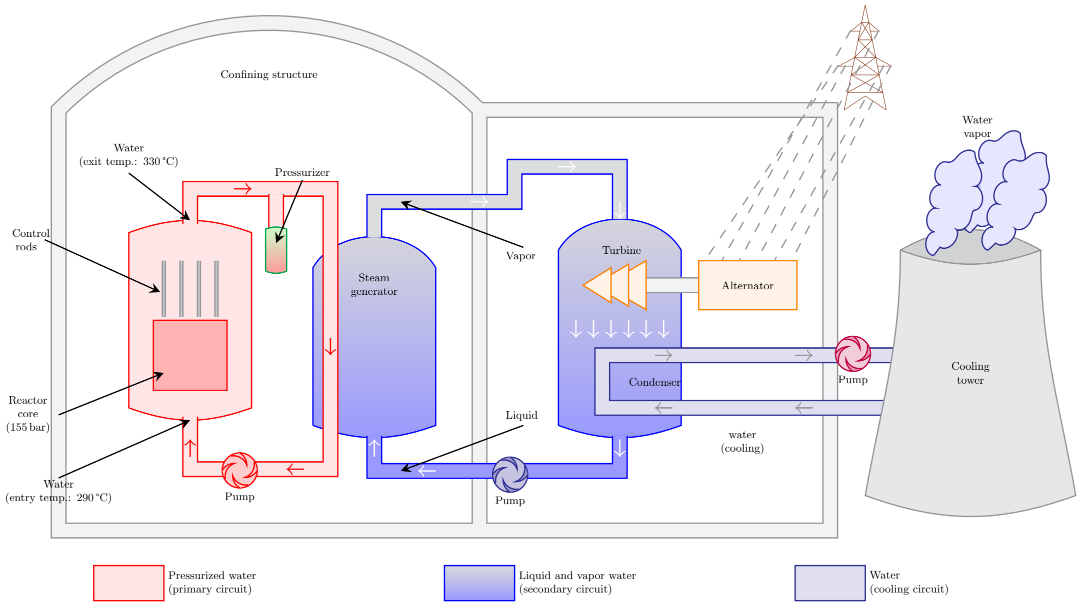

Figure 3.1: Scheme of a Pressurized Water Reactor from [82]

In this part, the pressurization at $p_* \simeq 155\,\text{bar}$ implies that liquid water enters the core with a given temperature and velocity (*i.e.* the flow is imposed), and is heated in the core by the nuclear reaction happening at the fuel rods. When leaving the core, the fluid is a mixture of liquid and vapor phase (see Figure 3.2).

3.1.2 Asymptotic models at low Mach number

A first natural approach is to represent the evolution of the fluid by a model for compressible diphasic flows, as it is done in industrial codes [24, 87, 157]. However, these models present several

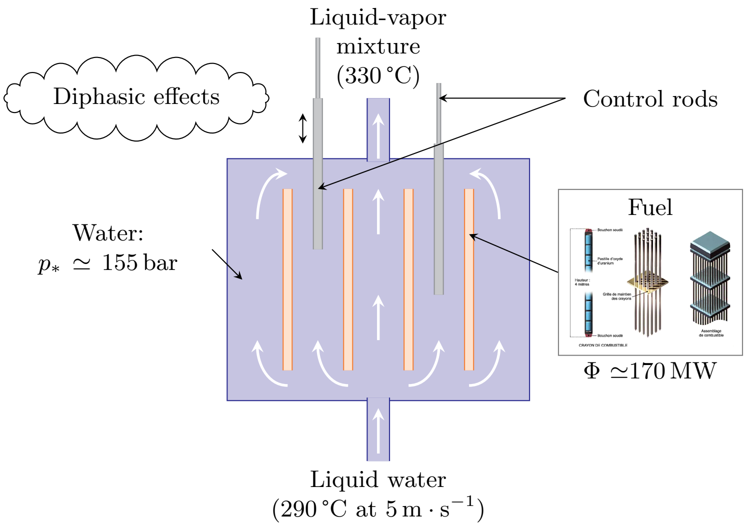

Figure 3.2: Scheme of the core of a PWR

mathematical and numerical difficulties [201, 110, 61]. Moreover, in nominal and incidental situations, as well as in some accidental situations studied in safety evaluations, the speed of sound is much higher that the nominal velocity of the fluid. Typically, the order of magnitude of the velocity $|\boldsymbol{u}|$ is about $5\,\mathrm{m}\cdot\mathrm{s}^{-1}$, whereas the speed of sound c_ℓ^* in liquid water at $p_* = 155\,\mathrm{bar}$ and $T = 300\,^\circ\mathrm{C}$ is about $10^3\,\mathrm{m}\cdot\mathrm{s}^{-1}$. This leads to a Mach number (measuring the compressibility of the flow) $\mathrm{Ma} = |\boldsymbol{u}|/c_\ell^*$ around $5 \times 10^{-3} \ll 1$. In the low Mach number regime, the acoustic phenomena can be neglected in the energy balance (no shock waves), although the flow is highly compressible due to thermal dilatation. Thus, whereas compressible models are too precise and costly, incompressible models do not describe satisfactorily the heat transfers in such flows. An appropriate low Mach number model has been derived by Dellacherie [62] by filtering out the acoustic waves through an asymptotic expansion. Let us mention that other low Mach number models have been derived in the literature [77, 154, 1]. Concretely, we start from the compressible Navier-Stokes equations

$$
\begin{cases}
\partial_t \rho + \mathrm{div}(\rho \boldsymbol{u}) = 0, & (3.1\mathrm{a}) \\
\partial_t(\rho \boldsymbol{u}) + \mathrm{div}(\rho \boldsymbol{u} \otimes \boldsymbol{u}) - \mathrm{div}\,\sigma(\boldsymbol{u}) + \nabla p = \rho \boldsymbol{g}, & (3.1\mathrm{b}) \\
\partial_t(\rho h) + \mathrm{div}(\rho h \boldsymbol{u}) = \Phi + \mathrm{div}(\lambda \nabla T) + \partial_t p + \boldsymbol{u} \cdot \nabla p + \sigma(\boldsymbol{u}) : \nabla \boldsymbol{u}, & (3.1\mathrm{c})
\end{cases}
$$

where the variables are $\boldsymbol{u}(t, \boldsymbol{x})$ the velocity of the fluid, $p(t, \boldsymbol{x})$ its pressure, $h(t, \boldsymbol{x})$ its enthalpy, $\rho(t, \boldsymbol{x})$ its density and $T(t, \boldsymbol{x})$ its temperature, with T, ρ, h and p being linked by an equation of state (EoS). The given data are $\Phi(t, \boldsymbol{x}) \geq 0$ the power density, $\boldsymbol{g}$ the gravity field, λ the thermal conductivity of the fluid, and $\sigma(\boldsymbol{u})$ the stress tensor involving the viscosity of the fluid. This model is known in the literature about homogeneous two-phase flows as the HEM model (Homogeneous Equilibrium Model) [195, 166, 57]. This model is posed in a domain $\boldsymbol{x} = (x, y) \in \Omega$, and has to be supplied with initial and boundary conditions. To this end, for a 2D domain $\Omega = [0, L_x] \times [0, L_y]$ representing the nuclear reactor core, we impose the following boundary conditions:

- ▷ at the entrance $\Gamma_{\mathrm{in}} = [0, L_x] \times \{0\}$, the density and the (vertical) flow rate are given

$$
\rho|_{\Gamma_{\mathrm{in}}} = \rho_e(t, x), \qquad \rho \boldsymbol{u}|_{\Gamma_{\mathrm{in}}} = (0, D_e(t, x));
$$

- ▷ on the lateral walls $\Gamma_{\text{lat}} = \{0\} \times [0, L_y] \cup \{L_x\} \times [0, L_y]$, we impose slip and adiabatic boundary conditions

$$\boldsymbol{u} \cdot \boldsymbol{n}|_{\Gamma_{\text{lat}}} = 0, \qquad \sigma(\boldsymbol{u})\boldsymbol{n} \cdot \boldsymbol{t}|_{\Gamma_{\text{lat}}} = 0, \qquad \lambda \nabla T \cdot \boldsymbol{n}|_{\Gamma_{\text{lat}}} = 0,$$

  where $\boldsymbol{n}$ is the normal and $\boldsymbol{t}$ the tangential vector to the boundary Γ_{lat};
- ▷ and at the exit $\Gamma_{\text{out}} = [0, L_x] \times \{L_y\}$, a free outflow and adiabatic conditions

$$(\sigma(\boldsymbol{u})\boldsymbol{n} - p\boldsymbol{n})|_{\Gamma_{\text{out}}} = -p_* \boldsymbol{n}|_{\Gamma_{\text{out}}}, \qquad \lambda \nabla T \cdot \boldsymbol{n}|_{\Gamma_{\text{out}}} = 0.$$

These boundary conditions can of course be extended to a 3D domain. Initial conditions are provided on the enthalpy and on the flow rate as

$$h(0, \boldsymbol{x}) = h^0(\boldsymbol{x}), \qquad (\rho \boldsymbol{u})(0, \boldsymbol{x}) = D^0(\boldsymbol{x}).$$

After writting the equations (3.1) in a non-dimensional form, it involves several dimensionless numbers, in particular the Mach number squared in front of ∇p in (3.1b). In the asymptotic regime we are interested in, it is assumed to be small of order ε. From an asymptotic expansion of the form

$$p = p^{(0)} + \varepsilon p^{(1)} + \varepsilon^2 p^{(2)} + \mathcal{O}(\varepsilon^3),$$

the $1/\varepsilon^2$ term in front of ∇p leads to $\nabla p^{(0)} = \nabla p^{(1)} = 0$. If one assumes the (exit) boundary condition p_* to be independent of time, it follows that

$$p(t, \boldsymbol{x}) = p_* + \varepsilon^2 \bar{p}(t, \boldsymbol{x}).$$

This means that the pressure is decomposed into a constant thermodynamic part p_* and a dynamic part $\bar{p}$ of order ε^2.

With asymptotic expansions on the other unknowns, we finally obtain at the main order the following asymptotic low Mach number model

$$\begin{cases} \partial_t \rho + \operatorname{div}(\rho \boldsymbol{u}) = 0, & (3.2a) \\ \partial_t(\rho \boldsymbol{u}) + \operatorname{div}(\rho \boldsymbol{u} \otimes \boldsymbol{u}) - \operatorname{div} \sigma(\boldsymbol{u}) + \nabla \bar{p} = \rho \boldsymbol{g}, & (3.2b) \\ \partial_t(\rho h) + \operatorname{div}(\rho h \boldsymbol{u}) = \Phi + \operatorname{div}(\lambda \nabla T), & (3.2c) \end{cases}$$

which is called the LMNC (Low Mach Nuclear Core) model.

To close the system, one has to provide an equation of state. As a consequence of the previous decomposition of the pressure, the thermodynamic description of the fluid involves the constant pressure p_*, which in particular prevents using it as a main variable for the equation of state, contrary to what is usually done for compressible models. Another important consequence for practical use is that the equation of state only depends on one scalar quantity (here h), and not two as in compressible models. We choose the enthalpy as a variable, and the density $\rho(h, p_*)$ (or equivalently the specific volume $\tau(h, p_*) = 1/\rho(h, p_*)$) and temperature $T(h, p_*)$ are given by the equation of state. Possible choices of equations of state are discussed in the next section 3.2.

In the case when the solutions are regular enough, it is convenient to rewrite the LMNC system under a non-conservative form, using the specific volume instead of the density, in the following way

$$\begin{cases} \operatorname{div} \boldsymbol{u} = \dfrac{1}{\zeta(h, p_*)}[\Phi + \operatorname{div}(\Lambda(h, p_*)\nabla h)], & (3.3a) \\ \partial_t \boldsymbol{u} + (\boldsymbol{u} \cdot \nabla)\boldsymbol{u} + \tau(h, p_*)\nabla \bar{p} = \tau(h, p_*) \operatorname{div} \sigma(\boldsymbol{u}) + \boldsymbol{g}, & (3.3b) \\ \partial_t h + \boldsymbol{u} \cdot \nabla h = \tau(h, p_*)\Big[\Phi + \operatorname{div}(\Lambda(h, p_*)\nabla h)\Big], & (3.3c) \end{cases}$$

where the equation of state defines the function $\tau(h, p_*)$ and where we introduced the following notations:

- ▷ the compressibility coefficient is $1/\zeta(h, p_*) := \dfrac{\partial \tau}{\partial h}(h, p_*)$;
- ▷ $\Lambda(h, p_*) := \lambda(h, p_*)/c_p(h, p_*)$, where $c_p(h, p_*)$ is the isobaric heat capacity computed by $1/c_p(h, p_*) = \partial T/\partial h(h, p_*)$, since the thermal diffusion term is rewritten as
$$\lambda(h, p_*)\nabla T = \frac{\lambda(h, p_*)}{c_p(h, p_*)}\nabla h = \Lambda(h, p_*)\nabla h;$$
- ▷ $\sigma(\boldsymbol{u})$ denotes the viscous stress tensor, given by $\sigma(\boldsymbol{u}) = \mu(h, p_*)\left(\nabla \boldsymbol{u} + (\nabla \boldsymbol{u})^{\mathsf{T}}\right) + \eta(h, p_*)(\operatorname{div} \boldsymbol{u})\,\mathrm{Id}$ (and the bulk viscosity $\eta(h, p_*)$ can be set to $-2\mu(h, p_*)/3$ under the Stokes hypothesis).

The boundary conditions become

$$\begin{gathered} h|_{\Gamma_{\text{in}}} = h_e(t, x), \qquad (\boldsymbol{u}/\tau)|_{\Gamma_{\text{in}}} = (0, D_e(t, x)), \\ \boldsymbol{u} \cdot \boldsymbol{n}|_{\Gamma_{\text{lat}}} = 0, \qquad (\sigma(\boldsymbol{u})\boldsymbol{n} \cdot \boldsymbol{t})|_{\Gamma_{\text{lat}}} = 0, \qquad \Lambda \nabla h \cdot \boldsymbol{n}|_{\Gamma_{\text{lat}}} = 0, \\ (\sigma(\boldsymbol{u})\boldsymbol{n} - \bar{p}\boldsymbol{n})|_{\Gamma_{\text{out}}} = 0, \qquad \Lambda \nabla h \cdot \boldsymbol{n}|_{\Gamma_{\text{out}}} = 0. \end{gathered}$$

Remark 3.1. *As far as the thermal diffusion term is concerned, we choose to work with the variable h instead of T, since the temperature is constant during the whole phase change process, making it a bad variable to describe the energy of the system during phase transition.*

Remark 3.2. *Note that this LMNC model is an intermediate model between a full compressible model and an incompressible model. It is much simpler than the compressible Euler model, since acoustic waves have been filtered out, but better captures the physics of the flow when heating occurs than an incompressible model (Boussinesq approximation). This can be observed for example on the stationary solutions of the different models, in the special case of a monophasic flow with the ideal gas equation of state, without gravity nor thermal diffusion nor viscosity, and with constant boundary conditions, in a 1D domain $\Omega = [0, 1]$. For the incompressible model, the steady solution for the velocity is given by $v^\infty(y) = v_e$, which does not see the heating, whereas the low Mach number model leads to $v^\infty(y) = v_e + \Phi y/\zeta(h_e, p_*)$. On the other hand, even in this very simple case, the analytical expression of the steady solution for the full compressible model is much more complex.*

Remark 3.3. *Despite the similarity of the conservative equations (3.1) and (3.2), the nature of the systems is not the same. The HEM model is a hyperbolic system, whereas the LMNC model is not hyperbolic and is closer to the incompressible Navier-Stokes equations (with non-zero but imposed divergence constraint on the velocity). This structure is visible on the non-conservative equations (3.3).*

3.2 Thermodynamic description of a diphasic flow

As we mentioned previously, in the context of a PWR, the high pressure values imply that the water is liquid in the primary circuit. However, in the range of possible temperature and pressures in nuclear cores, phase transition might occur. This event damages the capacity of the water to fulfill its function as a coolant. Phase transition thus has to be modelled in a precise and accurate way, in order to be prevented in nuclear applications.

There are many different approaches in the literature to describe multiphase flows. Locally, such a flow consists in monophasic fluids separated by an interface. We focus here on a Eulerian description of this interface, and we consider diffuse interface models, in which the transition zone is represented properly from a thermodynamical point of view, meaning that phase change is described accurately.

In the most general models, the phases evolve independently, and multiphase flows (and in particular diphasic flows) can be described by each phase having its own pressure, temperature, chemical potential and velocity. The models are then formulated as an hyperbolic system of equations, with source terms accounting for phase interactions. We focus here on the simplest possible model, where instantaneous equilibrium is assumed between the phases for all variables. We can thus consider monophasic models as described in the previous section, and phase change is taken into account *via* the equation of state.

3.2.1 Diphasic flow in a low Mach number model

As we saw in the previous section, in low Mach number models, the thermodynamic pressure p_* is constant. We will thus drop in the following the dependance of all thermodynamic variables on p_*, and only indicate the other variable in the equation of state.

The construction of a diphasic equation of state can be done as follows:

- both pure phases (liquid, denoted by $\kappa = \ell$, and gas, denoted by $\kappa = g$) are characterized by their own thermodynamic properties, given by an equation of state $h_\kappa(T)$ and $\tau_\kappa(T)$ (from which the Gibbs potential $G_\kappa(T)$ can be obtained);

- we can get rid of the variable T and express the equation of state of each pure phase as $\tau_\kappa(h)$, $\kappa = \ell, g$;

- the mixture is characterized by a temperature equilibrium between the two phases, meaning that the temperature T is constant equal to the saturation temperature T^s, defined by equalizing the Gibbs potentials of the two phases, *i.e.* $G_\ell(T^s) = G_g(T^s)$;

- saturation values for the liquid and the gas are now defined as follows, for $\kappa = \ell, g$

$$h_\kappa^s \overset{\text{def}}{=} h_\kappa(T^s), \qquad \tau_\kappa^s \overset{\text{def}}{=} \tau_\kappa(T^s).$$

- the diphasic equation of state is then defined piecewise by (see Figure 3.3):

$$\tau(h) = \begin{cases} \tau_\ell(h), & \text{if } h \leq h_\ell^s, \\ \tau_m(h) & \text{if } h_\ell^s < h < h_g^s, \\ \tau_g(h), & \text{if } h \geq h_g^s, \end{cases}$$

  where $\tau_m(h)$ still remains to be defined.

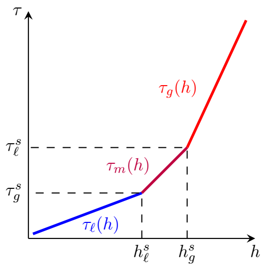

Figure 3.3: Piecewise equation of state

In a similar way, other thermodynamic quantities are defined piecewise, with phase boundaries being defined by the constants h_κ^s. Let us now describe precisely the construction of the mixture equation of state, as well as different possible choices for the pure phase equations of state.

3.2.2 Mixture at saturation

To describe the equation of state in the mixture, we denote φ the mass fraction of the vapor phase. The key idea is that, when phases coexist, they have the same temperature and pressure. Then, thermodynamic relations lead to

$$\tau = \varphi\tau_g^s + (1-\varphi)\tau_\ell^s \qquad \text{and} \qquad h = \varphi h_g^s + (1-\varphi)h_\ell^s, \qquad \text{for } h \in [h_\ell^s, h_g^s]. \tag{3.4}$$

Eliminating φ, we get the equation of state in the mixture

$$\tau_m(h) = \frac{h - q_m}{\zeta_m}, \tag{3.5}$$

where

$$\zeta_m \overset{\text{def}}{=} \frac{h_g^s - h_\ell^s}{\tau_g^s - \tau_\ell^s}, \qquad q_m \overset{\text{def}}{=} \frac{\tau_g^s h_\ell^s - \tau_\ell^s h_g^s}{\tau_g^s - \tau_\ell^s}.$$

Remark 3.4. *Equation (3.5) is very simple, since the specific volume is linear in h. In particular, without any simplifying assumption, the mixture equation of state with constant thermodynamic pressure always has the form of a stiffened gas law.*

Other thermodynamic quantities in the mixture can also be obtained. The mass fraction $\varphi_m(h)$ is obtained in a straightforward way from (3.4), and the temperature in the mixture is of course constant $T_m(h) = T^s$. Another important quantity is the speed of sound, which allows in particular to assess the validity of the LMNC model, by checking that the Mach number remains small. In [G-20, G-14], we derived from thermodynamic considerations explicit formulas for the speed of sound $c_m^*(h)$.

3.2.3 Pure phases

For pure phases, it is possible to choose various equations of state. On the one hand, simple analytical equations of state allow to obtain explicit (steady) solutions in some cases, but are of course limited when compared to experimental data. On the other hand, very complex analytical expressions, or using experimental data, lead to better accuracy of the results, but makes the analysis of the model more difficult. In practice, a compromise is often chosen. We explored different approaches, which are described shortly in the following.

Stiffened gas and Noble-Abel stiffened gas law

The simplest Equation of State (EoS) is the ideal gas law. However, for the liquid phase, it is vastly wrong, and a generalization has been introduced [166, 138] in the form of the stiffened gas (SG) law, which itself also has been generalized in the form of the Noble-Abel stiffened gas (NASG) law [140]. With a constant thermodynamic pressure, these equations of state are written under the following form, for $\kappa = \ell, g$

$$\tau_\kappa(h) = \frac{\gamma_\kappa - 1}{\gamma_\kappa}\frac{h - q_\kappa}{p_* + \pi_\kappa} + b_\kappa,$$

where $\gamma_\kappa > 1$ is the adiabatic coefficient, q_κ is the binding energy, π_κ is a reference pressure and b_κ is the covolume. When $b_\kappa = 0$, we obtain the stiffened gas law. Observe that computing the derivative of τ_κ with respect to h, we have

$$1/\zeta_\kappa(h) = \left.\frac{\partial\tau}{\partial h}\right|_{p_*}(h) = \frac{\gamma_\kappa - 1}{\gamma_\kappa}\frac{1}{p_* + \pi_\kappa},$$

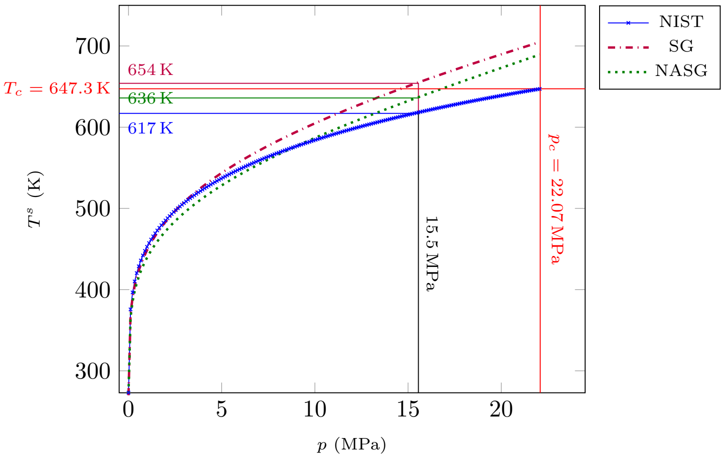

Figure 3.4: Temperature at saturation w.r.t. the pressure, data from [138, 139] (SG and NASG) and [141] (NIST)

which is independent of h, thus leading to another form of the EoS

$$\tau_\kappa(h) = \frac{h - q_\kappa}{\zeta_\kappa} + b_\kappa. \tag{3.6}$$

Other thermodynamic quantities for the (NA)SG EoS can also be obtained, such as the mass fraction $\varphi_\kappa(h)$, the temperature $T_\kappa(h)$ and the speed of sound $c_\kappa^*(h)$ [83].

Other analytical equations of state

Of course, other analytical equations of state can be used. Among them, a popular choice is the family of the so-called cubic EoS, which include the well-known Van der Waals law as well as many variants and extensions. Since the analysis of such EoS is of interest in a larger context than low Mach number models, and in particular for compressible models, we discuss these EoS in a separate section 3.2.4.

Equation of state from tabulated experimental data

The simple analytical EoS presented previously are not accurate enough to estimate precisely the thermodynamic behavior of the fluid (water in our case of interest), especially the saturation values. This might in turn lead to erroneous prediction of phase change. In particular, the temperature at saturation predicted by the SG law is larger than the critical temperature T_c at $p_* = 155$ bar (see Figure 3.4, where the NIST-curve is plotted from experimental data). The critical temperature is the temperature at which the liquid and vapor phases have the same density (and pressure), and it defines the critical point, which delimits the region where the two phases can coexist. It is thus non-physical to have a temperature at saturation larger than the critical temperature.

From this assessment, it seems natural to try using experimental values to construct analytical EoS which could describe the reality in a satisfactory way. In the literature, for example for water, many thermodynamic quantities are tabulated (*cf.* NIST data [202, 141]). In particular, for different thermodynamic pressures, these tables give, for both liquid and vapor phases, a large range of values for the enthalpy h, and the corresponding values of the density $\rho = 1/\tau$, the temperature T, the speed of sound c^*, the specific heat at constant volume c_v, the specific heat at constant pressure c_p, the thermal conductivity λ, and the viscosity μ among others. Observe that in the case of low Mach number models, the constant thermodynamic pressure allows to fit curves in order to define the EoS, whereas in compressible models one has to fit 2D surfaces.

The fitting procedure has to ensure some physical properties of the different thermodynamic variables (positivity and monotonicity of some variables, thermodynamic relations). More precisely, in each pure phase, the specific volume and the temperature have to be positive and increasing with respect to h, over the whole range of considered values for h. Moreover, ζ and τ are related by derivation, as well as $1/c_p$ being the derivative of T with respect to h. Let us describe the approach we chose for meeting these criteria.

- For $c_p(h)$, we compute a (polynomial) approximation $\widetilde{1/c_p}(h)$ of $1/c_p$ (which is tabulated); we then construct the approximation $\widetilde{T}(h)$ as the explicit integral of $\widetilde{1/c_p}$ (polynomial).
- For $\zeta(h)$, we observe that it is not a tabulated quantity, therefore it has to either be approximated as the derivative of τ, or computed from a thermodynamic relation. An example of such a thermodynamic relation is

  $$\frac{1}{\zeta} = \frac{\tau}{c^*\sqrt{T}}\sqrt{\frac{1}{c_v} - \frac{1}{c_p}}.$$

  The advantage of using such a relation is that it provides tabulated values for $1/\zeta$ from the tabulated values of τ, c^*, T, c_v and c_p. We can thus compute a polynomial approximation $\widetilde{1/\zeta}(h)$ of $1/\zeta$, and construct the approximation $\widetilde{\tau}(h)$ as the integral of $\widetilde{1/\zeta}$.

Remark 3.5. *Observe that having approximated τ (or T) and deriving these approximations could have risen some stability issues as well as positivity problems. Moreover, a finite-difference approximation of the derivatives could violate the consistency of thermodynamics [67]. We here avoid any of the aforementioned problems.*

Finally, we try to be as precise as possible for the saturation values, since they have a large influence on the possible predictions (for example apparition of the vapor phase). As far as the fitting procedure is concerned, we explored in [G-14] two different ways of approximating these experimental data by explicit analytical polynomial expressions:

- for each variable, computing fitting functions as polynomials of degree p in each phase, defined such as to minimize some error; this approach is called NIST-p;
- approximating each variable by a constant value in each phase, *i.e.* computing fitting functions as polynomials of degree 0; this approach is called NIST-0.

We then compared the results with the SG and NASG EoS (3.6). Consider a very simple setting representing a PWR (vertical) core in 1D, with liquid water injected at the entrance (bottom) with some fixed flow rate. We can investigate the influence of the equation of state on the steady solution. On Figure 3.5, we plot for the different possible choices of pure phase EoS the distribution of liquid, mixture and vapor phases in the reactor core. The errors upon the enthalpies at saturation and at the entrance when the EoS is ill-approximated can result in dramatic consequences: the computations with the SG EoS provide a late vaporisation. This highlights the importance of a precise description of the EoS when dealing with safety and design of nuclear reactors.

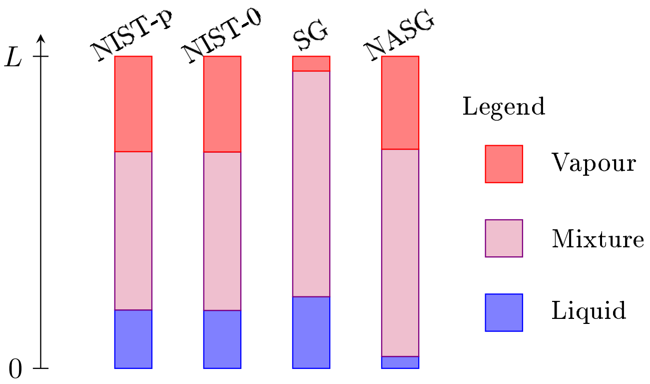

Figure 3.5: Comparison of the steady phase distribution in the core

Remark 3.6. *Note that the strategies for the computation of* ζ *and* c_p *are decoupled, since we are considering incomplete equations of state., due to the fact that we work at constant pressure* p_**. In particular, a NIST-*0 *for* $1/\zeta$ *and NIST-*0 *for* $1/c_p$ *strategy would mimic the NASG EoS in terms of algebraic formulation, except that these constant values are not related to each other.*

3.2.4 Cubic equation of state

As mentioned before, another family of analytical equations of state is the one of cubic laws [207, 151, 95]. We discuss here the construction of a cubic EoS in order to use it in a thermohydraulic model (compressible or in the low Mach number asymptotics).

Description of the cubic EoS

In a general (compressible) setting, cubic equations of state can be written under the following (incomplete) form

$$p(\tau, T) = \frac{rT}{\tau - b} - \frac{a\,\alpha(T)}{\tau(\tau + d) + c(\tau - d)}, \tag{3.7}$$

where r, a, b, c and d are constants and α is a temperature-dependent function, satisfying some positivity, monotonicity and convexity properties. The parameter b is usually interpreted as the volume occupied by the molecules, and r as the specific ideal gas constant. The second term in (3.7) can be thought of as representing the effect of intermolecular forces, and is non-positive. Such EoS are called cubic since the pressure definition leads to a polynomial equation of order 3 on τ. We focus in [G-7] on some special cubic EoS, which are widely used in the literature [168], simple enough to give analytical formulas and which could capture the essential physics of liquid-vapor phase transition:

- the Van der Waals EoS [199], obtained by setting $\alpha(T) = 1$ and $c = d = 0$;
- the Berthelot and Clausius EoS [56, 21], obtained by setting $\alpha(T) = 1/T$ and respectively $c = d = 0$ or c and d such that $c^2 + d^2 + 6cd = 0$;
- the Redlich-Kwong EoS [188], obtained by setting $\alpha(T) = 1/\sqrt{T}$ and $c = 0$, $d = b$;
- the Soave-Redlich-Kwong EoS [193], obtained by setting $\alpha(T) = (\sigma - \sqrt{T})^2$ and $c = 0$, $d = b$.

Equation (3.7) is not enough to describe the whole thermodynamic behavior of the fluid. Indeed, if we want to use it for example in a thermohydraulics model, such as a standard compressible model [174, 98, 187] or the LMNC model (3.3), we need to define the density (or the specific volume), meaning that quantities related to the energy (or the enthalpy) of the fluid remain to be given. The construction of a complete cubic EoS is detailed in [G-7], and relies on the combination of thermodynamic relations. This allows to define the specific internal energy $e(\tau, T)$ or the enthalpy $h(\tau, T)$.

Remark 3.7. *In the context of describing phase change in low Mach number models, it is more relevant to get rid of the thermodynamic variable* T*, as we did previously, and to express for example the equation of state on the specific volume* $\tau(h, p)$ *in terms of the enthalpy. In the case when* T *can be explicitly inverted from* (3.7)*, the enthalpy* $h(\tau, p)$ *can be deduced from the relation* $h(\tau, T)$*. The specific volume as a function of the enthalpy can possibly be obtained by inversion of a the cubic relation.*

Remark 3.8. *In the case of an incomplete EoS (or when the inversions needed in the thermodynamical relations are not possible analytically), the construction described in Section 3.2.1 cannot be applied, since for example the Gibbs potential is not known analytically. Yet, cubic equations of state can only describe in a satisfactory manner the properties of the fluid at the transition between liquid and vapor outside the spinodal zone (where the pressure increases for increasing volume). However, it is possible to define a mixture zone by Maxwell's construction (or Maxwell's Area Rule) [168], which allows to compute the saturation values of the mixture.*

Determination of the parameters of a cubic EoS

In the case of a cubic EoS, the parameters are not directly linked to physical quantities that could be measured experimentally, and thus have to be estimated. To determine these parameters, we make several choices [G-7]:

- ✍ We use the values at the critical point (which corresponds to liquid and vapor having the same density, temperature and pressure and delimits the spinodal zone), which are accessible experimentally, as in [168, 75]. Writing down the thermodynamic relations for the critical point, we can determine three relations between the parameters of the cubic EoS and values for the critical point T_c, τ_c and p_c.
- ✍ When the problem is under- or over-determined, we optimize the parameters in order to minimize the error on the saturation values at a chosen pressure ($p = p_*$).

Note that in our setting (high pressures), this second choice led us to modify the value of r from the ideal gas constant (which is also the case in another context in [93]). Of course, in another pressure regime, the parameters would have to be fitted again.

We compare the temperature $T(\tau, p)$ around saturation at pressure p_* for the best choice of parameters in each EoS on Figure 3.6, with experimental data denoted by IAPWS. We observe that whereas the Van der Walls, and to a lesser extent, the Redlich-Kwong EoS are not very precise, the three other EoS are very accurate on the saturation temperature. The phase boundaries are best described by the Clausius and Soave-Redlich-Kwong EoS, with slightly more precision with the Clausius one.

Remark 3.9. *As mentioned earlier, the interest for simple and accurate enough analytical EoS goes beyond the framework of low Mach number models. In particular, compressible diphasic*

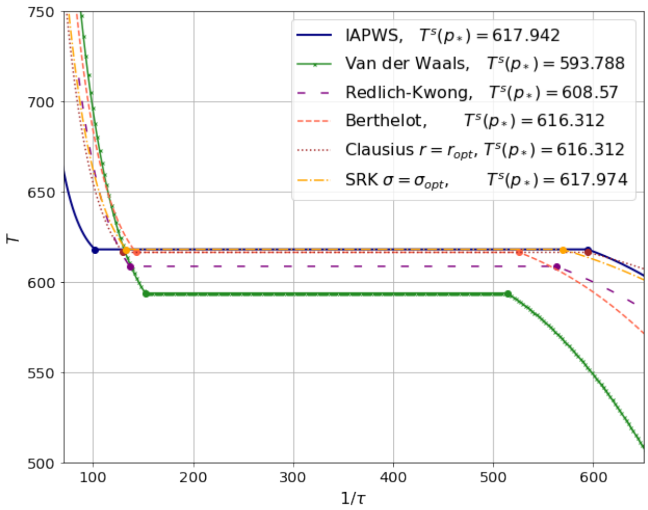

Figure 3.6: $T(\rho, p_*)$ with the best parameters for the different EoS

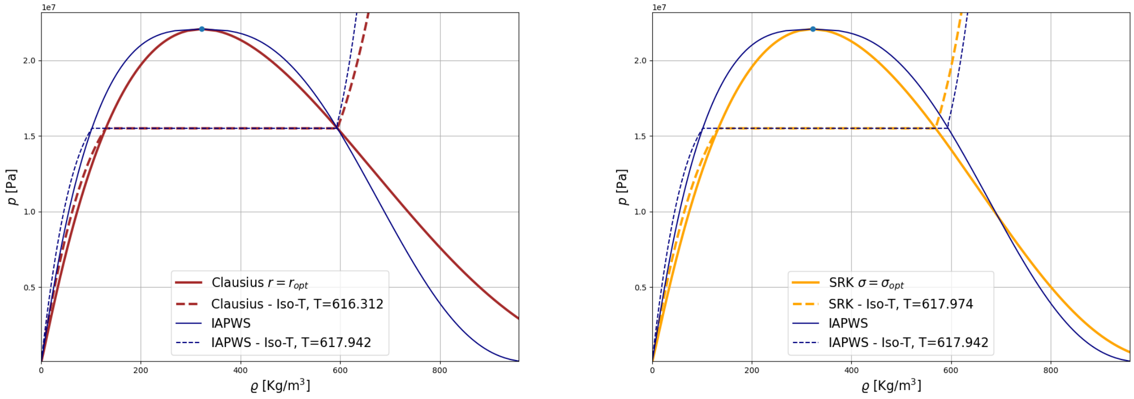

(a) Clausius EoS

(b) Soave-Redlich-Kwong EoS

Figure 3.7: Saturation domes in the (ρ, p) plane for the different EoS

*models (*e.g. *in thermohydraulics) can use a cubic EoS, in which case the pressure is also a thermodynamical variable. Fixing now the parameters at the optimal values obtained in the previous description for $p = p_*$, we want to assess the quality of the different cubic EoS and the quality of our parameter optimization procedure at a fixed pressure by comparing them with experimental data [202] at all pressures. This is done by compraing the phase boundaries $\tau^s_\kappa(p)$ for a large range of pressures. We plot on Figure 3.7 the saturation curve, separating the regions of pure phases from the region where the two phases coexist, at each pressure, for the two best cubic laws (Clausius and Soave-Redlich-Kwong). We observe that the coexistence zone is quite precise even for pressure values far from p_*.*

3.3 Mathematical and numerical analysis of the LMNC model

In this subsection, we mention some results obtained on the LMNC model (3.3) without thermal diffusion ($\Lambda = 0$). The mathematical analysis of the model in 3D (or in 2D) is a challenging task, since the model is highly coupled (with equations of both hyperbolic and parabolic types) and the inflow and outflow boundary conditions are not easy to handle.

However, in 1D, more results can be obtained. A crucial observation is that in this case, equation (3.3b) of the system (3.3) uncouples from the others, and $\bar{p}$ can be obtained as a post-treatment of the other unknowns $\boldsymbol{u}$ and h. Indeed, in 1D, the first equation giving $\operatorname{div} \boldsymbol{u}$ allows to recover the full velocity field, which is obviously not the case for higher space dimensions. Note that, for the application we have in mind, although the 1D setting is very simplified, it is still interesting to investigate, since the flow is mainly vertical in a nuclear reactor core. Moreover, the possibility of having explicit solutions in 1D is a great advantage for the validation of numerical codes in industry.

Denoting y the (vertical) space variable, and v the (vertical) component of the velocity, we are thus led to investigate the following simple 1D system

$$\begin{cases} \partial_y v = \dfrac{\Phi}{\zeta(h, p_*)}, & \text{(3.8a)} \\ \partial_t h + v \partial_y h = \tau(h, p_*)\Phi, & \text{(3.8b)} \end{cases}$$

and $\bar{p}$ can be obtained by integration in y of (3.3b). The domain is then simply $y \in [0, L]$, and the boundary conditions become $h(0,t) = h_e$ and $v(t,0)/\tau(t,0) = D_e$.

3.3.1 1D Steady-state and exact solutions

In the case of a two-phase flow with phase transition as described in the previous section, we can compute the exact solution of the 1D LMNC model (3.8) with the stiffened gas EoS.

Proposition 3.10 ([G-20])**.** *For a constant power density Φ, and constant boundary conditions h_e and $v_e = D_e \tau(h_e, p_*)$, we can define explicitly*

- *the phase boundaries y^s_κ, for $\kappa = \ell, g$,*
- *the spatiotemporal domains $\mathcal{L}$, $\mathcal{M}$ and $\mathcal{G}$ of existence of each phase as in Figure 3.8(a),*
- *the curves $t_\kappa(y)$ splitting the spatiotemporal domain between whether the foot of the characteristic curve reaches the boundary or not as in Figure 3.8(b).*

Then, the exact solution of the 1D LMNC model (3.8) with the stiffened gas EoS is given piecewise

- *the velocity $v(t,y)$ is piecewise affine in y, depending on the domain $\mathcal{L}$, $\mathcal{M}$ and $\mathcal{G}$;*
- *the enthalpy $h(t,y)$ is defined piecewise by*

$$h(t,y) = \begin{cases} q_\kappa + (h^0_\kappa - q_\kappa) e^{\Phi(t - t^0_\kappa)/\zeta_\kappa}, & (t,y) \in \mathcal{K} = \{\mathcal{L}, \mathcal{M}, \mathcal{G}\},\ t < t_\kappa(y),\ \kappa \in \{\ell, m, g\} \\ h_e + \frac{\Phi}{D_e} y & \textit{elsewhere}, \end{cases}$$

where $h^0_\kappa = h^0$ (resp. h^s_ℓ, h^s_g) and $t^0_\kappa = 0$ (resp. t^s_ℓ, t^s_g) for $\kappa = \ell$ (resp. m, g).

The proof of Proposition 3.10 is based on the characteristics method, and the construction of the phase boundaries and the curves $t_\kappa(y)$.

For more general cases (more complex EoS, variable data), even if the exact solution is not available, we can still compute the steady-state solution of the 1D LMNC model (3.8) with phase change for any EoS.

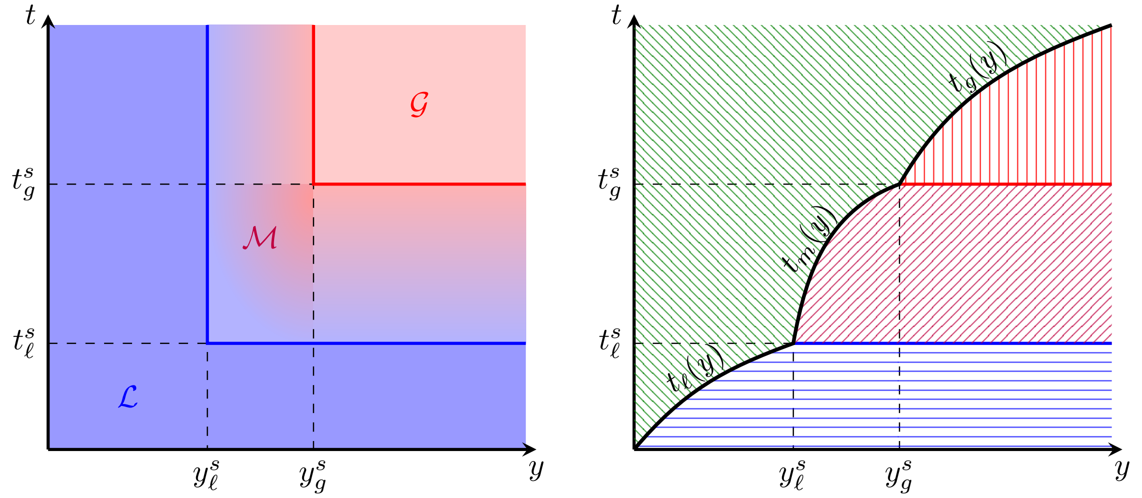

(a) Liquid ($\mathcal{L}$), mixture ($\mathcal{M}$) and vapor ($\mathcal{G}$) regions of the spatiotemporal domain $\mathbb{R}^+ \times \mathbb{R}^+$

(b) Definition of four regions of the spatiotemporal domain $\mathbb{R}^+ \times \mathbb{R}^+$ for the enthalpy

Figure 3.8: Definitions of regions for Proposition 3.10

Proposition 3.11 ([G-14])**.** *Assume that the inlet flow rate D_e, the entrance enthalpy h_e and the power density Φ have finite limits in time h_e^∞, D_e^∞ and $\Phi^\infty(y)$. Then, the steady-state solution of the 1D LMNC model* (3.8) *with any EoS is given by*

$$h^\infty(y) = h_e^\infty + \frac{1}{D_e^\infty} \int_0^y \Phi^\infty(z)\,\mathrm{d}z, \tag{3.9a}$$

$$v^\infty(y) = D_e^\infty \tau(h^\infty(y), p_*). \tag{3.9b}$$

Remark 3.12. *A distinctive feature of the LMNC model is that the steady-state enthalpy does not depend on the equation of state. Moreover, it is monotone increasing for a positive power density Φ. Its expression* (3.9a) *allows to determine which phases does the steady flow involve.*

3.3.2 1D numerical scheme

The decoupling of the equations in 1D allows to design an explicit scheme for the LMNC model (3.8), where (3.8b) is used to compute the enthalpy h, and (3.8a) to update the velocity v by simple integration. Let us mention a few details about possible numerical approaches for this system with the stiffened gas EoS (which could also be partially extended to NASG).

Computation of the enthalpy

The enthalpy h is computed by an explicit discretization of the transport equation (3.8b). The simplest way to do so is to use a first-order upwind scheme. Another possibility is to mimic the continuous approach for investigating the system and use the characteristics method, leading to unconditionally stable schemes. In this case, at each time step, we are first led to approximate the foot of the characteristic curve at the previous time, and then, if it lies in the domain, to interpolate the value of the enthalpy at this point. Finally, we update the enthalpy by integrating in time the ODE along the characteristic curve.

- ✍ The approximation of the foot of the characteristic curve can easily be done at order 1 or 2 in time [183]. When the foot of the characteristic curve falls into the domain, the interpolation of the enthalpy between the two neighboring points leads to a first-order scheme in space. To improve the order, one can use an additional neighboring point. Following [183], we choose a variable stencil and a procedure ensuring the maximum principle (which guarantees the positivity of the enthalpy and the density). Actually, when two possible stencils preserve the maximum principle in the cell, a convex combination of the two interpolations is used, and allows to reach order 3 in space. An extension to the 2D case of this scheme is tackled in [G-2].

- ✍ For the update of the enthalpy, we can integrate with a classic Euler-type method the ODE over the appropriate time interval. For more accuracy, we can take advantage of the particular structure of the source term with the stiffened gas EoS $\tau(h) = (h - q(h))/\zeta(h)$. Indeed, it becomes $(h-q(h))\Phi/\zeta(h)$, where $q(h)$ and $\zeta(h)$ are piecewise constant. Therefore, the ODE becomes

  $$\frac{\zeta(h)}{h - q(h)} \frac{\mathrm{d}h}{\mathrm{d}t} = \Phi.$$

  If we define by $R(h)$ the primitive function of $\zeta(h)/(h - q(h))$, we have the following integration formula

  $$h_i^{n+1} = R^{-1}\Big(R(h_i^n) + \int_{t^n}^{t^{n+1}} \Phi(\tau)\,\mathrm{d}\tau\Big),$$

  and the functions R and R^{-1} are computed explicitly for each phase.

Update of the velocity

From (3.8a), we can integrate to obtain the velocity v^{n+1}. However, since $\zeta(h, p_*)$ is piecewise constant, and thus discontinuous at phase change points, we take special care of the cells where the phase changes, by approximating in a linear way the position of the phase boundary and splitting the cell into two subcells on either side of the phase boundary. In this case, we compute the right-hand side of the equation depending on the phase in the subcell.

Well-balanced property

The numerical approach proposed before allows to reach order 2, but is not well-balanced, in the sense that the numerical solutions do not satisfy at the discrete level the properties of the steady-state solution stated in Proposition 3.11, in particular the conservation of the inflow rate $v = D_e\tau(h, p_*)$, and thus the constant slope of the enthalpy Φ/D_e for constant Φ. Indeed, although the splitting procedure in the update of the velocity allows to preserve the thermodynamical quantities accurately at the discrete level, the method of characteristics for the enthalpy does not ensure the conservation of the inflow rate at the discrete level. However, a simple explicit upwind scheme for the enthalpy coupled with the same approach for the velocity is proved to be well-balanced in [G-9]. The proof relies on preserving at the discrete level the thermodynamical definition of $1/\zeta = \partial\tau/\partial h$, which appears on the right-hand side of (3.8a). The following discretization suffices

$$\frac{v_i - v_{i-1}}{\Delta y} = \Phi\frac{\tau(h_i) - \tau(h_{i-1})}{h_i - h_{i-1}}. \tag{3.10}$$

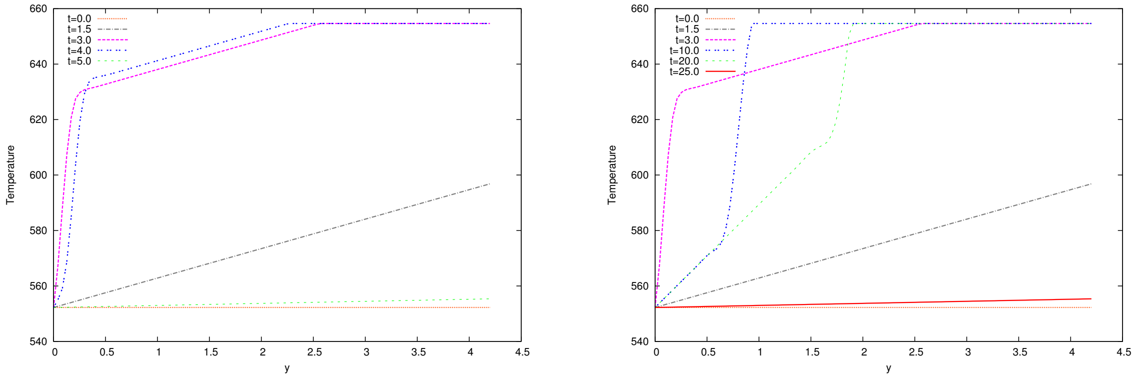

(a) Pumps restart at $t \simeq 2\,\mathrm{s}$ (b) Pumps restart at $t \simeq 18\,\mathrm{s}$

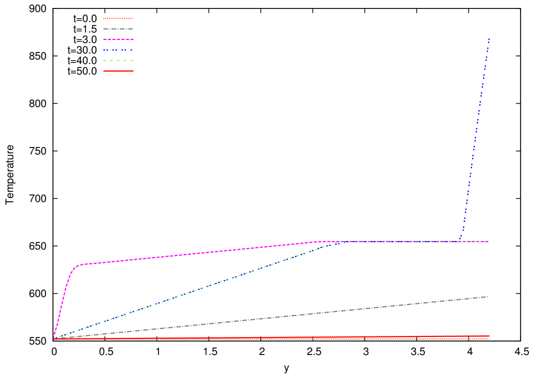

(c) Pumps restart at $t \simeq 38\,\mathrm{s}$

Figure 3.9: Temperature at different times in the different accidental scenarii, depending on the time before the pumps are restarted

From this, combining the two discretized equations of (3.8), we deduce that at a steady-state, the relation $\tau\partial_y v = v\partial_y \tau$ is preserved at the discrete level, meaning that v/τ is constant, thus ensuring the well-balanced property.

Numerical results

With the 1D LMNC model, one can already obtain some numerical results for simulating thermohydraulic phenomena in a nuclear reactor core. In [G-20], we considered a simplified scenario for an accidental transient regime: a main coolant pum trip (Loss of Flow Accident). This corresponds to a sudden decrease of the flow rate at the inlet of the core (when the pumps stop working). The control rods then drop into the core to decrease the power density. By taking into account phase transition, we can describe the thermohydynamics of the system and observe possible apparition of the vapor phase in the core if the pumps are not restarted soon enough, which impairs the cooling in the core (with possible dramatic consequences). Starting with a core filled with fluid phase in nominal regime, the velocity is drastically reduced in the core in a time interval of various lengths ($\simeq 2\,\mathrm{s}$, $18\,\mathrm{s}$ and $38\,\mathrm{s}$). On Figure 3.9, we plot the temperature at different times for the three different scenarii, and observe that while a short interruption of the pumps does not lead to the apparition of the vapor phase, a longer interruption does.

Remark 3.13. *Of course, it would be interesting to extend these 1D approaches to obtain 2D/3D*

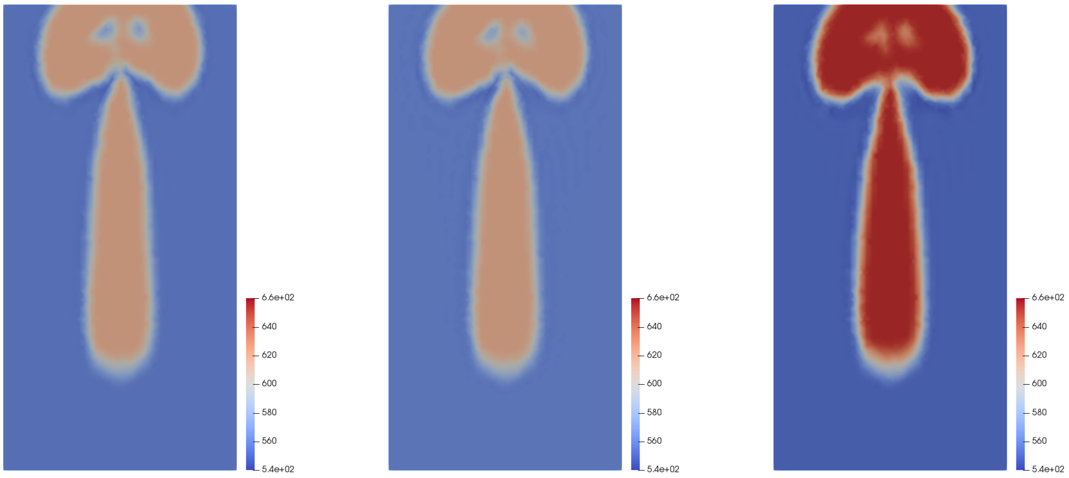

(a) NIST-p (b) NIST-0 (c) Stiffened Gas

Figure 3.10: Temperature in the core for different EoS

simulations. Preliminary 2D numerical results were obtained in [G-14] with finite elements using `FreeFem++`*, with the method of characteristics for the transport term. We investigated in particular the extension of Figure 3.5, in which we compared the influence of the EoS on the steady solution and the apparition of vapor. In this test case, in order to recover a genuine 2D case, the power density $\Phi(t,x)$ is not constant but localized in a disc in the lower part of the core. With the vertical flow, the temperature is then increased along time in the whole upper part of the domain. We plot on Figure 3.10 the temperature at some fixed time and observe again the unsuitability of the simple stiffened gas EoS for the prediction of apparition of the vapor phase in the core. We also notice that the NIST-0 strategy for handling tabulated data described in Section 3.2.3 is sufficient to describe the thermodynamics needed in the test case. We also see the influence of 2D effects in the heating process in the core in comparison to the 1D case (*cf. *Figure 3.5).*

3.4 Disequilibrium of Gibbs potential between the phases

We mentioned in the previous section that multiphase flows can be described by each phase having its own pressure, temperature, chemical potential and velocity. One can obtain a hierarchy of compressible models [88, 153, 152, 144], each with partial equilibrium (instant relaxation) in one or more of the aforementioned variables. Our aim is to consider the analogous of this hierarchy in the case of low Mach number models. We focus here on homogeneous models, meaning that a single velocity is used to describe the flow, and the flow is treated as a single fluid (as in previous sections). Our first step towards such a hierarchy is to consider the relaxation of the Gibbs potential between the phases (with equality of both pressures and temperatures), in a similar way as for the Homogeneous Relaxed Model (HRM) model [88, 153] in the compressible hierarchy. It corresponds to allowing non-instantaneous mass transfer between the two phases. This translates into a fourth equation in the LMNC model on the mass fraction, with a relaxation source term towards the equilibrium (saturation) value.

3.4.1 Obtention of the 4-LMNC model

More precisely, in the low Mach number limit, the system (3.2) is modified by considering the additional equation

$$\partial_t(\rho\varphi) + \operatorname{div}(\rho\varphi\boldsymbol{u}) = \rho\mathcal{R}_\varepsilon,$$

where the variable φ is the vapor mass fraction, and $\mathcal{R}_\varepsilon$ is a term describing mass exchanges between the two phases. Observe that in this case, the EoS $\rho(h, \varphi, p_*)$ does not depend on the only variable h but on both h and φ. Before explaining how the thermodynamics is extended to this case, let us proceed as for system (3.3) and write the non-conservative form on the specific volume, with no thermal diffusion term ($\Lambda = 0$)

$$\begin{cases} \operatorname{div}\boldsymbol{u} = \dfrac{\Phi}{\zeta(h,\varphi,p_*)} + \dfrac{\mathcal{R}_\varepsilon}{\tau(h,\varphi,p_*)}\dfrac{\partial\tau}{\partial\varphi}, \\ \partial_t\boldsymbol{u} + (\boldsymbol{u}\cdot\nabla)\boldsymbol{u} + \tau(h,\varphi,p_*)\nabla\bar{p} = \tau(h,\varphi,p_*)\operatorname{div}\sigma(\boldsymbol{u}) + \boldsymbol{g}, \\ \partial_t h + \boldsymbol{u}\cdot\nabla h = \tau(h,\varphi,p_*)\Phi, \\ \partial_t\varphi + \boldsymbol{u}\cdot\nabla\varphi = \mathcal{R}_\varepsilon, \end{cases} \tag{3.11}$$

where $1/\zeta(h, \varphi, p_*) = \partial\tau/\partial h(h, \varphi, p_*)$. This model is called 4-LMNC, by analogy with the 4-equations compressible model. This system is equipped with the same boundary conditions as the LMNC model with an additional condition at the entrance Γ_{in}, where the mass fraction is prescribed $\varphi|_{\Gamma_{\text{in}}} = \varphi_e(t, x)$.

As for the LMNC system, in 1D, the first equation on $\operatorname{div}\boldsymbol{u}$ allows to recover the full velocity field, and $\bar{p}$ can thus be handled as a post-treatment. In this case, with the same 1D notations as before, the system (3.11) becomes

$$\begin{cases} \partial_y v = \dfrac{\Phi}{\zeta(h,\varphi)} + \dfrac{\mathcal{R}_\varepsilon}{\tau(h,\varphi)}\dfrac{\partial\tau}{\partial\varphi}, \\ \partial_t h + v\partial_y h = \tau(h,\varphi)\Phi, \\ \partial_t\varphi + v\partial_y\varphi = \mathcal{R}_\varepsilon, \end{cases} \tag{3.12}$$

and the closure by the equation of state consists in determining $\tau(h, \varphi)$. This is done by adapting the construction of Section 3.2.1 of the EoS. As before, the pure phases are described by their own EoS (SG for simplicity), and the saturation values are determined from the Gibbs potential equality. For the mixture, we extend the work of Section 3.2.2. The mixture being isothermal and isobaric, we obtain the following expression for the specific volume

$$\tau_m(h,\varphi) = \frac{h - q(\varphi)}{\zeta(\varphi)},$$

where

$$q(\varphi) = \varphi q_g + (1-\varphi)q_\ell, \qquad \zeta(\varphi) = \frac{\varphi\zeta_g\tau_g^s + (1-\varphi)\zeta_\ell\tau_\ell^s}{\varphi\tau_g^s + (1-\varphi)\tau_\ell^s}.$$

As for the source term, mass transfer between the two phases can be modelled by the following relaxation term [11, 116, 2, 120, 122], involving a characteristic time ε

$$\mathcal{R}_\varepsilon(h,\varphi) = \frac{\varphi^s(h) - \varphi}{\varepsilon}, \tag{3.13}$$

where the mass fraction $\varphi^s(h)$ corresponds either to a pure phase ($\varphi = 0, 1$) or to a mixture at saturation ($\varphi \in (0,1)$):

$$\varphi^s(h) = \begin{cases} 0, & \text{if } h \leq h_\ell^s, \\ \frac{h-h_\ell^s}{h_g^s-h_\ell^s}, & \text{if } h_\ell^s < h < h_g^s, \\ 1, & \text{if } h \geq h_g^s. \end{cases}$$

As for the LMNC model, the steady-state solution of (3.12) is known almost explicitly: the enthalpy is the same as for the LMNC model, and the stationary mass fraction is the solution of an ODE, as stated in the following proposition.

Proposition 3.14 ([G-9])**.** *Assume that the inlet flow rate D_e, the entrance enthalpy h_e, the entrance mass fraction φ_e and the power density Φ are constant in time. Then, the steady-state solution of the 1D 4-LMNC model (3.12) with any EoS is given by*

$$\begin{aligned} h^\infty(y) &= h_e + \frac{1}{D_e}\int_0^y \Phi^\infty(z)\,\mathrm{d}z, \\ (\varphi^\infty(y))' &= \frac{\mathcal{R}_\varepsilon(h^\infty(y),\varphi^\infty(y))}{D_e\tau(h^\infty(y),\varphi^\infty(y))}, \qquad \varphi^\infty(0) = \varphi_e, \\ v^\infty(y) &= D_e\tau(h^\infty(y),\varphi^\infty(y)). \end{aligned}$$

The proof is very easy and relies on the relation between τ and its derivatives

$$\partial_y\tau = \frac{1}{\zeta(\varphi)}\partial_y h + \frac{\partial\tau}{\partial\varphi}\partial_y\varphi. \tag{3.14}$$

Indeed, from the stationary equations on h and φ, we have that $v\partial_y h = \tau\Phi$ and $v\partial_y\varphi = \mathcal{R}_\varepsilon$, and thus, in the equation on v, we recognize

$$\partial_y v = \frac{\Phi}{\zeta(h,\varphi)} + \frac{\mathcal{R}_\varepsilon}{\tau(h,\varphi)}\frac{\partial\tau}{\partial\varphi} = \frac{v}{\tau}\partial_y\tau. \tag{3.15}$$

This means that the flow rate v/τ is constant (equal to D_e). We shall see in the following that suitable analysis of the model relies on preserving this property.

Moreover, the method of characteristics (splitting the domain into subdomains to take into account initial/boundary conditions and phase change) allows again to obtain some properties on the model. In particular, a maximum principle can be proved for the mass fraction, ensuring its nonnegativity and the nonnegativity of the relaxation term $\mathcal{R}_\varepsilon$. This means that there is a delay (due to the non-instanteneous relaxation) between the evolution of h and the one of φ. For example, h can become greater that h_ℓ^s while φ is still equal to zero. Therefore, it is now the value of φ that determines the phase in which the fluid is (and not h as for the LMNC model).

Well-balanced property

As far as numerical approaches are concerned, the same ideas as for the LMNC model can be used to obtain a well-balanced scheme (*cf.* Section 3.3.2).

The computation of the velocity is done in the same way, with a special care at the phase change points, through dividing the corresponding cell into two sub-cells. The well-balanced property comes from preserving, at the discrete level, the equivalent of the relation (3.10) for the LMNC model. This is done with a suitable discretization of the relation (3.14), which can be rewritten using the form of the SG EoS as

$$\partial_y \tau = \frac{\partial_y h}{\zeta(h,\varphi)} + \frac{(q_g - q_\ell)\zeta(h,\varphi) - (\zeta_g - \zeta_\ell)(h - q(\varphi))}{\zeta(h,\varphi)^2}\partial_y \varphi.$$

Then, if the discretization of the right-hand side of the first equation of (3.12) is compatible with this relation, we shall recover, as for the continuous case, the discretization of (3.15) and thus the fact that v/τ is constant at the discrete level.

As far as the equation on the mass fraction is concerned, the only care we have to take is to discretize the source term implicitly, in order to avoid any restriction on the CFL condition in the case of a stiff source term ($\varepsilon \ll 1$). However, since this term is linear in φ, this does not induce additional difficulties in the scheme.

3.4.2 Relaxation towards the LMNC model

As we stated, the 4-LMNC model (3.11) describes a two-phase flow under the assumption of instantaneous mechanical and thermal equilibrium, but generally not of chemical equilibrium, whereas all three equilibria are assumed to be reached for the LMNC model (3.3). With the choice (3.13) of the relaxation source term, we show that the model (3.3) is formally as the instantaneous relaxation limit of (3.11) (instantaneous phase change).

Proposition 3.15 ([G-9]). *The solution* $(v_\varepsilon, h_\varepsilon, \varphi_\varepsilon)$ *of the 4-LMNC model* (3.12) *with relaxation term* (3.13) *converges formally to* $(\bar{v}, \bar{h}, \varphi^s(\bar{h}))$ *as* $\varepsilon \to 0$, *where* $(\bar{v}, \bar{h})$ *is the solution of the LMNC model* (3.8).

Let us mention the main steps of the proof.

- An asymptotic expansion of each variable in ε is performed, and the leading order (ε^{-1}) gives that at the main order, $\varphi_\varepsilon = \varphi^s(h_\varepsilon)$. From this, up to introducing a regularization of φ^s to allow derivation, we deduce, at the main order, that $\partial_t \varphi_\varepsilon + v\partial_y \varphi_\varepsilon = (\varphi^s)'(h_\varepsilon)(\partial_t h_\varepsilon + v\partial_y h_\varepsilon)$.
- A crucial point is the compatibility of the EoS between the two models, meaning that $\tau(h, \varphi^s(h)) = \tau(h)$, where $\tau(h,\varphi)$ denotes the EoS in the 4-LMNC model, whereas $\tau(h)$ denotes the one of the LMNC model (with a slight abuse of notation). This allows to obtain, from the transport equation on h_ε, that h_ε converges formally to $\bar{h}$. Observe that this compatibility is satisfied although $q(\varphi^s(h)) \neq q(h)$ and $\zeta(\varphi^s(h)) \neq \zeta(h)$.
- Last, the equation on v_ε combined with the relation betwwen the derivatives of the EoS

  $$\frac{\partial \tau}{\partial h} + \varphi^{s\prime}(h)\frac{\partial \tau}{\partial \varphi} = \frac{\mathrm{d}}{\mathrm{d}\,h}\tau(h, \varphi^s(h)) = \tau'(h)$$

  and the equation on φ_ε allow to obtain that v_ε converges formally to $\bar{v}$.

Moreover, we were able to derive in [G-9] an asymptotic-preserving (AP) scheme for the 4-LMNC model (3.11), which recovers solutions of the LMNC model in the limit of small relaxation time ε.

An important feature of such an AP-scheme is that it allows to consider the spatial coupling of non-instantaneous and instantaneous regimes with only one numerical scheme, by letting the value of ε vary in space. This avoids to determine artificial boundary conditions on the coupling interface.

Let us mention the main ideas of the construction of this scheme.

- In a standard way [126, 86, 127], the scheme relies on a time splitting between the relaxation step (stiff, thus implicit) and the transport one (explicit). More precisely, the source term of the equation on h is easily treated explicitly to update an intermediate value of h, which is then used in the equation on φ to compute the relaxation term, whose linearity in φ allow to be treated implicitly without any additional difficulty (and thus avoiding restrictions on the CFL condition).

- Further, the velocity is updated by integrating its (1D) equation, using in an adequate way either the value h^n, φ^n at the previous time or the intermediate values h^*, φ^* of h and φ in the right-hand side. Let us explain briefly how to construct the right balance of the different times.

    - For a well-balanced scheme for the LMNC model, we preserve in (3.10) the fact that the right-hand side Φ/ζ of the equation on v was also (from the definition $1/\zeta = \partial\tau/\partial h$) $\Delta\tau/\Delta h$, where Δ denotes some variation (in this steady-state case, related to space: $\Delta\star = \star_i - \star_{i-1}$).
    - For the relaxation limit of the 4-LMNC model, the continuous analysis relied also on the preservation of the derivatives of τ ($\partial\tau/\partial h$ and $\partial\tau/\partial\varphi$).
    - Inspired by these observations, we preserve with the balance of the different times the same type of relations. In particular, $\mathcal{R}_\varepsilon(h,\varphi)/\tau(h,\varphi) \times \partial\tau/\partial\varphi$ is discretized as something of the form $\mathcal{R}_\varepsilon(h^*,\varphi^*)/\tau(h^n,\varphi^n) \times \Delta\tau/\Delta\varphi$, using the equation of state for τ, where the variation is here related to time $\Delta\star = \star^* - \star^n$.

- The transport part is computed in a standard way. The scheme is then proved to be weakly-AP, meaning that its numerical solution is an $\mathcal{O}(\varepsilon)$-approximation of the numerical solution of the LMNC model, discretized in a standard way with the same splitting in time.

We show on Figure 3.11 the AP-property of the scheme, where we plotted the norm of the difference between the solutions of the 4-LMNC model (denoted by $\star_4$) and the LMNC model (denoted by $\star_3$) along time for different values of ε (with fixed discretization parameters). A relaxed-AP behavior is observed, meaning that, at least for the enthalpy and the mass fraction, the error is of order ε (or less) after some time (around 1.5 s).

Remark 3.16. *This analysis on the 4-LMNC model could be extended to a 5-LMNC model, in which the temperature relaxation is not instaneous. The construction of the EoS would have to be extended, but the structure of the equations would not be altered, and a similar analysis could be performed.*

3.5 Future works and prospects

In this section, I mention possible future works and perspectives on low Mach number models, some of which are already collaborations in progress.

3.5.1 Taking into account thermal diffusion

In all previous analysis, we neglected thermal diffusion effects by setting $\Lambda = 0$. Physically, thermal diffusion is negligible for water in the physical conditions of a PWR. However, other

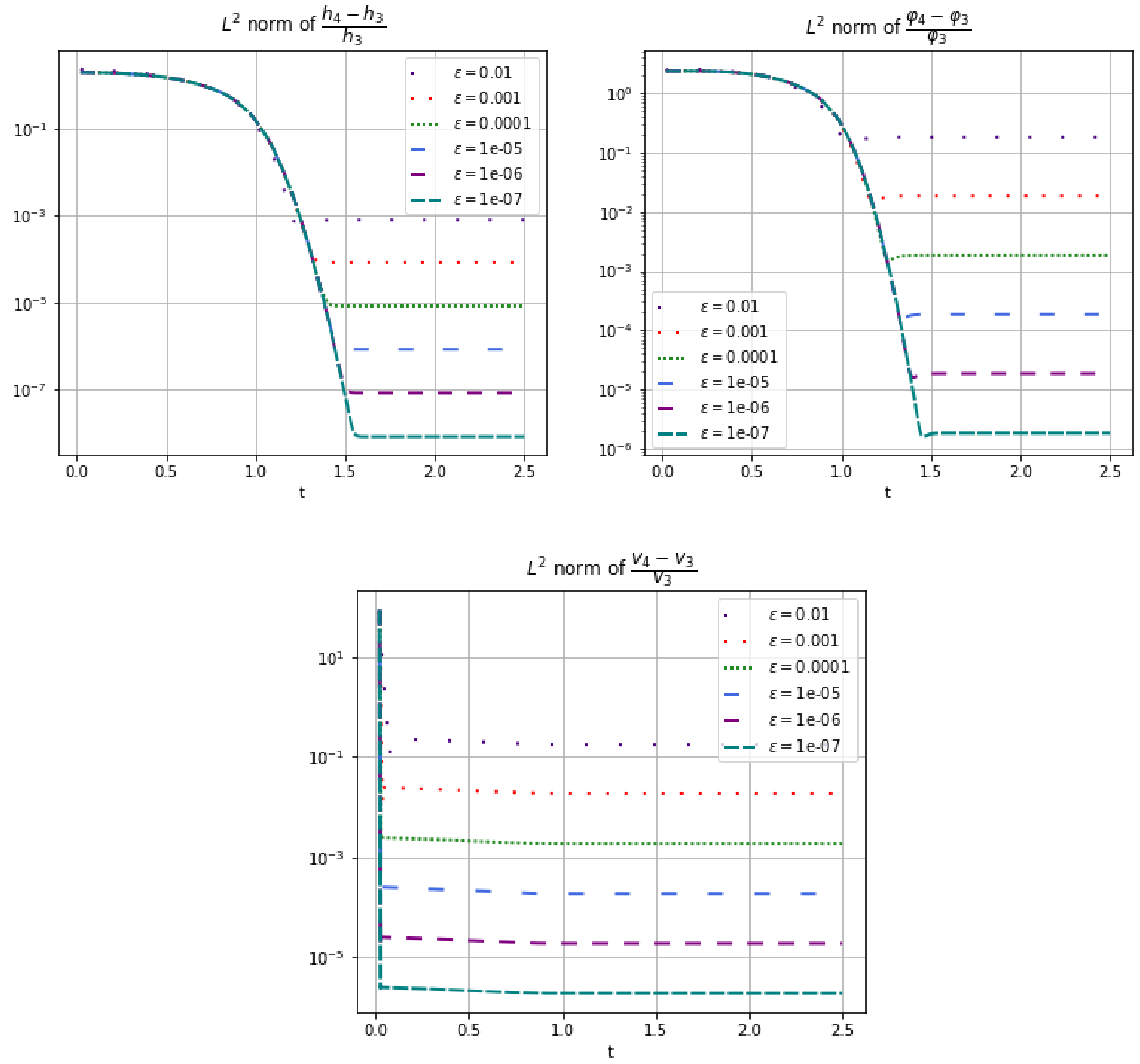

Figure 3.11: Asymptotic-preserving property of the scheme

settings or other coolants may require to take into account this effect (*e.g.* sodium-cooled fast reactors). It is thus of interest to analyze the LMNC model when taking into account thermal diffusion. This is done by keeping the term $\nabla \cdot (\Lambda(h)\nabla h)$ in (3.2c). Observe that this term is obtained from $\nabla \cdot (\lambda(h)\nabla T(h))$, which is relevant in pure phases. In the mixture, since $T = T^s$ is constant, the term vanishes (meaning that $\Lambda(h) = 0$ in the mixture).

A 1D toy model has been studied in [84], in which the density is assumed to be constant. This simplifies highly the model, which reduces to a single advection-diffusion equation for the enthalpy (no velocity equation). However, the diffusion coefficient already presents a degeneracy, since it is zero in the mixture whereas it is positive in the pure phases. Because of this degenerate coefficient, the enthalpy exhibits a discontinuity at the appearance of the vapor phase (liquid-gas or mixture-gas transition point).

With Gloria Faccanoni and Cédric Galusinski, we tackle the full 1D LMNC model with thermal diffusion and phase change

$$\begin{cases} \partial_t(\rho(h)) + \partial_y(\rho(h)v) = 0, \\ \partial_t(\rho(h)h) + \partial_y(\rho(h)hv) = \Phi + \partial_y(\Lambda(h)\partial_y h), \end{cases} \tag{3.16}$$

where we dropped the equation on the momentum as usual in a 1D setting, since $\bar{p}$ can be computed as a post-treatment. Because of the discontinuities in the solution, the non-conservative form cannot be used, and usual analysis for low Mach number models does not apply. We show that the degeneracy induces discontinuities on the solution, both on the enthalpy and the velocity. We are able to provide explicit steady-state and traveling wave solutions, and to describe the existing phases depending on the data. In particular, we can show the disappearance of the mixture phase for hight heat transfers with a large diffusion coefficient in the gas phase. We then derive suitable numerical schemes able to capture the moving discontinuities. This requires the use of a gradient scheme (discretize the diffusion term as $\partial_y^2 \mathcal{L}(h)$), and, for the time discretization, either a full implicit scheme, or a predictor-corrector approach (after some rewriting of the system to avoid possible antidiffusion).

A natural extension of this work is then to tackle numerically the full 2D or 3D model (3.2), in which the decoupling of the pressure does not happen anymore. As in 1D, because of the discontinuities in the solution, the non-conservative form cannot be used. Without viscosity, the structure of the additional equation to handle is similar. However, when adding the viscosity, special care has to be taken, even to check that this second-order term is well-defined with discontinuous solutions. If the pressure is discontinuous, the validity of the low Mach number assumption might be questioned at the jumps.

For this analysis, we could start on investigating the compressible model with phase change and thermal diffusion (and thus degenerate diffusion) in pure phases and at transition points, and further its low Mach number limit. One could also consider the limit regime of evanescent viscosity.

We observe that the 4-LMNC model does not present such discontinuities, since the term $\lambda\nabla T(h,\varphi)$ gives two contributions in ∇h and $\nabla\varphi$. The fact that in the mixture, the temperature is constant does not lead anymore to a degenerate term in ∇h. Investigating the relaxation of the 4-LMNC model with thermal diffusion towards the LMNC model is then of interest, and could also suggest possible numerical approaches in 2D or 3D.

3.5.2 Theoretical analysis for the LMNC model

Whereas the mathematical analysis of the LMNC system is easy in 1D, where we can exhibit explicit solutions, the well-posedness of the model in higher dimensions is not studied yet. In the case of a closed system (with periodic boundary conditions), the existence and uniqueness of a solution to the LMNC model has been proved in [182, 184] (for small time or small data). The proof relies on the Hodge decomposition for the Navier-Stokes part, and on the characteristics method for the transport part, and is based on Picard iterates in regular enough function spaces.

However, for an open system, with inflow boundary conditions, the mathematical analysis is more intricate, and remains to be done. It is not obvious that the same method of proof can be applied, since working in very regular function spaces for the transport equation with inflow boundary conditions is not straightforward.

Further, it could be extended to the 4-LMNC model. This would provide the first step to prove the rigorous convergence between the two models in the relaxation limit. However, of course, such a limit would require to control the smallness assumption on the data (or existence time), or alternatively to first obtain the existence of a global solution.

3.5.3 Hierarchy of low Mach number models

We tackled in Section 3.4 the first step towards a hierarchy of low Mach number models, by considering the relaxation of the Gibbs potential between the phases. In a general averaged two-phase flow model, the flow will consist of two fluids which evolve independently. In the compressible hierarchy for immiscible two-phase fluids, many models have been derived starting from the Baer-Nunziato model [7, 190], endowed with source terms driving towards different equilibria. Let us describe briefly this model, neglecting here thermal diffusion, viscosity and gravity. Denoting α_κ the volume fraction of phase $\kappa \in \{1,2\}$, and $E_\kappa = e_\kappa + \boldsymbol{u}_\kappa^2/2$ the total energy of each phase, the Baer-Nunziato model (also called 7-equations model) is usually written in the variables $\alpha_\kappa\rho_\kappa$, $\alpha_\kappa\rho_\kappa\boldsymbol{u}_\kappa$, $\alpha_\kappa\rho_\kappa E_\kappa$ and one of the volume fractions, for example α_1, as follows

$$\begin{cases} \partial_t(\alpha_\kappa\rho_\kappa) + \nabla\cdot(\alpha_\kappa\rho_\kappa\boldsymbol{u}_\kappa) = \mathcal{R}_\kappa^{\mu}, \\ \partial_t(\alpha_\kappa\rho_\kappa\boldsymbol{u}_\kappa) + \nabla\cdot(\alpha_\kappa\rho_\kappa\boldsymbol{u}_\kappa\otimes\boldsymbol{u}_\kappa + \alpha_\kappa p_\kappa\,\mathrm{Id}) - p_I\nabla\alpha_\kappa = \mathcal{R}_\kappa^{\mu,\boldsymbol{u}}, \\ \partial_t(\alpha_\kappa\rho_\kappa E_\kappa) + \nabla\cdot(\alpha_\kappa\rho_\kappa E_\kappa\boldsymbol{u}_\kappa + \alpha_\kappa p_\kappa\boldsymbol{u}_\kappa) - p_I\boldsymbol{u}_I\cdot\nabla\alpha_\kappa = \mathcal{R}_\kappa^{\mu,\boldsymbol{u},p,T}, \\ \partial_t\alpha_1 + \boldsymbol{u}\cdot\operatorname{div}\alpha_1 = \mathcal{R}_1^{p}, \end{cases} \tag{3.17}$$

where the relaxation terms $\mathcal{R}_\kappa^\star$ are imposed to drive the system towards the equilibrium in the different variables, and the so-called interface velocity and pressure u_I and p_I have to be defined.

Of course, this model can be rewritten in the variables ρ_κ, $\rho_\kappa\boldsymbol{u}_\kappa$, $\rho_\kappa h_\kappa$ and α_1 in a more similar way to (3.1), involving again relaxation source terms. From this model, we can consider the equilibrium limits of each relaxation process, assuming the corresponding process to be instantaneous. This leads to a hierarchy of models, with 6, 5, 4 or 3 equations. The order of these relaxations is not imposed, leading to several branches coexisting in the literature and being studied separately. For example, homogeneous models [116, 153, 120] (as the ones we studied previously) start with momentum relaxation, meaning velocity equilibrium, whereas other models [144] consider first mechanical relaxation, meaning pressure equilibrium. When considering all four possible relaxations, all these branches converge of course to the same model, the HEM one, corresponding to (3.1) (without thermal diffusion, viscosity or gravity). However, even in the compressible hierarchy, not all models of the different branches have been studied.

For a hierarchy of low Mach number models, many additional questions arise.

- ▹ Which asymptotic low Mach number model is correct from the Baer-Nunziato model? Indeed, depending on the form we start with (*i.e.* the chosen variables), different models can be obtained, in particular since the definition of the Mach number depends on the velocity, and thus on the phase, and the pressure variable is split into a dynamic and a thermodynamic part.
- ▹ Do the limits commute, *i.e.* can we consider first an instantaneous relaxation process and then its low Mach number limit, or the instaneous relaxation process of an already asymptotic low Mach number model, and obtain the same model?

One could also consider miscible fluids, in which the volume fractions of the two phases (or fluids) satisfy $\alpha_1 = \alpha_2 = 1$. In this case, we already have to adapt the description of the equation of state with phase change (construction of Section 3.2.1), since the pressures of the two fluids are not equal at saturation. In a low Mach number context, we would expect the total pressure (sum of the two fluid pressures) to be the thermodynamic one. The derivation and study of a hierarchy of models in this case would then be of interest.

3.5.4 Mesoscopic description to justify the macroscopic models

A natural question, which makes a bridge with the models of Chapter 2, is to investigate whether such macroscopic diphasic models can be derived from a mesoscopic description. Some results have been obtained recently [66]. We aim at investigating this question with Frédéric Hérau and Hélène Mathis, starting with the Baer-Nunziato model (3.17). Can this Baer-Nunziato model be derived from the Boltzmann equation for two fluids? In particular, the source terms used in the literature involve the differences of the fluid velocities, pressures, temperatures (and possibly Gibbs potential with mass transfers), and nonconservative terms involve the interface velocity and pressure, which are imposed without a complete physical justification, and are often discussed in the literature: one can thus wonder whether they can be derived from a kinetic description. However, the nonconservative form of the equations makes the derivation from the (conservative) Boltzmann equation intricate, and the obtention of the volume fraction α (for immiscible fluids) from a kinetic description is not straightforward [121].

A first step in this direction is to describe at the microscopic or mesoscopic level the immiscibility property. To this end, we investigate a kinetic equation for two species i and j, in which the particules of phase i are strongly repulsed by the particles of the other phase j *via* a force $-\frac{1}{\eta}\nabla V_j$, for a mean field potential V_j related to the density n_j. From this modelling, one could expect to derive, in the limit $\eta \to 0$ and the hydrodynamic limit, a macroscopic equation for the volume fraction α, linked to the characteric function of the domain of existence of the corresponding phase.

We first tackle the monospecies case, with a given repulsion potential (scaled in $1/\eta$) with the simplest "kinetic" model (overdamped Langevin dynamics), and study its limit of strong repulsion $\eta \to 0$ towards the heat equation, without and then with a moving boundary (corresponding to the other fluid). Further, we enrich the kinetic equation by considering an inhomogeneous Fokker-Planck equation. The return to equilibrium can then be proved depending on both η and ε (corresponding to the scaling in $1/\varepsilon$ of the term acting in velocity in the Fokker-Planck equation). In this process, a very interesting question arises first on the convergence of the model when η tends to zero to a kinetic model with specular boundary conditions. Moreover, using the hypocoercivity formalism, it seems that both limits could be made rigorous (as a first step for simplified collision kernels).

CHAPTER 4

Models for the respiratory system

Content of this chapter

This chapter is based on the works [G-30, G-27, G-28, G-11, G-4], in collaboration with L. Boudin, C. Grandmont and S. Martin, as well as A. Devys, D. Götz, B. Maury, A. Mecherbet, F. Noël and D. Yakoubi during CEMRACS projects.

This chapter is dedicated to some contributions on the description of the respiratory system, as well as the propagation and deposition of aerosols in the airways. In particular, we discuss a reduced 1D model taking into account the multiscale aspect of the airways and the presence of different species in the air breathed by the patient. We also describe in a precise way the gas exchanges in the alveoli, with non-linear effects due to the combined presence of O_2 and CO_2. This appears as a source term in the 1D model, and investigate different pathological tendencies. Moreover, we study the coupling of aerosol particles with the airflow in the airways, in simple geometries such as branched structures (similar to a bifurcation in the lung). The airflow is described by a fluid model, and a kinetic description is used for the aerosol particles. We investigate the coupling, as well as the evolution in temperature and radius of the particles, and their influence on the deposition of the aerosol in some academic test cases, showing the importance of taking into account the different effects in some situations.

In this chapter, we are concerned with the description of the respiration process, and the behavior of aerosols in the respiratory system. The respiration process implies the transport of air in the upper airways from the mouth to the pulmonary alveoli, where the gas exchanges occur (diffusion of oxygen and carbon dioxide). These alveoli are surrounded by a a viscoelastic tissue, the parenchyma, which is involved in the mechanical effects of respiration, such as the displacement of the diaphragm and the ribs. The understanding of the respiration process is crucial for example for the development of aerosol therapies, for which the particles need to

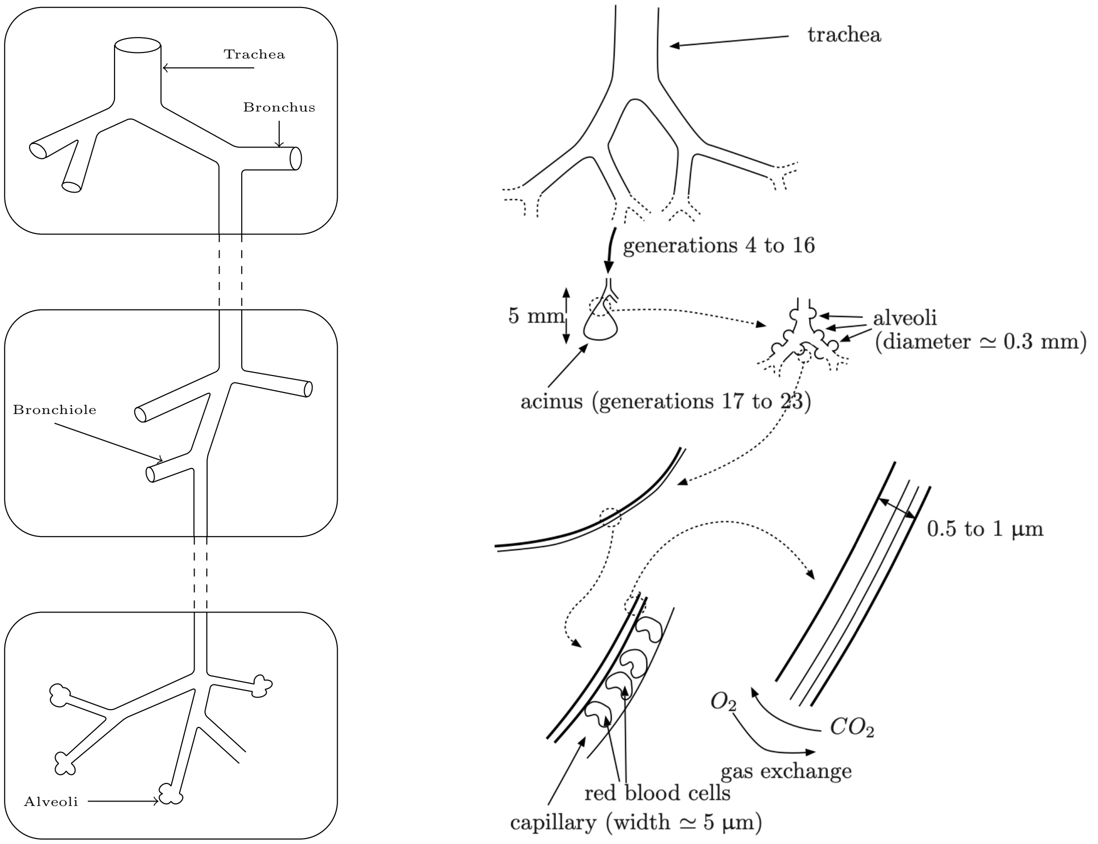

(a) Scheme of the human lung (b) Overall view of the oxygen transfer into blood (from [158])

Figure 4.1: Schematic view of the lung and the oxygen transfer

reach precisely the region that has to be treated. We are thus interested in this chapter in developing mathematical models at different scales, for the description of the respiration process (transport of air in the airways and gas exchanges in the alveoli), and of the behavior of aerosols in the respiratory system (transport and deposition, with possible size variations). Numerical simulations of these models could then help the comprehension of the respiration process, the diagnosis of respiratory diseases, and the optimization of therapeutic protocols.

4.1 Description of air in the airways

The bronchial tree can be schematically divided into three parts (see Figure 4.1(a)):

- the higher airways (up to the 7th generation), in which air can be assumed to be Newtonian, viscous and incompressible; the Navier-Stokes equations are a good approximation for the flow in this part;
- the medium airways (the bronchioles, from the 8th to the 16th generation), in which the flow can be supposed to be laminar;
- the acini and alveolar bags (from the 17th to the 23rd generation), surrounded by the parenchyma, in which the gas exchanges occur.

A detailed description of the physiology of the human lung can be found in [203, 206].

4.1.1 Multiscale modelling

Several approaches for modelling the airflow in this multiscale geometry have been proposed in the literature.

One possible approach [106, 8, 105], which we tackled briefly numerically in [G-30], is to consider the Navier-Stokes equations in some domain Ω, representing the upper airways of the bronchial tree. Further, a Poiseuille law is supposed to be satisfied in each branch; the flow in one branch i can thus be characterized by a single equivalent resistance R_i. This resistance can be computed from an analogy with an electric circuit [180, 16]. We then model the behavior of the diaphragm, which drives the respiration, by assuming that the bronchial tree comes out into a box, whose one side can move in one direction linked to a fixed wall by a spring. This modelling translates into non standard non-local boundary conditions on the stress tensor involving the alveolar pressure, which in turns is deduced from an ordinary differential equation on the position of the diaphragm.

Many other approaches have also been developed, involving differential equations, possibly with different compartments [191], or partial differential equations, in 0D, 1D [181, 204, 89, 197, 196, 125, 176] or 3D coupled with 0D models for the lower parts of the lung [161, 186, 46]. Some of these models also take into account the deformation of the lung *via* fluid-structure interaction effects.

Let us describe in more details the approach by Martin and Maury [158], which consists in a 1D model taking into account the multiscale aspect of the geometry and the heterogeneity of oxygen exchange (see Fig. 4.1(b)). The main elements of the model are the following.

- A 0D mechanical model provides the volume $V(t)$ and the variation of volume $\dot{V}(t)$

  $$R\dot{V}(t) + E(V(t) - V_{\text{FRC}}) = -P_{\text{ext}}(t), \tag{4.1}$$

  where R is the resistance of the airways, E is the elastance of the lung, V_{FRC} is the functional residual capacity, and $P_{\text{ext}}(t)$ is the exterior pressure accounting for the effort of the diaphragm ($P_{\text{ext}} < 0$ for inspiration) and possibly muscles of the abdomen during forced expiration ($P_{\text{ext}} \geq 0$).

- From geometrical data of a 24-generation lung, a lineic version $\tilde{V}(t,x)$ of the volume of the lung $V(t)$ is defined through piecewise constant functions. This corresponds to the volume of the lung at each generation, including the volume of all alveoli for alveolar generations. We thus write $\tilde{V}(t,x) = S_b(x) + S_a(t,x)$, where $S_b(x)$ is the (constant) volume of the bronchial tree, and $S_a(t,x)$ is the volume of the alveoli.

- Denoting by $u(t,x)$ the longitudinal velocity of the air along the tree, it is determined by the conservation of air volume, considered as incompressible

  $$\partial_t \tilde{V}(t,x) + \partial_x (S_b(x) u(t,x)) = 0.$$

- The oxygen concentration $c(t,x)$ is computed by a convection-diffusion equation, with a source term $\mathcal{S}$ describing the oxygen exchanges in the alveoli

  $$\partial_t (\tilde{V}(t,x) c(t,x)) + \partial_x (S_b(x) u(t,x) c(t,x)) - D \partial_x (S_b(x) \partial_x c(t,x)) = -\mathcal{S}(t,x).$$

- The source term describes the oxygen flux from the alveoli to the blood. The main idea of the model is that a quantity V_c of venous blood is brought instantaneously in the neighborhood of the alveoli, stays there during a time τ_b, allowing exchanges to take place, and is periodically evacuated and replaced by the same amount of venous blood. In this case, denoting by σ the solubility of oxygen in the blood, the initial concentration of oxygen in the plasma is σP^v, with P^v the partial pressure of the venous blood, and the final concentration is σP^{atm}, if one assumes that the equilibrium between the partial pressures is reached within the time of stay of the blood in the alveoli. If needed, it can be modified in order to take into account kinetic limitation on the oxygen transfer. The source term is given by

$$\mathcal{S}(t,x) = \alpha(x)\frac{V_c}{\tau_b}\Big[\sigma c(t,x)P^{\mathrm{atm}} - \sigma P^v + 4C_{\mathrm{Hb}}\Big(\mathcal{H}(c(t,x)P^{\mathrm{atm}}) - \mathcal{H}(P^v)\Big)\Big], \tag{4.2}$$

where C_{Hb} is the concentration of hemoglobin in the blood, $\mathcal{H}(y) = y^{2.5}/(26^{2.5} + y^{2.5})$ is the Hill function [132], and $\alpha(x)$ is the proportion of exchange surface at the corresponding generation.

4.1.2 Choice of the diffusion model for air

The previous models do not take into account the multi-species nature of the gas flowing in the airways. In particular, air is obviously a mixture of several species (mainly nitrogen, oxygen, carbon dioxide and water vapor). Moreover, in some therapeutical applications, a mixture of helium (instead of nitrogen) and oxygen (so-called heliox) can be inhaled.

Because of the discussion in Chapter 2 about the importance of the diffusion model in the case of mixtures, we investigate the need to use a cross-diffusion model for the air/heliox in the airways.

In [G-27], we considered a very simplified setting, consisting in a 2D bifurcation with characteristic size corresponding to the 17th generation. In this part of the lung, the convection is negligible, and the diffusion is the main transport mechanism. We considered the air to be a mixture of three species (O_2, CO_2, N_2), and we compared the results of a standard diffusion model with a cross-diffusion model of Maxwell-Stefan type. In this toy configuration, we observed that a cross-diffusion model is not needed to describe the evolution of air. However, when considering heliox (O_2, CO_2, He), the cross-diffusion model is more relevant, because of the different binary diffusivities of the species.

Work in progress

It thus seems important to investigate further the influence of the diffusion model for different gases in the airways. Since the diffusion in the distal part of the lung has to be coupled with the air transport in the higher airways and the gas exchanges in the alveoli, we are currently working with Laurent Boudin, Céline Grandmont and Sébastien Martin on the extension of the model of [158] described in Section 4.1.1 to the multi-species setting. This full 1D ventilation-perfusion model, taking into account the geometrical aspects of the lung and the gas exchanges in the alveoli, allows to investigate the influence of the diffusion model in the airways, as well as the influence of the gas carrier (nitrogen vs. helium). A first step for developing such a model is the description of both oxygen and carbon dioxide gas exchanges, which is described in the next Section 4.1.3. Incorporating an accurate description of the gas exchanges in the alveoli generalizes previous works not taking the coupling into account [176, 175].

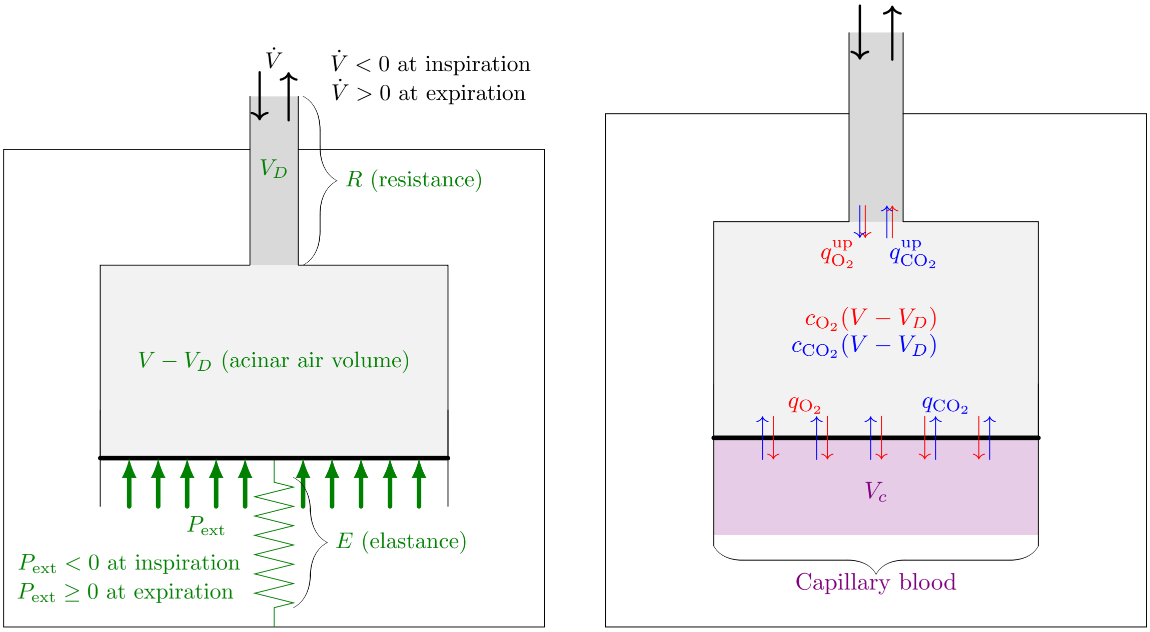

(a) Schematic view of the lung mechanics

(b) Schematic view of the gas exchange model

Figure 4.2: Schematic view of the elements of the 0D model with gas exchanges

4.1.3 Gas exchange modelling

The gas exchanges in the alveoli are a crucial part of the respiration, and are driven by the blood-alveolar partial pressure of each species. In [G-4], we proposed an integrated dynamical model for oxygen and carbon dioxide transfer from the lung into the blood, coupled with the lumped mechanical model (4.1) for the ventilation process. Chemically, the affinity of hemoglobin with respect to oxygen depends on the blood pressure of carbon dioxide, which is referred to as the Haldane and Bohr effects in the literature [118, 206, 107, 114, 156]. Those effects induce a nonlinear coupling in the dynamics of the diffusion process of each species, which we took into account.

Let us describe the 0D model in more details.

- The same mechanical model (4.1) provides the variation of volume $\dot V(t)$. One important ingredient of our model is to take into account the so-called dead volume V_D of the lung [206, 114], *i.e.* the volume which does not contribute to the gas exchanges (see Figure 4.2(a)). This volume is split into two contributions, a (constant) anatomic one, and one depending on the patient state. This last contribution is chosen depending on the patient breathing at each respiratory cycle.

- Let us now explain how to determine the mole fractions of oxygen c_{O_2} and of carbon dioxide c_{CO_2} in the alveoli. The mole balances in the alveolar space (see Figure 4.2(b)) give the evolution of these quantities as

  $$\frac{\mathrm{d}}{\mathrm{d}t}\Big(c_\kappa(t)(V(t) - V_D)\Big) = q_\kappa^{\text{up}}(t) - q_\kappa(t), \qquad \kappa \in \{O_2, CO_2\},$$

  where $q_\kappa^{\text{up}}(t)$ is expressed from $c_\kappa(t)$ and $\dot V(t)$ depending on the sign of $\dot V(t) \lessgtr 0$ (inspiration/expiration), and $q_\kappa(t)$ is the quantity of κ transferred to the blood.

- ✍ Observe that in 1D, (4.2) can be rewritten under the following form

  $$\mathcal{S}(t,x) = \alpha(x)\frac{V_c}{\tau_b}\Big[\mathcal{C}(P^a(t,x)) - \mathcal{C}(P^v)\Big],$$

  where $P^a(t,x) = c(t,x)P^{\text{atm}}$, and the function $\mathcal{C}(P) = \sigma P + 4C_{\text{Hb}}\mathcal{H}(P)$ describes the concentration of oxygen in the blood, through the Hill function $\mathcal{H}$. In the same way, we determine the instantaneous alveolo-capillary fluxes in our 0D model by

  $$q_\kappa(t) = \frac{V_c}{\tau_b}\Big[\mathcal{C}_\kappa(P^a_{\text{O}_2}(t), P^a_{\text{CO}_2}(t)) - \mathcal{C}_\kappa(P^v_{\text{O}_2}, P^v_{\text{CO}_2})\Big], \qquad \kappa \in \{\text{O}_2, \text{CO}_2\},$$

  where it remains to compute the instantaneous partial pressures in arterial blood P^a_κ, and to express the functions describing the gas exchanges $\mathcal{C}_\kappa$.

- ✍ When neglecting kinetic limitation, the arterial pressures are given by $P^a_\kappa(t) \simeq c_\kappa(t)P^{\text{atm}}$, but for some pathological situations, or breathing scenarios, we can take into account the kinetic limitation, which is described by a nonlinear system of differential equations allowing to define P^a_κ. These equations involve the important parameters $D_{m,\kappa}$, which are the diffusion coefficients of the alveolar membrane for each species.

- ✍ Last, the function $\mathcal{C}_{\text{O}_2}$ is chosen to take into account the Bohr effect, meaning that the oxygen-binding affinity is shifted with respect to both pH and carbon dioxide concentration. To this end, the Hill function $\mathcal{H}(P)$ in $\mathcal{C}$ is modified into a function $\widetilde{\mathcal{H}}(P_{\text{O}_2}, P_{\text{CO}_2}, \text{pH})$. In our model, the pH is supposed to be a constant parameter, but it could also be extended and coupled with CO_2 (acid-base equilibrium).

- ✍ The function $\mathcal{C}_{\text{O}_2}$ on the other hand is chosen to take into account the Haldane effect, meaning that blood oxygen increases the carbon dioxide removal. This is achieved through a phenomenological formula, called the Meade formula [165], describing the blood carbon dioxide concentration in a highly nonlinear way.

In this model, the standard values of the parameters (R, E, $D_{m,\kappa}$) are well described in the literature. The model, used with parameters corresponding to a healthy situation, allows to recover physically relevant values of the averaged quantities over a time period (denoted by $\langle\cdot\rangle$), in terms of fluxes, arterial pressures, and gas concentrations for both species, as showed in Table 4.1. The ratio $\text{RQ} = |q_{\text{CO}_2}/q_{\text{O}_2}|$ is the respiratory quotient, used in the literature as a possible indicator for some pathological states (for example chronic obstructive pulmonary disease).

$\langle q_{\text{O}_2}\rangle$	$\langle q_{\text{CO}_2}\rangle$	RQ	$\langle P^a_{\text{O}_2}\rangle$	$\langle P^a_{\text{CO}_2}\rangle$	$\langle c_{\text{O}_2}\rangle$	$\langle c_{\text{CO}_2}\rangle$	V_D
256 mL/min	−203 mL/min	0.793	97.6 mmHg	41 mmHg	13.7%	5.74%	0.152 L

Table 4.1: Averaged quantities in the healthy case with standard breathing parameters.

Further, a sensitivity analysis with respect to the parameters can be performed. This allows to relate some physiological quantities to the parameters of the model. To this end, we fix one parameter equal to its healthy value, and we let the two other parameters vary from their reference value. For example, for a healthy value of R, we observe on Figure 4.3(a) that the oxygen arterial pressure is sensitive to D_m, in particular for small values of E, whereas the

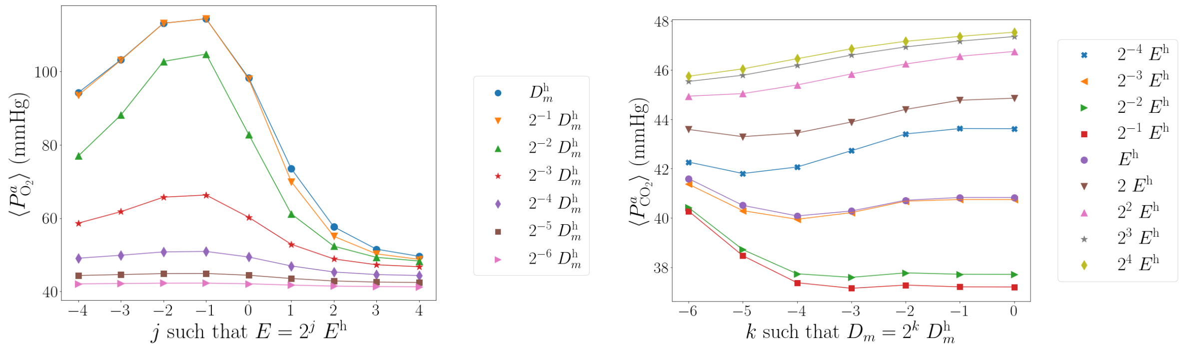

(a) $\langle P^a_{O_2} \rangle$ w.r.t. E for various values of D_m

(b) $\langle P^a_{O_2} \rangle$ w.r.t. D_m for various values of E

Figure 4.3: Crossed sensitivity analysis of the arterial pressures with respect to E and D_m

carbon dioxide arterial pressure could be seen as a good indicator for the lung stiffness (Fig. 4.3(b).

We can also consider characteristic pathological situations, for which correct tendencies can be recovered with the model. For example, asthma is roughly characterized by an increase of the resistance R of the bronchial tree. When increasing R by a factor 4, we give in Table 4.2 the relative variations (denoted by $\Delta\cdot$) of the different quantities with respect to the healthy case. We observe that the carbon dioxide flux drastically goes down, leading to rising CO_2 concentrations in both the lung and the blood, and consequently to acidosis. We also observe a significant increase of the dead volume. Different respiration scenarii can be then tested to compare their efficiency.

$\Delta\langle q_{O_2} \rangle$	$\Delta\langle q_{CO_2} \rangle$	RQ	$\Delta\langle P^a_{O_2} \rangle$	$\Delta\langle P^a_{CO_2} \rangle$	$\Delta\langle c_{O_2} \rangle$	$\Delta\langle c_{CO_2} \rangle$	ΔV_D
−24.6%	−69.4%	0.323	−31.5%	11.7%	−31.2%	12%	53.9%

Table 4.2: Relative variations of the averaged quantities with respect to the healthy case for increased R (asthma)

Other pathological situations have been considered, such as happy hypoxia (related to D_m), fibrosis or emphysema (related to E).

4.2 Aerosols in the airways

Several types of particles are inhaled and transported in the airways, such as therapeutical aerosols or pollution particles. These particles can interact with the respiratory system. In the case of pollution particles, they have to be filtered by the airways before reaching the alveoli, whereas therapeutical aerosols need to reach the exact region of the lungs where they are needed. Therefore, mathematical models can be useful to understand the transport of these particles in the airways, and possibly optimize the protocols of inhalation.

Such particles can be described at different scales [65], either at the microscopic scale, as individual particles, which quickly becomes out of hand for numerous particles, or at macroscopic scale, as a continuous phase, which is however not accurate for diluted sprays. The mesoscopic scale is therefore often chosen to describe the particles, either for so-called thick sprays (in the sense that the volume occupied by the particles is of the same order of magnitude as the one occupied by the fluid) [159], or, when the interactions (collisions) between the particles can be neglected, the context of thin sprays, which is the one we will focus on. For such models, the particles are a dispersed phase in the air, and can thus be described by a kinetic equation on the distribution function f of the particles, which depends at least on (t, x, v), but can also depend on other variables, such as the radius r of the particles or their temperature T, and satisfies a Vlasov-type equation [198, 10]. On the other hand, the air can be described by fluid equations (for example the Navier-Stokes equations) on macroscopic quantities such as the velocity u and the pressure p, which depend on (t, x).

More precisely, for the airflow, the gas is assumed to be incompressible, with a constant density $\rho_{\mathrm{air}} = 1.11\,\mathrm{kg}\cdot\mathrm{m}^{-3}$, and a dynamic viscosity μ. The aerosol is also assumed to be an incompressible fluid very similar to water, so that its volumic mass is $\rho_{\mathrm{aero}} = 1000\,\mathrm{kg}\cdot\mathrm{m}^{-3}$. The full model can be written as

$$\rho_{\mathrm{air}}\Big(\partial_t u(t,x) + \nabla\big(u(t,x)\otimes u(t,x)\big)\Big) - \mu\Delta u(t,x) + \nabla p(t,x) = \mathcal{F}_{\mathrm{aero}}(t,x), \tag{4.3a}$$

$$\nabla\cdot u(t,x) = 0, \tag{4.3b}$$

$$\partial_t f(t,x,v,r) + \nabla\cdot\Big(vf(t,x,v,r)\Big) + \nabla_v\cdot\Big(a(t,x,v,r)f(t,x,v,r)\Big) = 0, \tag{4.3c}$$

where $\mathcal{F}_{\mathrm{aero}}$ is a force term due to the presence of the particles (acting as a source term in the Navier-Stokes equations), and a is the acceleration of the particles, which is mainly due to the Stokes force exerted by the fluid on the aerosol. The acceleration is given by

$$a(t,x,v,r) = \frac{6\pi\mu r}{m(r)}(u(t,x) - v),$$

where the mass of a particle of radius r is $m(r) = \frac{4}{3}\pi r^3\rho_{\mathrm{aero}}$. The retroaction force of the particles on the fluid is given by

$$\mathcal{F}_{\mathrm{aero}}(t,x) = \int_{\mathbb{R}^3\times\mathbb{R}^+} m(r)a(t,x,v,r)f(t,x,v,r)\,\mathrm{d}r\,\mathrm{d}v.$$

The system is supplemented by boundary conditions, which depend on the chosen domain Ω but can be formulated generically as follows. Assume that the boundary $\Gamma = \partial\Omega$ consists in three parts:

- ▷ the entrance part Γ_{in}, on which the flow of the air and the distribution function of particles f are prescribed;
- ▷ the lateral parts Γ_{lat}, on which a zero Dirichlet condition is imposed for the velocity of the air, and the particles deposit if they hit the wall, meaning that $f(t,x,v,r) = 0$ if $v\cdot n < 0$;
- ▷ the exit part Γ_{out}, on which a homogeneous Neumann boundary condition is imposed for the fluid: the particles exit the domain through Γ_{out}.

In the case of variable radius particles, an additional equation on the evolution of r has to be added to the model (see Section 4.2.2).

Numerically, the airflow can be solved by a standard P^2 (for the velocity) and P^1 (for the pressure) finite element method, and the aerosol by a particle method. Since this is standard, we do not detail the numerical method here. The deposition (resp. exiting) of particles is taken into account by considering that a particle deposits if its distance to the wall Γ_{lat} (resp. Γ_{out}) is smaller than its radius. Moreover, one needs to perform a sub-cycling in time for the aerosol computation. Without it, the particles could go across several mesh cells during one single fluid time step, and not follow the correct trajectory.

Many phenomena can be observed with such models. In this section, we focus on two preparatory contributions, in which two types of effects are taken into account: the influence on the airflow of the presence of the particles, and the radius growth of the particles due to humidity in the respiratory system.

4.2.1 Influence of the particles on the airflow

As we mentioned, the inhalation of an aerosol can induce mechanical effects on the respiration. While the drag force exerted by the air on the particles is well studied, the literature is not always in agreement on whether to neglect the retroaction force exerted by the particles on the fluid (assumption of a very thin spray) or not. We therefore focused in [G-28] on determining the range of size and velocities in which this retroaction force $\mathcal{F}_{\text{aero}}$ can be neglected.

Let us mention that the mathematical analysis of system (4.3) with retroaction (without any dependence on r) has been performed in [37], where the authors proved that the incompressible Navier-Stokes-Vlasov system admits a weak solution in suitable function spaces, with an energy inequality.

Preliminary numerical simulations were provided in [G-28], emphasizing that the retroaction force is not negligible in the case of large particles, or in the case of a very large number of particles (which can be the case for some nebulizers) and can induce a significant modification of the airflow. Moreover, we observed that the deposition of the particles on the walls of the airways could also be modified when taking into account this force, underlining the importance of further works. This model has then been more thoroughly investigated in [38], where first 3D numerical simulations are provided. In the context of respiration and deposition of aerosols for the rat, further numerical simulations can be found in [177–179], with an agent-based model to describe the aerosol in the airways.

4.2.2 Variable size and temperature

The aerosol particles in the lung happen to have hygroscopic properties, and can vary in size due to the humidity in the airways [149, 150]. Note that these hygroscopic properties strongly rely on thermal effects, which hints that also the particles temperature should be taken into account. Assuming that the droplets remain spherical, we studied the influence of radius growth on deposition in [G-11], by introducing an extension of the previous model (4.3), in which the air temperature, the mass fraction of the water vapor in the air, and the radius and temperature of the particles are taken into account. We assume that in each particle, one can find active products (the drug of the aerosol), a possible excipient, and (possibly) water. Therefore, the mass $m(r)$ of a particle of radius r is corrected with respect to the previous expression by taking into account the mass densities of the drug and the excipient with equivalent radii.

The Vlasov equation (4.3c) is replaced by a similar equation on $f(t, x, v, r, T)$ of the form

$$\partial_t f + \nabla \cdot (vf) + \nabla_v \cdot (af) + \partial_r(a_r f) + \partial_T(a_t f) = 0,$$

where a_r and a_T represent the radius and temperature growth of the particles. These functions are built following the approach in [149].

- ✍ The function a_r depends on r, T, on the mass fraction of the water vapor in the air $Y_{v,\text{air}}$. It involves the evaporating water flux at the surface of the particle Q_{v}, proportional to the water vapor mass fraction difference between the particles and the air $Y_{\text{v,aero}} - Y_{\text{v,air}}$, where $Y_{\text{v,aero}}$ depends in a highly non-linear way on r and T.

- The function a_T depends on r, T, $Y_{\mathrm{v,air}}$ and the air temperature T_{air}. It involves Q_{v} and the heat flux Q_{h} between the particles and the air, proportional to the temperature difference between the particles and the air $T - T_{\mathrm{air}}$, as well as the same evaporating water flux as in a_r.

Of course, we then need additional equations for the air quantities $Y_{\mathrm{v,air}}$ (resp. T_{air}). They both satisfy an advection-diffusion equation, with a source term S_{v} accounting for the water mass exchanges between the bronchial air and the aerosol for $Y_{\mathrm{v,air}}$ (resp. S_T accounting for the heat transfer between the air and the aerosol for T_{air}). These source terms are expressed in terms of the evaporating water flux Q_{v} and the heat flux Q_{h} as

$$S_{\mathrm{v}}(t,x) = \int_{\mathbb{R}^3 \times \mathbb{R}_*^+ \times \mathbb{R}_*^+} 4\pi r^2 Q_{\mathrm{v}}(r, T, Y_{\mathrm{v,air}}) f(t,x,v,r,T)\,\mathrm{d}r\,\mathrm{d}T\,\mathrm{d}v,$$

$$S_T(t,x) = \int_{\mathbb{R}^3 \times \mathbb{R}_*^+ \times \mathbb{R}_*^+} 4\pi r^2 Q_{\mathrm{h}}(r, T, T_{\mathrm{air}}) f(t,x,v,r,T)\,\mathrm{d}r\,\mathrm{d}T\,\mathrm{d}v.$$

For numerical simulations, we consider the following 2D experimental context. The domain is supposed to be the trachea and the first bifurcation, with geometrical data from [203], taking into account a 3D-2D correction for each branch length. The air temperature is initially a 37 °C, as well as the boundary condition at the walls. The entrance temperature of both air and the particles is 24 °C (room temperature). The initial and boundary conditions on $Y_{\mathrm{v,air}}$ also are chosen to be physically relevant. We consider 5 injections of 100 numerical particles (representing 100×10^4 physical particles), periodically released between the initial time and $t = 0.25\,\mathrm{s}$. On Figure 4.4, we plot for different times the positions of the particles, and the air temperature in the domain. One can observe the influence of the asymetry of the domain on the airflow, and thus on the convection of the aerosol. The presence of the particles has an influence on the air temperature: there is a local air temperature increase at the particles location (*cf.* Figure 4.5). This effect is not explained by direct thermal phenomena, but from water vapor mass exchange between air and the particles.

Moreover, the radius growth and temperature evolution along time of a particle (here chosen from the second release) can be observed on Figure 4.6, where we compare the full model presented here (blue curve) with the one in which the temperature of the aerosol is constant (therefore, there is no variation in T of f) (red curve) and the classical one without any radius nor temperature variation (yellow curve). As far as the particle temperature is concerned (full model only), we see that since the droplet belongs to the second release, it evolves in ambient air temperature, which means that its temperature evolution is triggered by hygroscopic phenomena. Moreover, when neglecting the temperature variation, the radius growth is overestimated, which obviously heavily impacts the deposition of the particles in a non-physical way.

Let us mention that further analysis of this model (extended to a time-dependent domain) has been the topic of the PhD of David Michel, and the existence of a weak solution has been proved in [40]. 3D numerical simulations in a branched structure are provided in [39], where they discussed possible simplifications of the model, such as the fact that the water vapor mass fraction in the air may be considered to be constant in standard breathing conditions.

Prospect

> The hygroscopic effects in the lung are still not well known, and there is a need to understand how the bioaerosols, loaded with viruses such as SARS-CoV-2, are transported inside the airways. In that spirit, we could also consider an improvement of the model, by taking into

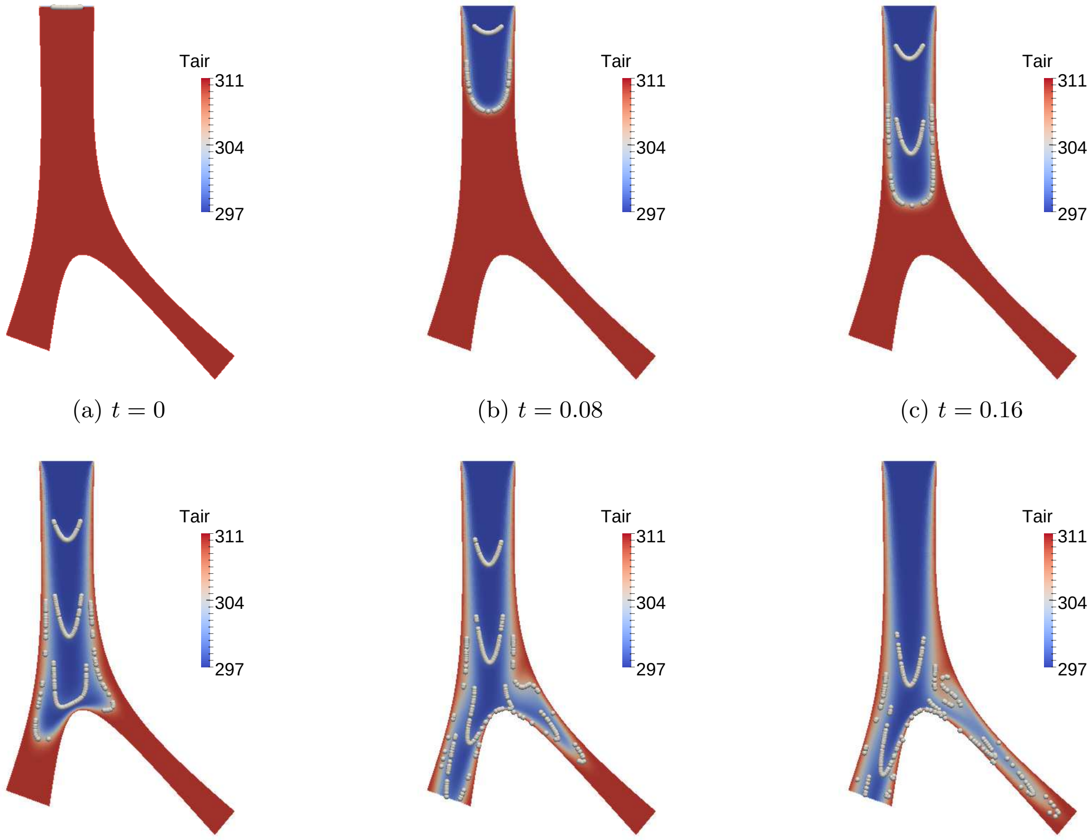

(a) $t = 0$ (b) $t = 0.08$ (c) $t = 0.16$

(d) $t = 0.24$ (e) $t = 0.32$ (f) $t = 0.4$

Figure 4.4: Dynamics of the particles and air temperature at different times $t = 0.08k$, $0 \leq k \leq 5$

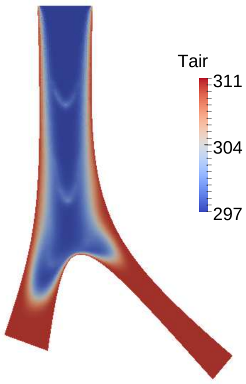

Figure 4.5: Local effects of the aerosol on the air temperature at time $t = 0.25$

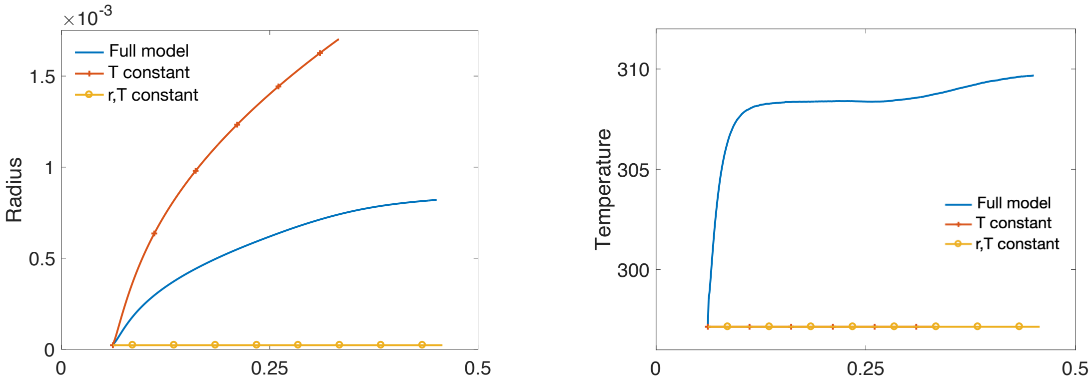

Figure 4.6: Radius and temperature evolution of a particle from the second release for different models

account the water vapor and heat exchanges of the airways with the mucus, remembering that a significant part of aerosol is deposited on the mucus.

Prospect

More generally, in the context of fluid/kinetic models describing air and particles in the lung, or possibly in closed domains (typically for viruses in closed rooms), many extensions could be investigated. First, depending on the application, the orders of magnitude have to be studied, to determine the right description of the spray: thin or (very) thick spray, taking into account a force acting on the particles as a pressure gradient from the fluid, and/or possibly collisions between the particles [63, 80], which involve similar models as the ones studied in Chapter 2. Further, the fact that the gases are polyatomic could be taken into account in these models, as mentioned in Section 2.8.2.

Prospect

From the numerical point of view, suitable strategies also have to be developed for the extended fluid/kinetic models suggested before. In particular, a special care has to be taken to satisfy the conservation of physical quantities at the discrete level, as it can be proved at the continuous level. Moreover, as in Section 2.8.1, the different involved scales (fluid and kinetic) and their coupling might require new numerical approaches. This has been for example considered recently in [90] in the case of thick sprays, where numerical strategies are proposed to handle the fluid and kinetic equations coupled through the fluid volume fraction.

CHAPTER 5

Author’s publications

[G-1] N. Bernhoff, L. Boudin, M. Čolić, and B. Grec. “Compactness of linearized Boltzmann operators for polyatomic gases”. *Proceedings of the Final Conference of COST Action “CA18232: Mathematical models for interacting dynamics on networks”, Springer* (2025), to appear.

[G-2] B. Grec, D. Kumozec, and Y. Penel. “Unconditionally stable numerical scheme for the 2D transport equation”. *Comput. Math. Appl.* (2025), to appear.

[G-3] B. Grec and S. Simic. “Numerical Study of the Higher-Order Maxwell-Stefan Model of Diffusion”. *Proceedings of the Final Conference of COST Action “CA18232: Mathematical models for interacting dynamics on networks”, Springer* (2025), to appear.

[G-4] L. Boudin, C. Grandmont, B. Grec, and S. Martin. “A coupled model for the dynamics of gas exchanges in the human lung with Haldane and Bohr’s effects”. *J. Theoret. Biol.* (2023), p. 111590.

[G-5] L. Boudin, B. Grec, M. Pavić-Čolić, and S. Simić. “Energy method for the Boltzmann equation of monatomic gaseous mixtures”. *Commun. Math. Sci.* (2023).

[G-6] M. Briant and B. Grec. “Rigorous derivation of the Fick cross-diffusion system from the multi-species Boltzmann equation in the diffusive scaling”. *Asymptot. Anal.* 135 (1-2) (2023), pp. 55–80.

[G-7] G. Faccanoni and B. Grec. “Comparison of several complete cubic laws for two-phase flow models”. *ESAIM: ProcS* 72 (2023), pp. 117–142.

[G-8] B. Grec and S. Simić. “Higher-order Maxwell-Stefan model of diffusion”. *Matematica* (2023).

[G-9] G. Faccanoni, B. Grec, and Y. Penel. “A homogeneous relaxation low Mach number model”. *ESAIM Math. Model. Numer. Anal.* 55 (4) (2021), pp. 1569–1598.

[G-10] A. Bondesan, L. Boudin, M. Briant, and B. Grec. “Stability of the spectral gap for the Boltzmann multi-species operator linearized around non-equilibrium Maxwell distributions”. *Commun. Pure Appl. Anal.* 19 (5) (2020), pp. 2549–2573.

[G-11] L. Boudin, C. Grandmont, B. Grec, S. Martin, A. Mecherbet, and F. Noël. “Fluid-kinetic modelling for respiratory aerosols with variable size and temperature”. *ESAIM: ProcS* 67 (2020), pp. 100–119.

[G-12] A. Bondesan, L. Boudin, and B. Grec. “A numerical scheme for a kinetic model for mixtures in the diffusive limit using the moment method”. *Numer. Methods Partial Differential Equations* 35 (3) (2019), pp. 1184–1205.

[G-13] L. Boudin, B. Grec, and V. Pavan. “Diffusion models for mixtures using a stiff dissipative hyperbolic formalism”. *J. Hyperbolic Differ. Equ.* 16 (2) (2019), pp. 293–312.

[G-14] S. Dellacherie, G. Faccanoni, B. Grec, and Y. Penel. “Accurate steam-water equation of state for two-phase flow LMNC model with phase transition”. *Appl. Math. Model.* 65 (2019), pp. 207–233.

[G-15] B. Grec, B. Maury, N. Meunier, and L. Navoret. “A 1D model of leukocyte adhesion coupling bond dynamics with blood velocity”. *J. Theoret. Biol.* 452 (2018), pp. 35–46.

[G-16] L. Boudin, B. Grec, and V. Pavan. “The Maxwell-Stefan diffusion limit for a kinetic model of mixtures with general cross sections”. *Nonlinear Anal.* 159 (2017), pp. 40–61.

[G-17] G. Bayada, L. Chupin, and B. Grec. “Some theoretical results concerning diphasic flows in thin films”. *Nonlinear Anal.* 116 (2015), pp. 153–179.

[G-18] L. Boudin, B. Grec, and F. Salvarani. “The Maxwell-Stefan diffusion limit for a kinetic model of mixtures”. *Acta Appl. Math.* 136 (2015), pp. 79–90.

[G-19] C. Etchegaray, B. Grec, B. Maury, N. Meunier, and L. Navoret. “An integro-differential equation for 1D cell migration”. *Integral methods in science and engineering.* Birkhäuser/Springer, Cham, 2015, pp. 195–207.

[G-20] M. Bernard, S. Dellacherie, G. Faccanoni, B. Grec, and Y. Penel. “Study of a low Mach nuclear core model for two-phase flows with phase transition I: Stiffened gas law”. *ESAIM Math. Model. Numer. Anal.* 48 (6) (2014), pp. 1639–1679.

[G-21] S. Dellacherie, G. Faccanoni, B. Grec, E. Nayir, and Y. Penel. “2D numerical simulation of a low Mach nuclear core model with stiffened gas using Freefem++”. *ESAIM: ProcS* 45 (2014), pp. 138–147.

[G-22] L. Boudin, B. Grec, M. Pavić, and F. Salvarani. “Diffusion asymptotics of a kinetic model for gaseous mixtures”. *Kinet. Relat. Models* 6 (1) (2013), pp. 137–157.

[G-23] M. Bernard, S. Dellacherie, G. Faccanoni, B. Grec, O. Lafitte, T.-T. Nguyen, and Y. Penel. “Study of a low Mach nuclear core model for single-phase flows”. *ESAIM: Proc.* 38 (2012), pp. 118–134.

[G-24] L. Boudin, B. Grec, and F. Salvarani. “A mathematical and numerical analysis of the Maxwell-Stefan diffusion equations”. *Discrete Contin. Dyn. Syst. Ser. B* 17 (5) (2012), pp. 1427–1440.

[G-25] L. Chupin and B. Grec. “Steady state solutions for a lubrication multi-fluid flow”. *European J. Appl. Math.* 22 (6) (2011), pp. 581–612.

[G-26] G. Bayada, L. Chupin, and B. Grec. “A new model of diphasic fluids in thin films”. *Advances in mathematical fluid mechanics.* Springer, Berlin, 2010, pp. 25–35.

[G-27] L. Boudin, D. Götz, and B. Grec. “Diffusion models of multicomponent mixtures in the lung”. *ESAIM: Proc.* 30 (2010), pp. 90–103.

[G-28] L. Boudin, C. Grandmont, B. Grec, and D. Yakoubi. “Influence of the spray retroaction on the airflow”. *ESAIM: Proc.* 30 (2010), pp. 153–165.

[G-29] G. Bayada, L. Chupin, and B. Grec. “Viscoelastic fluids in thin domains: a mathematical proof”. *Asymptot. Anal.* 64 (3-4) (2009), pp. 185–211.

[G-30] A. Devys, C. Grandmont, B. Grec, B. Maury, and D. Yakoubi. “Numerical method for the 2D simulation of the respiration”. *ESAIM: Proc.* 28 (2009), pp. 162–181.

[G-31] G. Bayada, L. Chupin, and B. Grec. “An unconditional existence result for elastohydrodynamic piezoviscous lubrication problems with Elrod-Adams model of cavitation”. *Differential Integral Equations* 21 (1-2) (2008), pp. 41–62.

[G-32] B. Grec and E. V. Radkevich. “Newton's polygon method and the local solvability of free boundary problems”. *J. Math. Sci. (N.Y.)* 143 (4) (2007). Trudy Seminara im. I. G. Petrovskogo (Petrovskii Seminars) No. 26 (2007), pp. 3253–3292.

[G-33] M. Geissert, B. Grec, M. Hieber, and E. Radkevich. “The model-problem associated to the Stefan problem with surface tension: an approach via Fourier-Laplace multipliers”. *Differential equations: inverse and direct problems.* Vol. 251. Lect. Notes Pure Appl. Math. Chapman & Hall/CRC, Boca Raton, FL, 2006, pp. 171–182.

CHAPTER 6

Bibliography

[1] A. Almgren, J. Bell, C. Rendleman, and M. Zingale. “Low Mach number modeling of type Ia supernovae. I. Hydrodynamics”. *Astrophys. J.* 637 (2) (2006), p. 922.

[2] A. Ambroso, J.-M. Hérard, and O. Hurisse. “A method to couple HEM and HRM two-phase flow models”. *Comput. Fluids* 38 (2009), pp. 738–756.

[3] V. Anaya, M. Bendahmane, and M. Sepúlveda. “Numerical analysis for a three interacting species model with nonlocal and cross diffusion”. *ESAIM Math. Model. Numer. Anal.* 49 (1) (2015), pp. 171–192.

[4] P. Andries, K. Aoki, and B. Perthame. “A consistent BGK-type model for gas mixtures”. *J. Statist. Phys.* 106 (5-6) (2002), pp. 993–1018.

[5] B. Anwasia and S. Simić. “Maximum entropy principle approach to a non-isothermal Maxwell-Stefan diffusion model”. *Appl. Math. Lett.* 129 (2022), Paper No. 107949, 9.

[6] K. Asano and S. Ukai. “On the fluid dynamical limit of the Boltzmann equation”. *Recent topics in nonlinear PDE.* Vol. 98. North-Holland, 1984, pp. 1–19.

[7] M. R. Baer and J. W. Nunziato. “A two-phase mixture theory for the deflagration-to-detonation transition (DDT) in reactive granular materials”. *Int. J. Multiphase Flow* 12 (1986), pp. 861–889.

[8] L. Baffico, C. Grandmont, and B. Maury. “Multiscale modelling of the respiratory tract”. *Math. Models Methods Appl. Sci.* (2010), pp. 59–93.

[9] R. Bailo and T. Rey. “Projective and telescopic projective integration for non-linear kinetic mixtures”. *J. Comput. Phys.* 458 (2022), p. 111082.

[10] C. Baranger, L. Boudin, P.-E. Jabin, and S. Mancini. “A modeling of biospray for the upper airways”. *ESAIM: Proc.* 14 (2005), pp. 41–47.

[11] T. Barberon and P. Helluy. “Finite volume simulation of cavitating flows”. *Comput. Fluids* 34 (7) (2005), pp. 832–858.

[12] C. Bardos, F. Golse, and C. D. Levermore. “Fluid dynamic limits of kinetic equations. II. Convergence proofs for the Boltzmann equation”. *Comm. Pure Appl. Math.* 46 (5) (1993), pp. 667–753.

[13] C. Bardos, F. Golse, and D. Levermore. “Fluid dynamic limits of kinetic equations. I. Formal derivations”. *J. Stat. Phys.* 63 (1-2) (1991), pp. 323–344.

[14] C. Bardos and S. Ukai. “The classical incompressible Navier-Stokes limit of the Boltzmann equation”. *Math. Models Methods Appl. Sci.* 1 (2) (1991), pp. 235–257.

[15] N. Bellomo. *Lecture notes on the mathematical theory of the Boltzmann equation.* Vol. 33. World Scientific, 1995.

[16] A. Ben-Tal. “Simplified models for gas exchange in the human lungs”. *J. Theoret. Biol.* 238 (2) (2006), pp. 474–495.

[17] M. Bennoune, M. Lemou, and L. Mieussens. “Uniformly stable numerical schemes for the Boltzmann equation preserving the compressible Navier-Stokes asymptotics”. *J. Comput. Phys.* 227 (8) (2008), pp. 3781–3803.

[18] N. Bernhoff. “Linearized Boltzmann collision operator: I. Polyatomic molecules modeled by a discrete internal energy variable and multicomponent mixtures”. *Acta Appl. Math.* 183 (2023), Paper No. 3, 45.

[19] N. Bernhoff. “Linearized Boltzmann collision operator: II. Polyatomic molecules modeled by a continuous internal energy variable”. *Kinet. Relat. Models* 16 (6) (2023), pp. 828–849.

[20] N. Bernhoff. “Compactness property of the linearized Boltzmann collision operator for a multicomponent polyatomic gas”. *J. Math. Anal. Appl.* 537 (1) (2024), Paper No. 128625, 31.

[21] D. Berthelot. “Sur une méthode purement physique pour la détermination des poids moléculaires des gaz et des poids atomiques de leurs éléments”. *J. Phys. Theor. Appl.* 8 (1) (1899), pp. 263–274.

[22] M. Bessemoulin-Chatard, M. Herda, and T. Rey. “Hypocoercivity and diffusion limit of a finite volume scheme for linear kinetic equations”. *Math. Comp.* 89 (323) (2020), pp. 1093–1133.

[23] M. Bessemoulin-Chatard, T. Laidin, and T. Rey. “Discrete hypocoercivity for a nonlinear kinetic reaction model”. *IMA J. Numer. Anal.* (2025), to appear.

[24] D. Bestion. “The physical closure laws in the CATHARE code”. *Nucl. Eng. Des.* 124 (3) (1990), pp. 229–245.

[25] P. L. Bhatnagar, E. P. Gross, and M. Krook. “A Model for Collision Processes in Gases. I. Small Amplitude Processes in Charged and Neutral One-Component Systems”. *Phys. Rev.* 94 (3 1954), pp. 511–525.

[26] M. Bisi, T. Borsoni, and M. Groppi. “A General Framework for the Kinetic Modelling of Polyatomic Gases”. *Commun. Math. Phys.* 392 (2022), pp. 215–266.

[27] M. Bisi, T. Borsoni, and M. Groppi. “An internal state kinetic model for chemically reacting mixtures of monatomic and polyatomic gases”. *Kinet. Relat. Models* 17 (2) (2024), pp. 276–311.

[28] M. Bisi, M. Groppi, and G. Martalò. “Macroscopic equations for inert gas mixtures in different hydrodynamic regimes”. *J. Phys. A* 54 (8) (2021), Paper No. 085201, 23.

[29] A. Bondesan. “Asymptotique diffusive de l’équation de Boltzmann pour les mélanges gazeux, étude mathématique et numérique”. PhD thesis. Université Paris Descartes, 2019.

[30] A. Bondesan and M. Briant. “Stability of the Maxwell-Stefan system in the diffusion asymptotics of the Boltzmann multi-species equation”. *Comm. Math. Phys.* 382 (1) (2021), pp. 381–440.

[31] A. Bondesan and M. Briant. “Perturbative Cauchy theory for a flux-incompressible Maxwell-Stefan system”. *Discrete Contin. Dyn. Syst.* 42 (6) (2022), pp. 2747–2773.

[32] T. Borsoni, L. Boudin, and F. Salvarani. “Compactness property of the linearized Boltzmann operator for a polyatomic gas undergoing resonant collisions”. *J. Math. Anal. Appl.* 517 (2023), p. 126579.

[33] S. Boscarino, S. Y. Cho, M. Groppi, and G. Russo. “BGK models for inert mixtures: comparison and applications”. *Kinet. Relat. Models* 14 (5) (2021), pp. 895–928.

[34] D. Bothe. “On the Maxwell-Stefan approach to multicomponent diffusion”. *Parabolic problems.* Vol. 80. Progr. Nonlinear Differential Equations Appl. Springer Basel, 2011, pp. 81–93.

[35] D. Bothe and W. Dreyer. “Continuum thermodynamics of chemically reacting fluid mixtures”. *Acta Mech.* 226 (6) (2015), pp. 1757–1805.

[36] F. Bouchut and L. Desvillettes. “A proof of the smoothing properties of the positive part of Boltzmann’s kernel”. *Rev. Mat. Iberoamericana* 14 (1) (1998), pp. 47–61.

[37] L. Boudin, L. Desvillettes, C. Grandmont, and A. Moussa. “Global existence of solutions for the coupled Vlasov and Navier-Stokes equations”. *Differential Integral Equations* 22 (11-12) (2009), pp. 1247–1271.

[38] L. Boudin, C. Grandmont, A. Lorz, and A. Moussa. “Modelling and Numerics for Respiratory Aerosols”. *Commun. Comput. Phys.* 18 (3) (2015), pp. 723–756.

[39] L. Boudin and D. Michel. “Three-dimensional numerical study of a fluid-kinetic model for respiratory aerosols with variable size and temperature”. *J. Comput. Theor. Transp.* 50 (5) (2021), pp. 507–527.

[40] L. Boudin, D. Michel, and A. Moussa. “Global existence of weak solutions to the incompressible Vlasov-Navier-Stokes system coupled to convection-diffusion equations”. *Math. Models Methods Appl. Sci.* 30 (8) (2020), pp. 1485–1515.

[41] J.-F. Bourgat, L. Desvillettes, P. Le Tallec, and B. Perthame. “Microreversible collisions for polyatomic gases and Boltzmann’s theorem”. *European J. Mech. B Fluids* 13 (2) (1994), pp. 237–254.

[42] M. Briant and E. S. Daus. “The Boltzmann Equation for a Multi-species Mixture Close to Global Equilibrium”. *Arch. Ration. Mech. Anal.* 222 (2016), pp. 1367–1443.

[43] M. Briant. “From the Boltzmann equation to the incompressible Navier-Stokes equations on the torus: a quantitative error estimate”. *J. Differential Equations* 259 (11) (2015), pp. 6072–6141.

[44] S. Brull, J. Schneider, and V. Pavan. “A BGK model for gas mixtures”. *Acta Appl. Math.* 132 (2014), pp. 117–125.

[45] S. Brull, M. Shahine, and P. Thieullen. “Fredholm property of the linearized Boltzmann operator for a polyatomic single gas model”. *Kinet. Relat. Models* 17 (2) (2024), pp. 234–252.

[46] M. Brunengo, B. R. Mitchell, A. Nicolini, B. Rousselet, and B. Mauroy. “Optimal efficiency of high-frequency chest wall oscillations and links with resistance and compliance in a model of the lung”. *Phys. Fluids* 33 (12) (2021), p. 121909.

[47] R. E. Caflisch. “Asymptotics of the Boltzmann equation and fluid dynamics”. *Kinetic theory and gas dynamics*. Vol. 293. CISM Courses and Lect. Springer, Vienna, 1988, pp. 95–133.

[48] R. E. Caflisch. “The fluid dynamic limit of the nonlinear Boltzmann equation”. *Comm. Pure Appl. Math.* 33 (5) (1980), pp. 651–666.

[49] C. Cancès, V. Ehrlacher, and L. Monasse. “Finite volumes for the Stefan–Maxwell cross-diffusion system”. *IMA J. Numer. Anal.* 44 (2) (2023), pp. 1029–1060.

[50] J. A. Carrillo, T. Goudon, P. Lafitte, and F. Vecil. “Numerical schemes of diffusion asymptotics and moment closures for kinetic equations”. *J. Sci. Comput.* 36 (1) (2008), pp. 113–149.

[51] C. Cercignani. *Rarefied gas dynamics*. Cambridge Texts in Applied Mathematics. Cambridge University Press, 2000.

[52] C. Cercignani, R. Illner, and M. Pulvirenti. *The mathematical theory of dilute gases*. Vol. 106. Applied Mathematical Sciences. Springer-Verlag, New York, 1994.

[53] C. Cercignani and M. Lampis. “On the kinetic theory of a dense gas of rough spheres”. *J. Stat. Phys.* 53 (3-4) (1988), pp. 655–672.

[54] S. Chapman and T. G. Cowling. *The mathematical theory of non-uniform gases: an account of the kinetic theory of viscosity, thermal conduction and diffusion in gases*. Cambridge university press, 1990.

[55] G. Q. Chen, C. D. Levermore, and T.-P. Liu. “Hyperbolic conservation laws with stiff relaxation terms and entropy”. *Comm. Pure Appl. Math.* 47 (6) (1994), pp. 787–830.

[56] R. Clausius. “Über das Verhalten der Kohlensäure in Bezug auf Druck, Volumen und Temperatur”. *Ann. Phys.* 245 (3) (1880), pp. 337–357.

[57] S. Clerc. “Numerical Simulation of the Homogeneous Equilibrium Model for Two-Phase Flows”. *J. Comput. Phys.* 161 (1) (2000), pp. 354–375.

[58] E. S. Daus, A. Jüngel, and B. Q. Tang. “Exponential time decay of solutions to reaction-cross-diffusion systems of Maxwell-Stefan type”. *Arch. Ration. Mech. Anal.* 235 (2) (2020), pp. 1059–1104.

[59] A. De Masi, R. Esposito, and J. L. Lebowitz. “Incompressible Navier-Stokes and Euler limits of the Boltzmann equation”. *Comm. Pure Appl. Math.* 42 (8) (1989), pp. 1189–1214.

[60] A. Decoster, P. A. Markowich, and B. Perthame. *Modeling of collisions.* Vol. 2. Series in Applied Mathematics (Paris). North-Holland, Amsterdam, 1998.

[61] S. Dellacherie. “Analysis of Godunov type schemes applied to the compressible Euler system at low Mach number”. *J. Comput. Phys.* 229 (4) (2010), pp. 978–1016.

[62] S. Dellacherie. “On a low Mach nuclear core model”. *ESAIM: Proc.* 35 (2012), pp. 79–106.

[63] L. Desvillettes and J. Mathiaud. “Some Aspects of the Asymptotics Leading from Gas-Particles Equations Towards Multiphase Flows Equations”. *J. Stat. Phys.* 141 (2010), pp. 120–141.

[64] L. Desvillettes, R. Monaco, and F. Salvarani. “A kinetic model allowing to obtain the energy law of polytropic gases in the presence of chemical reactions”. *Eur. J. Mech. B Fluids* 24 (2) (2005), pp. 219–236.

[65] L. Desvillettes. “Some aspects of the modeling at different scales of multiphase flows”. *Comput. Methods Appl. Mech. Engrg.* 199 (21-22) (2010), pp. 1265–1267.

[66] C. B. Didier Bresch and F. Lagoutière. “Mathematical justification of a compressible bifluid system with different pressure laws: a continuous approach”. *Appl. Anal.* 101 (12) (2022), pp. 4235–4266.

[67] G. A. Dilts. “Consistent thermodynamic derivative estimates for tabular equations of state”. *Phys. Rev. E* 73 (6 2006), p. 066704.

[68] G. Dimarco and L. Pareschi. “Exponential Runge-Kutta methods for stiff kinetic equations”. *SIAM J. Numer. Anal.* 49 (5) (2011), pp. 2057–2077.

[69] G. Dimarco and L. Pareschi. “High order asymptotic-preserving schemes for the Boltzmann equation”. *C. R. Math. Acad. Sci. Paris* 350 (9-10) (2012), pp. 481–486.

[70] G. Dimarco and L. Pareschi. “Asymptotic preserving implicit-explicit Runge-Kutta methods for nonlinear kinetic equations”. *SIAM J. Numer. Anal.* 51 (2) (2013), pp. 1064–1087.

[71] G. Dimarco and L. Pareschi. “Multi-scale control variate methods for uncertainty quantification in kinetic equations”. *J. Comput. Phys.* 388 (2019), pp. 63–89.

[72] J. Dolbeault, C. Mouhot, and C. Schmeiser. “Hypocoercivity for linear kinetic equations conserving mass”. *Trans. Amer. Math. Soc.* 367 (6) (2015), pp. 3807–3828.

[73] W. Dreyer. “Maximisation of the entropy in nonequilibrium”. *J. Phys. A* 20 (18) (1987), pp. 6505–6517.

[74] J. B. Duncan and H. L. Toor. “An experimental study of three component gas diffusion”. *AIChE Journal* 8 (1) (1962), pp. 38–41.

[75] I. G. Economou. “Cubic and generalized Van der Waals equations of state”. *Applied Thermodynamics of Fluids.* Royal Society of Chemistry, 2010, pp. 53–83.

[76] R. S. Ellis and M. A. Pinsky. “The first and second fluid approximations to the linearized Boltzmann equation”. *J. Math. Pures Appl. (9)* 54 (1975), pp. 125–156.

[77] P. Embid. “Well-posedness of the nonlinear equations for zero Mach number combustion”. *Comm. Partial Differential Equations* 12 (11) (1987), pp. 1227–1283.

[78] P. Embid. “On the reactive and nondiffusive equations for zero Mach number flow”. *Comm. Partial Differential Equations* 14 (8-9) (1989), pp. 1249–1281.

[79] D. Enskog. “Kinetische Theorie der Vorgänge in mässig verdünnten Gasen.” PhD thesis. Uppsala Universitet, 1917.

[80] L. Ertzbischoff and D. Han-Kwan. “Some Aspects of the Asymptotics Leading from Gas-Particles Equations Towards Multiphase Flows Equations”. *Mem. Eur. Math. Soc.* (2024), to appear.

[81] R. Esposito, J. L. Lebowitz, and R. Marra. “The Navier-Stokes limit of stationary solutions of the nonlinear Boltzmann equation”. Vol. 78. 1-2. 1995, pp. 389–412.

[82] G. Faccanoni. “Étude d’un modèle fin de changement de phase liquide-vapeur”. PhD thesis. École Polytechnique, 2008.

[83] G. Faccanoni, S. Kokh, and G. Allaire. “Modelling and Simulation of Liquid-Vapor Phase Transition in Compressible Flows Based on Thermodynamical Equilibrium”. *ESAIM Math. Model. Numer. Anal.* 46 (2012), pp. 1029–1054.

[84] G. Faccanoni and C. Galusinski. “Influence of a nonlinear degenerate diffusion on an advection-diffusion equation in a diffuse interface framework”. *ESAIM: ProcS* 72 (2023), pp. 143–162.

[85] A. Fick. “Ueber Diffusion”. *Ann. Phys.* 170 (1) (1855), pp. 59–86.

[86] F. Filbet and S. Jin. “A class of asymptotic-preserving schemes for kinetic equations and related problems with stiff sources”. *J. Comput. Phys.* 229 (20) (2010), pp. 7625–7648.

[87] P. Fillion, A. Chanoine, S. Dellacherie, and A. Kumbaro. “FLICA-OVAP: A new platform for core thermal–hydraulic studies”. *Nucl. Eng. Des.* 241 (11) (2011), pp. 4348–4358.

[88] T. Flåtten and H. Lund. “Relaxation two-phase flow models and the subcharacteristic condition”. *Math. Models Methods Appl. Sci.* 21 (12) (2011), pp. 2379–2407.

[89] A. Foucquier. “Dynamique du transport et du transfert de l’oxygène au sein de l’acinus pulmonaire humain”. PhD thesis. École Polytechnique, 2010.

[90] V. Fournet. “Mathematical and Numerical Study of Thick Spray Models”. PhD thesis. Sorbonne Université, 2025.

[91] E. Gabetta, L. Pareschi, and G. Toscani. “Relaxation schemes for nonlinear kinetic equations”. *SIAM J. Numer. Anal.* 34 (6) (1997), pp. 2168–2194.

[92] I. M. Gamba, S. Jin, and L. Liu. “Micro-macro decomposition based asymptotic-preserving numerical schemes and numerical moments conservation for collisional nonlinear kinetic equations”. *J. Comput. Phys.* 382 (2019), pp. 264–290.

[93] S. Gavrilyuk and H. Gouin. “Theoretical model of the Leidenfrost temperature”. *Phys. Rev. E: Stat. Phys. Plasmas Fluids Relat. Interdiscip. Top.* 106 (5) (2022).

[94] J. Geiser, J. L. Hueso, and E. Martínez. “Adaptive Iterative Splitting Methods for Convection-Diffusion-Reaction Equations”. *Mathematics* 8 (3) (2020).

[95] P. N. Ghoderao, V. H. Dalvi, and M. Narayan. “A four parameter cubic equation of state with temperature dependent covolume parameter”. *Chin. J. Chem. Eng.* 27 (5) (2019), pp. 1132–1148.

[96] V. Giovangigli. “Convergent iterative methods for multicomponent diffusion”. *Impact Comput. Sci. Engrg.* 3 (3) (1991), pp. 244–276.

[97] V. Giovangigli. *Multicomponent flow modeling.* Modeling and Simulation in Science, Engineering and Technology. Boston, MA: Birkhäuser Boston Inc., 1999.

[98] V. Giovangigli and L. Matuszewski. “Supercritical fluid thermodynamics from equations of state”. *Physica D* 241 (6) (2012), pp. 649–670.

[99] F. Golse and L. Saint-Raymond. “The Navier-Stokes limit of the Boltzmann equation for bounded collision kernels”. *Invent. Math.* 155 (1) (2004), pp. 81–161.

[100] F. Golse and L. Saint-Raymond. “The incompressible Navier-Stokes limit of the Boltzmann equation for hard cutoff potentials”. *J. Math. Pures Appl. (9)* 91 (5) (2009), pp. 508–552.

[101] H. Grad. “Principles of the Kinetic Theory of Gases”. *Thermodynamik der Gase / Thermodynamics of Gases.* Springer, 1958.

[102] H. Grad. “On the kinetic theory of rarefied gases”. *Comm. Pure Appl. Math.* 2 (4) (1949), pp. 331–407.

[103] H. Grad. “Asymptotic theory of the Boltzmann equation. II”. *Rarefied Gas Dynamics (Proc. 3rd Internat. Sympos.)* Vol. Supplement 2. Adv. Appl. Mech. Academic Press, New York-London, 1963, pp. 26–59.

[104] T. Graham. “Researches on the arseriates, phosphates, and modifications of phosphoric acid”. *Phil. Trans. R. Soc.* 123 (1833), pp. 253–284.

[105] C. Grandmont and S. Martin. “Existence of solutions and continuous and semi-discrete stability estimates for 3D/0D coupled systems modelling airflows and blood flows”. *ESAIM Math. Model. Numer. Anal.* 55 (5) (2021), pp. 2365–2419.

[106] C. Grandmont, B. Maury, and A. Soualah. “Multiscale modelling of the respiratory track : a theoretical framework”. *ESAIM: Proc.* 23 (2008), pp. 10–29.

[107] B. J. Grant. “Influence of Bohr-Haldane effect on steady-state gas exchange”. *Journal of Applied Physiology* 52 (5) (1982), pp. 1330–1337.

[108] S. R. de Groot and P. Mazur. *Non-equilibrium thermodynamics.* Series in Physics. Interscience Publishers Inc., New York: North-Holland Publishing Co., Amsterdam, 1962.

[109] M. Groppi, S. Monica, and G. Spiga. “A kinetic ellipsoidal BGK model for a binary gas mixture”. *Europhys. Lett.* 96 (6) (2011), p. 64002.

[110] H. Guillard and C. Viozat. “On the behaviour of upwind schemes in the low Mach number limit”. *Comput. Fluids* 28 (1) (1999), pp. 63–86.

[111] Y. Guo. “Classical solutions to the Boltzmann equation for molecules with an angular cutoff”. *Arch. Ration. Mech. Anal.* 169 (4) (2003), pp. 305–353.

[112] Y. Guo. “The Vlasov-Maxwell-Boltzmann system near Maxwellians”. *Invent. Math.* 153 (3) (2003), pp. 593–630.

[113] Y. Guo. “The Boltzmann equation in the whole space”. *Indiana Univ. Math. J.* 53 (4) (2004), pp. 1081–1094.

[114] A. Guyton and J. Hall. *Textbook of medical physiology, 11th.* Elsevier Inc., 2006.

[115] M. Heckl and I. Müller. “Frame dependence, entropy, entropy flux, and wave speeds in mixtures of gases”. *Acta Mech.* 50 (1983), pp. 71–95.

[116] P. Helluy and N. Seguin. “Relaxation models of phase transition flows”. *ESAIM Math. Model. Numer. Anal.* 40 (02) (2006), pp. 331–352.

[117] D. Hilbert. “Begründung der kinetischen Gastheorie”. *Math. Ann.* 72 (1912), pp. 562–577.

[118] E. Hill, G. Power, and L. Longo. “Mathematical simulation of pulmonary O 2 and CO 2 exchange”. *Am. J. Physiol.* 224 (4) (1973), pp. 904–917.

[119] X. Huo, H. Liu, A. E. Tzavaras, and S. Wang. “An Energy Stable and Positivity-Preserving Scheme for the Maxwell–Stefan Diffusion System”. *SIAM J. Numer. Anal.* 59 (5) (2021), pp. 2321–2345.

[120] O. Hurisse. “Application of an homogeneous model to simulate the heating of two-phase flows”. *Int. J. Finite Vol.* 11 (2014), pp. 1–37.

[121] O. Hurisse. “Simulation des écoulements industriels diphasiques compressibles”. PhD thesis. Habilitation à diriger des recherches, Université de Strasbourg, 2017.

[122] O. Hurisse and L. Quibel. “A homogeneous model for compressible three-phase flows involving heat and mass transfer.” *ESAIM: ProcS* 66 (2019), pp. 84–108.

[123] H. Hutridurga and F. Salvarani. “Maxwell-Stefan diffusion asymptotics for gas mixtures in non-isothermal setting”. *Nonlinear Anal.* 159 (2017), pp. 285–297.

[124] H. Hutridurga and F. Salvarani. “On the Maxwell-Stefan diffusion limit for a mixture of monatomic gases”. *Math. Methods Appl. Sci.* 40 (3) (2017), pp. 803–813.

[125] M. Ismail, A. Comerford, and W. A. Wall. “Coupled and reduced dimensional modeling of respiratory mechanics during spontaneous breathing”. *Int. J. Numer. Methods Biomed. Eng.* 29 (11) (2013), pp. 1285–1305.

[126] S. Jin. “Runge-Kutta methods for hyperbolic conservation laws with stiff relaxation terms”. *J. Comput. Phys.* 122 (1) (1995), pp. 51–67.

[127] S. Jin. “Asymptotic preserving (AP) schemes for multiscale kinetic and hyperbolic equations: a review”. *Riv. Math. Univ. Parma (N.S.)* 3 (2) (2012), pp. 177–216.

[128] S. Jin and Q. Li. “A BGK-penalization-based asymptotic-preserving scheme for the multispecies Boltzmann equation”. *Numer. Methods Partial Differential Equations* 29 (3) (2013), pp. 1056–1080.

[129] S. Jin, L. Pareschi, and G. Toscani. “Uniformly accurate diffusive relaxation schemes for multiscale transport equations”. *SIAM J. Numer. Anal.* 38 (3) (2000), pp. 913–936.

[130] S. Jin and Y. Shi. “A micro-macro decomposition-based asymptotic-preserving scheme for the multispecies Boltzmann equation”. *SIAM J. Sci. Comput.* 31 (6) (2009), pp. 4580–4606.

[131] A. Jüngel and I. V. Stelzer. “Existence analysis of Maxwell-Stefan systems for multicomponent mixtures”. *SIAM J. Math. Anal.* 45 (4) (2013), pp. 2421–2440.

[132] J. Keener and J. Sneyd. “Mathematical Physiology”. *Interdiscip. Appl. Math.* (1998).

[133] A. Klar. “An asymptotic-induced scheme for nonstationary transport equations in the diffusive limit”. *SIAM J. Numer. Anal.* 35 (3) (1998), pp. 1073–1094.

[134] G. M. Kremer. *An introduction to the Boltzmann equation and transport processes in gases.* Interaction of Mechanics and Mathematics. Springer, Dordrecht, 2010, pp. xviii+303.

[135] R. Krishna and J. A. Wesselingh. “The Maxwell-Stefan approach to mass transfer”. *Chem. Eng. Sci.* 52 (6) (1997), pp. 861–911.

[136] T. Laidin. “Hybrid kinetic/fluid numerical method for the Vlasov-BGK equation in the diffusive scaling”. *Kinet. Relat. Models* 16 (6) (2023), pp. 913–947.

[137] T. Laidin and T. Rey. “Hybrid Kinetic/Fluid Numerical Method for the Vlasov-Poisson-BGK Equation in the Diffusive Scaling”. *Finite Volumes for Complex Applications X—Volume 2, Hyperbolic and Related Problems.* Springer, 2023, pp. 229–237.

[138] O. Le Métayer, J. Massoni, and R. Saurel. “Elaborating equations of state of a liquid and its vapor for two-phase flow models”. *Int. J. Therm. Sci.* 43 (3) (2004), pp. 265–276.

[139] O. Le Métayer, J. Massoni, and R. Saurel. “Modelling evaporation fronts with reactive Riemann solvers”. *J. Comput. Phys.* 205 (2) (2005), pp. 567–610.

[140] O. Le Métayer and R. Saurel. “The Noble-Abel Stiffened-Gas equation of state”. *Phys. Fluids* 28 (2016), p. 046102.

[141] E. W. Lemmon, M. O. McLinden, and D. G. Friend. *Thermophysical Properties of Fluid Systems.* http://webbook.nist.gov. National Institute of Standards and Technology. 2012.

[142] M. Lemou. “Relaxed micro-macro schemes for kinetic equations”. *C. R. Math. Acad. Sci. Paris* 348 (7-8) (2010), pp. 455–460.

[143] C. D. Levermore. “Moment closure hierarchies for kinetic theories”. *J. Stat. Phys.* 83 (5-6) (1996), pp. 1021–1065.

[144] G. Linga and T. Flåtten. “A hierarchy of non-equilibrium two-phase flow models”. *ESAIM: ProcS* 66 (2019), pp. 109–143.

[145] P.-L. Lions. “Compactness in Boltzmann’s equation via Fourier integral operators and applications. I, II”. *J. Math. Kyoto Univ.* 34 (2) (1994), pp. 391–427, 429–461.

[146] T.-P. Liu, T. Yang, and S.-H. Yu. “Energy method for Boltzmann equation”. *Phys. D* 188 (3-4) (2004), pp. 178–192.

[147] T.-P. Liu and S.-H. Yu. “Boltzmann equation: micro-macro decompositions and positivity of shock profiles”. *Comm. Math. Phys.* 246 (1) (2004), pp. 133–179.

[148] T.-P. Liu and S.-H. Yu. “Initial-boundary value problem for one-dimensional wave solutions of the Boltzmann equation”. *Comm. Pure Appl. Math.* 60 (3) (2007), pp. 295–356.

[149] P. W. Longest and M. Hindle. “CFD simulations of enhanced condensational growth (ECG) applied to respiratory drug delivery with comparisons to in vitro data”. *J. Aerosol Sci.* 41 (8) (2010), pp. 805–820.

[150] P. W. Longest and M. Hindle. “Numerical Model to Characterize the Size Increase of Combination Drug and Hygroscopic Excipient Nanoparticle Aerosols”. *Aerosol Sci. Technol.* 45 (7) (2011), pp. 884–899.

[151] J. S. Lopez-Echeverry, S. Reif-Acherman, and E. Araujo-Lopez. “Peng-Robinson equation of state: 40 years through cubics”. *Fluid Phase Equilib.* 447 (2017), pp. 39–71.

[152] M. de Lorenzo. “Modelling and numerical simulation of metastable two-phase flows”. PhD thesis. Université Paris-Saclay, 2018.

[153] H. Lund. “A Hierarchy of Relaxation Models for Two-Phase Flow”. *SIAM J. Appl. Math.* 72 (6) (2012), pp. 1713–1741.

[154] A. Majda and K. Lamb. *Simplified equations for low Mach number combustion with strong heat release.* Vol. 35. IMA Vol. Math. Appl. Springer-Verlag, 1991, pp. 167–211.

[155] A. Majda and J. Sethian. “The Derivation and Numerical Solution of the Equations for Zero Mach Number Combustion”. *Combust. Sci. Technol.* 42 (3-4) (1985), pp. 185–205.

[156] H. Malte and G. Lykkeboe. “The Bohr/Haldane effect: a model-based uncovering of the full extent of its impact on O2 delivery to and CO2 removal from tissues”. *J. Appl. Physiol.* 125 (3) (2018), pp. 916–922.

[157] J. P. Mañes, V. H. Sánchez Espinoza, S. Chiva Vicent, M. Böttcher, and R. Stieglitz. “Validation of NEPTUNE-CFD two-phase flow models using experimental data”. 2014 (2014).

[158] S. Martin and B. Maury. “Modeling of the oxygen transfer in the respiratory process”. *ESAIM Math. Model. Numer. Anal.* 47 (4) (2013), pp. 935–960.

[159] J. Mathiaud. “A study of gas-particles systems”. PhD thesis. École normale supérieure de Cachan - ENS Cachan, 2006.

[160] B. Mauroy. “Hydrodynamique dans le poumon, relations entre flux et geometries”. PhD thesis. École Normale Supérieure de Cachan, 2004.

[161] B. Mauroy, M. Filoche, J. S. Andrade, and B. Sapoval. “Interplay between Geometry and Flow Distribution in an Airway Tree”. *Phys. Rev. Lett.* 90 (14 2003), p. 148101.

[162] B. Maury. *The Respiratory System in Equations.* MS&A. Springer, 2013.

[163] J. C. Maxwell. “On the dynamical theory of gases”. *Phil. Trans. R. Soc.* 157 (1867), pp. 49–88.

[164] M. McLeod and Y. Bourgault. “Mixed finite element methods for addressing multi-species diffusion using the Maxwell–Stefan equations”. *Comput. Methods Appl. Mech. Engrg.* 279 (2014), pp. 515–535.

[165] F. Meade. “A formula for the carbon dioxide dissociation curve”. *Br. J. Anaesth.* 44 (6) (1972), p. 630.

[166] R. Menikoff and B. Plohr. “The Riemann problem for fluid flow of real materials”. *Rev. Mod. Phys.* 61 (1) (1989), pp. 75–130.

[167] T. F. Morse. “Kinetic Model Equations for a Gas Mixture”. *Phys. Fluids* 7 (12) (1964), pp. 2012–2013.

[168] R. Mortimer. *Physical Chemistry.* Harcourt/Academic Press, 2000.

[169] C. Mouhot. “Explicit coercivity estimates for the linearized Boltzmann and Landau operators”. *Comm. Partial Differential Equations* 31 (7-9) (2006), pp. 1321–1348.

[170] C. Mouhot and L. Neumann. “Quantitative perturbative study of convergence to equilibrium for collisional kinetic models in the torus”. *Nonlinearity* 19 (4) (2006), pp. 969–998.

[171] C. Mouhot and C. Villani. “Regularity theory for the spatially homogeneous Boltzmann equation with cut-off”. *Arch. Ration. Mech. Anal.* 173 (2) (2004), pp. 169–212.

[172] I. Müller. “A thermodynamic theory of mixtures of fluids”. *Arch. Ration. Mech. Anal.* 28 (1968), pp. 1–39.

[173] I. Müller and T. Ruggeri. *Extended thermodynamics.* Vol. 37. Springer Tracts in Natural Philosophy. Springer-Verlag, New York, 1993, pp. xii+230.

[174] S. Müller and A. Voss. “The Riemann Problem for the Euler Equations with Nonconvex and Nonsmooth Equation of State: Construction of Wave Curves”. *SIAM J. Sci. Comput.* 28 (2) (2006), pp. 651–681.

[175] F. Noël, C. Karamaoun, J. Dempsey, and B. Mauroy. “The origin of the allometric scaling of lung ventilation in mammals”. *PCI Math. Comp. Biol.* 2 (e2) (2022).

[176] F. Noël and B. Mauroy. “Interplay between optimal ventilation and gas transport in a model of the human lung”. *Front. Physiol.* 10 (2019).

[177] J. Oakes, A. Marsden, C. Grandmont, S. C. Shadden, C. Darquenne, and I. E. Vignon-Clementel. “Airflow and Particle Deposition Simulations in Health and Emphysema: From In Vivo to In Silico Animal Experiments”. *Ann. Biomed. Eng.* 42 (2014), pp. 899–914.

[178] J. M. Oakes, A. L. Marsden, C. Grandmont, C. Darquenne, and I. E. Vignon-Clementel. “Distribution of aerosolized particles in healthy and emphysematous rat lungs: Comparison between experimental and numerical studies”. *J. Biomech.* 48 (6) (2015), pp. 1147–1157.

[179] J. M. Oakes, S. C. Shadden, C. Grandmont, and I. E. Vignon-Clementel. “Aerosol transport throughout inspiration and expiration in the pulmonary airways”. *Int. J. Numer. Methods Biomed. Eng.* 33 (9) (2017), e2847.

[180] M. Olufsen. “Structured tree outflow condition for blood flow in larger systemic arteries”. *Am. J. Physiol.* 276 (1) (1999), H257–H268.

[181] M. Paiva and L. A. Engel. “Model analysis of gas distribution within human lung acinus”. *J. Appl. Physiol.* 56 (2) (1984), pp. 418–425.

[182] Y. Penel. “Étude théorique et numérique de la déformation d’une interface séparant deux fluides non-miscibles à bas nombre de Mach”. PhD thesis. Université Paris 13, 2010.

[183] Y. Penel. “An explicit stable numerical scheme for the 1D transport equation”. *Discrete Contin. Dyn. Syst. Ser. S* 5 (3) (2012), pp. 641–656.

[184] Y. Penel, S. Dellacherie, and O. Lafitte. “Theoretical Study of an Abstract Bubble Vibration Model”. *Z. Anal. Anwend.* 32 (1) (2013), pp. 19–36.

[185] J. Polewczak. “A review of the kinetic modelings for non-reactive and reactive dense fluids: questions and problems”. Vol. 4*. 2001, pp. 23–55.

[186] N. Pozin, S. Montesantos, I. Katz, M. Pichelin, I. Vignon-Clementel, and C. Grandmont. “A tree-parenchyma coupled model for lung ventilation simulation”. *Int. J. Numer. Methods Biomed. Eng.* 33 (11) (2017), e2873.

[187] L. Quibel. “Simulation of water-vapor two-phase flows with non-condensable gas.” PhD thesis. Université de Strasbourg, 2020.

[188] O. Redlich and J. N. Kwong. “On the thermodynamics of solutions. V. An equation of state. Fugacities of gaseous solutions.” *Chem. Rev.* 44 (1) (1949), pp. 233–244.

[189] P. Résibois. “H theorem for the (modified) nonlinear Enskog equation”. *Phys. Rev. Lett.* 40 (22) (1978), pp. 1409–1411.

[190] R. Saurel and R. Abgrall. “A Multiphase Godunov Method for Compressible Multifluid and Multiphase Flows”. *J. Comput. Phys.* 150 (2) (1999), pp. 425–467.

[191] T. Similowski and J. Bates. “Two-compartment modelling of respiratory system mechanics at low frequencies: gas redistribution or tissue rheology?” *European Respiratory Journal* 4 (3) (1991), pp. 353–358.

[192] L. Sirovich. “Kinetic Modeling of Gas Mixtures”. *Phys. Fluids* 5 (8) (1962), pp. 908–918.

[193] G. Soave. “Equilibrium constants from a modified Redlich-Kwong equation of state”. *Chem. Eng. Sci.* 27 (6) (1972), pp. 1197–1203.

[194] J. Stefan. “Über das Gleichgewicht und die Bewegung, insbesondere die Diffusion von Gasgemengen”. *Wiener Sitzungsberichte* 63 (1871), pp. 63–124.

[195] H. Stewart and B. Wendroff. “Two-phase flow: Models and methods”. *J. Comput. Phys.* 56 (3) (1984), pp. 363–409.

[196] A. J. Swan, A. R. Clark, and M. H. Tawhai. “A computational model of the topographic distribution of ventilation in healthy human lungs”. *J. Theoret. Biol.* 300 (2012), pp. 222–231.

[197] A. J. Swan and M. H. Tawhai. “Evidence for minimal oxygen heterogeneity in the healthy human pulmonary acinus”. *J. Appl. Physiol.* 110 (2) (2011), pp. 528–537.

[198] T. E. C. Tevfik Gemci and N. Chigier. “A Numerical and Experimental Study of Spray Dynamics in a Simple Throat Model”. *Aerosol Sci. Technol.* 36 (1) (2002), pp. 18–38.

[199] J. Van der Waals. “Continuity of the gaseous and liquid state of matter”. PhD thesis. 1873.

[200] C. Villani. “A review of mathematical topics in collisional kinetic theory”. *Handbook of mathematical fluid dynamics, Vol. I.* North-Holland, Amsterdam, 2002, pp. 71–305.

[201] G. Volpe. “Performance of compressible flow codes at low Mach numbers”. *AIAA J.* 31 (1) (1993), pp. 49–56.

[202] W. Wagner and H.-J. Kretzschmar. *IAPWSIF’97 International Steam Tables: Properties of Water and Steam.* Springer-Verlag, Berlin, 2008.

[203] E. R. Weibel. *Morphometry of the Human Lung.* Springer Verlag and Academic Press, New York, 1963.

[204] E. R. Weibel, B. Sapoval, and M. Filoche. “Design of peripheral airways for efficient gas exchange”. *Respir. Physiol. Neurobiol.* 148 (1) (2005), pp. 3–21.

[205] B. Wennberg. “Regularity in the Boltzmann equation and the Radon transform”. *Comm. Partial Differential Equations* 19 (11-12) (1994), pp. 2057–2074.

[206] J. West. *Respiratory Physiology - The Essentials.* Baltimore: Williams & Wilkins, 1974.

[207] G. Wilczek-Vera and J. H. Vera. “Understanding cubic equations of state: A search for the hidden clues of their success”. *AIChE Journal* 61 (9) (2015), pp. 2824–2831.

[208] F. Williams. *Combustion Theory.* Second edition. Benjamin Cummings, 1985.